13

AD

AD736851

FUNDAMENTAL STUDIES OF SEMICONDUCTOR HETEROEPITAXY

THIRD SEMIANNUAL REPORT

Ind. Rept. unlimited
AD-886 667L

ARPA Support Office
Research, Development, Engineering and Missile Systems Laboratory
United States Army Missile Command AMSMI RND
Redstone Arsenal
Huntsville, Alabama

Contract No. DAAH01-70-C-1311

DDC
RECEIVED
FEB 11 1972
A

Distribution of this document
is unlimited.

Sponsored by:
Advanced Research Projects Agency
ARPA Order No. 1585

Reproduced by
NATIONAL TECHNICAL
INFORMATION SERVICE
Springfield, Va. 22151

96

BEST
AVAILABLE COPY

This research was sponsored by the Advanced Research Projects Agency of the Department of Defense under ARPA Order 1585 and was monitored by the U.S. Army Missile Command under Contract Number DAAH01-70-C-1311. Views and conclusions expressed herein are the primary responsibility of the author or the contractor and should not be interpreted as representing the official opinion or policy of USAMICOM, ARPA, DOD or any other agency of the Government.

The findings in this report are not to be construed as an official Department of the Army position unless so designated by other authorized documents.

CFSTI
DDC
JUSTIFICATION
DISTRIBUTION/AVAILABILITY CODES
AVAIL. and/or SPECIAL
A

Security Classification

DOCUMENT CONTROL DATA - R & D

(Security classification of title, body of abstract and indexing annotation must be entered when the overall report is classified)

1. ORIGINATING ACTIVITY *(Corporate author)*
North American Rockwell Corp, Electronics Group
Research and Technology Division
Anaheim, California

2a. REPORT SECURITY CLASSIFICATION

2b. GROUP

3. REPORT TITLE

Fundamental Studies of Semiconductor Heteroepitaxy

4. DESCRIPTIVE NOTES *(Type of report and inclusive dates)*
Semiannual Report, July 1971 through December 1971

5. AUTHOR(S) *(First name, middle initial, last name)*

Ralph P. Ruth

6. REPORT DATE
January 1972

7a. TOTAL NO. OF PAGES
~~100~~ 96

7b. NO. OF REFS
25

8a. CONTRACT OR GRANT NO.
DAAH01-70-C-1311

b. PROJECT NO.

c.

d.

9a. ORIGINATOR'S REPORT NUMBER(S)
C71-66.3/501

9b. OTHER REPORT NO(S) *(Any other numbers that may be assigned this report)*

10. DISTRIBUTION STATEMENT

Distribution of this document is unlimited

11. SUPPLEMENTARY NOTES

12. SPONSORING MILITARY ACTIVITY
Advanced Research Projects
Agency, ARPA Order No. 1585
Washington, D.C.

13. ABSTRACT

The objective of this program is to carry out a fundamental study of nucleation and film growth mechanisms in heteroepitaxial semiconductor thin films, and to apply the results to the preparation of improved films and thin-film devices on insulating substrates. Both theoretical and experimental investigations are involved, with emphasis on chemical vapor deposition (CVD) techniques applied to the Si-on-$A\ell_2O_3$ and GaAs-on-$A\ell_2O_3$ systems. The accomplishments of the third six-month period are described in terms of seven program subtasks.

Two theoretical approaches to modeling the heteroepitaxial interface are being investigated. The first involves the use of interatomic potentials which fulfill certain stability conditions and are stable against transformation to other crystal structures. The stability conditions for the $A\ell_2O_3$ lattice have been determined to the extent required. The ultimate goal of this approach is the computer simulation of the growth of Si films on $A\ell_2O_3$ substrates. The second approach involves application of the electron-on-network theory to the problem of determining surface configurations and interfacial binding energies in heteroepitaxial systems. Normalized eigenvectors have been developed as a basis for a secular equation whose solution is fundamental to the total solution desired.

Mass spectrometic analysis of samples of SiH_4 and trimethylgallium used for Si and GaAs CVD experiments has identified several impurities, some of potential importance in determining film properties. Analysis of extensive data demonstrating the effects of changes in deposition parameters on $Si/A\ell_2O_3$ film properties reveals strong interrelationships among the various parameters important to the optimization of film properties. Identification of

(continued on following sheet)

DD FORM 1 NOV 65 1473

Security Classification

14 KEY WORDS	LINK A ROLE	LINK A WT	LINK B ROLE	LINK B WT	LINK C ROLE	LINK C WT
Epitaxy						
GaAs						
Si						
$A\ell_2O_3$ (sapphire)						
$MgA\ell_2O_4$ (spinel)						
Chemical vapor deposition (CVD)						
In situ film growth						
Electron microscopy						
Epitaxy theory						
Heteroepitaxy						
Thin-film devices						
Semiconductors						
Film nucleation						
Transport properties						
Metalorganic compounds						
Physical vapor deposition (PVD)						
Substrate						
Polishing						
Gas-phase etching						

conditions for optimized Si film growth on various $A\ell_2O_3$ orientations is nearly complete. The importance of the reactor configuration in determining film growth and properties has been demonstrated. The extent of $A\ell$ autodoping from the $A\ell_2O_3$ substrate has been established, and appropriate annealing procedures for minimizing these effects have been determined. $A\ell_2O_3$ substrate orientations not previously used have resulted in Si films at least as good as any previously grown. Si deposition by SiH_4 pyrolysis at reduced pressures (1 to 10 torr) indicates single-crystal growth can be obtained over a wide temperature range on both $A\ell_2O_3$ and $MgA\ell_2O_4$ when deposition conditions are optimized.

An improved technique for polishing $(10\bar{1}4)$ $A\ell_2O_3$ has been developed; excellent surfaces in this orientation have been obtained. Gas-phase etching/polishing techniques have been further developed and used in several different experimental procedures. Ion-beam sputter-etching techniques are being developed for preparation of very thin (~200 A) $A\ell_2O_3$ substrates for the in situ CVD experiments in the electron microscope. A series of in situ PVD experiments has been carried out in the electron microscope with $A\ell$ deposited onto heated carbon substrates; various facets of film nucleation and island coalescence mechanisms have been observed. Microscope modification for the CVD experiments is nearly complete, including design of the CVD microchamber.

Work functions of several metals have been determined by measurement of photoemission of electrons from heteroepitaxial semiconductor films on $A\ell_2O_3$, and the mechanism of electron transport through the insulator is being investigated. Measurement of high-field transport properties of Si and GaAs heteroepitaxial films has been initiated. Design of a Schottky-barrier FET has been completed for experimental fabrication of 1 GHz devices in GaAs/insulator films. Preliminary results on carrier lifetime in $Si/A\ell_2O_3$ films by the measurement of C-V characteristics of MOS structures have been obtained.

A summary of the work planned for the next six months is included.

AD

FUNDAMENTAL STUDIES OF SEMICONDUCTOR HETEROEPITAXY

THIRD SEMIANNUAL REPORT

R. P. Ruth

Research and Technology Division of North American Rockwell

January 1972

ARPA Support Office

Research, Development, Engineering and Missile Systems Laboratory

United States Army Missile Command AMSMI RND

Redstone Arsenal

Huntsville, Alabama

Contract No. DAAH01-70-C-1311

Distribution of this document
is unlimited.

Sponsored by:

Advanced Research Projects Agency

ARPA Order No. 1585

ABSTRACT

The objective of this program is to carry out a fundamental study of nucleation and film growth mechanisms in heteroepitaxial semiconductor thin films, and to apply the results to the preparation of improved films and thin-film devices on insulating substrates. Both theoretical and experimental investigations are involved, with emphasis on chemical vapor deposition (CVD) techniques applied to the Si-on-$A\ell_2O_3$ and GaAs-on-$A\ell_2O_3$ systems. The accomplishments of the third six-month period are described in terms of seven program subtasks.

Two theoretical approaches to modeling the heteroepitaxial interface are being investigated. The first involves the use of interatomic potentials which fulfill certain stability conditions and are stable against transformation to other crystal structures. The stability conditions for the $A\ell_2O_3$ lattice have been determined to the extent required. The ultimate goal of this approach is the computer simulation of the growth of Si films on $A\ell_2O_3$ substrates. The second approach involves application of the electron-on-network theory to the problem of determining surface configurations and interfacial binding energies in heteroepitaxial systems. Normalized eigenvectors have been developed as a basis for a secular equation whose solution is fundamental to the total solution desired.

Mass spectrometic analysis of samples of SiH_4 and trimethylgallium used for Si and GaAs CVD experiments has identified several impurities, some of potential importance in determining film properties. Analysis of extensive data demonstrating the effects of changes in deposition parameters on $Si/A\ell_2O_3$ film properties reveals strong interrelationships among the various parameters important to the optimization of film properties. Identification of conditions for optimized Si film growth on various $A\ell_2O_3$ orientations is nearly complete. The importance of the reactor configuration in determining film growth and properties has been demonstrated. The extent of $A\ell$ autodoping from the $A\ell_2O_3$ substrate has been established, and appropriate annealing procedures for minimizing these effects have been determined. $A\ell_2O_3$ substrate orientations not previously used have resulted in Si films at least as good as any previously grown. Si deposition by SiH_4 pyrolysis at reduced pressures (1 to 10 torr) indicates single-crystal growth can be obtained over a wide temperature range on both $A\ell_2O_3$ and $MgA\ell_2O_4$ when deposition conditions are optimized.

An improved technique for polishing $(10\bar{1}4)$ $A\ell_2O_3$ has been developed; excellent surfaces in this orientation have been obtained. Gas-phase etching/polishing techniques have been further developed and used in several different experimental procedures. Ion-beam sputter-etching techniques are being developed for preparation of very thin (~200Å) $A\ell_2O_3$ substrates for the in situ CVD experiments in the electron microscope. A series of in situ PVD experiments has been carried out in the electron microscope with $A\ell$ deposited onto heated carbon substrates; various facets of film nucleation and island coalescence mechanisms have been observed. Microscope modification for the CVD experiments is nearly complete, including design of the CVD microchamber.

Work functions of several metals have been determined by measurement of photoemission of electrons from heteroepitaxial semiconductor films on $A\ell_2O_3$, and the mechanism of electron transport through the insulator is being investigated. Measurement of high-field transport properties of Si and GaAs heteroepitaxial films has been initiated. Design of a Schottky-barrier FET has been completed for experimental fabrication of 1 GHz devices in GaAs/insulator films. Preliminary results on carrier lifetime in $Si/A\ell_2O_3$ films by the measurement of C-V characteristics of MOS structures have been obtained.

A summary of the work planned for the next six months is included.

CONTENTS

Page

I. Introduction 1

1. Program Objectives 1
2. Program Scope 2
3. Program Description by Subtask 3

II. Results and Discussion 5

1. Subtask 1: Theory of Epitaxy and Heteroepitaxial Interfaces 5
2. Subtask 2: Deposition Studies and Film Preparation 11
3. Subtask 3. Analysis and Purification of CVD Reactants 19
4. Subtask 4. Preparation and Characterization of Substrates 20
5. Subtask 5: Studies of In Situ Film Growth in the Electron Microscope 31
6. Subtask 6: Evaluation of Film Properties 41
7. Subtask 7: Design and Fabrication of Devices 67

III. Work Planned for Next Six Months 72

1. Subtask 1: Theory of Epitaxy and Heteroepitaxial Interfaces 72
2. Subtask 2: Deposition Studies and Film Preparation 72
3. Subtask 3: Analysis and Purification of CVD Reactants 72
4. Subtask 4: Preparation and Characterization of Substrates 73
5. Subtask 5: Studies of In Situ Film Growth in the Electron Microscope 73
6. Subtask 6: Evaluation of Film Properties 73
7. Subtask 7: Design and Fabrication of Devices 74

IV. Program Summary to Date 75

1. Subtask 1. Theory of Epitaxy and Heteroepitaxial Interfaces 76
2. Subtask 2. Deposition Studies and Film Preparation 77
3. Subtask 3. Analysis and Purification of CVD Reactants 78
4. Subtask 4. Preparation and Characterization of Substrates 78
5. Subtask 5. Studies of In Situ Film Growth in the Electron Microscope 79
6. Subtask 6. Evaluation of Film Properties 79
7. Subtask 7. Design and Fabrication of Devices 80

Appendix A. Interim Report on Analysis and Purification of CVD Reactants . . . 81

Appendix B. Bibliography: Electron Microscope In Situ Nucleation and Growth Studies 89

ILLUSTRATIONS

Figures		Page
1.	Variation of Hall Mobility with Growth Temperature for N-Type $Si/A\ell_2O_3$ Films Grown in Horizontal Reactor	12
2.	Typical Surface Finish Obtained on $(10\bar{1}4)$ $A\ell_2O_3$ Substrate with Special Cast Iron Laps with Slurry of 1 μm Synthetic Diamond on Optical Polisher	22
3.	a. Surface Finish on $(10\bar{1}4)$ $A\ell_2O_3$ Substrate after Using Special Brass Lap with Slurry of 0.5 μm Synthetic Diamond on Optical Polisher. b. Same Area after 66 Hr Polishing on Vibratory Polisher Using 0.25 μm Synthetic Diamond on Nylon Cloth	23
4.	Surface Structure of $(10\bar{1}4)$ $A\ell_2O_3$ after Removal ~7 μm of $A\ell_2O_3$ by Freon Etch at 1550 C (Etch Rate ~0.1 μm/min)	24
5.	The Surface of Verneuil-Grown $(10\bar{1}4)$ $A\ell_2O_3$ after Etching with Freon at 1500 C for ~3 Hr at Nominal Rate of 0.6 μm/min	25
6.	The Surface of Czochralski-Grown $(01\bar{1}2)$ $A\ell_2O_3$ after Etching at 1500 C with Freon at a Flow Rate of 13 ccpm for (a) 25 min, (b) 50 min, (c) 75 min, and (d) 100 min	27
7.	The Surface of Different Substrates of Verneuil-Grown ~$(11\bar{2}0)$ $A\ell_2O_3$ after Etching at 1500 C with Freon at a Flow Rate of 13 ccpm for (a) 25 min, (b) 50 min, (c) 75 min, and (d) 100 min	28
8.	The Surface of (0001) $A\ell_2O_3$ after Etching at 1500 C with Freon at a Flow Rate of 13 ccpm for (a) 25 min, (b) 50 min, (c) 75 min, and (d) 100 min	29
9.	Surface of $(10\bar{1}4)$ $A\ell_2O_3$ (a) after Mechanical Polishing in the NR Laboratory; (b) after a 10 min Etch with Freon at 1400 C; (c) after a 30 min Etch with Freon at 1400 C (~0.6 μm removed.)	30
10.	Overall View of EM6 Electron Microscope as Modified for <u>in situ</u> Film Growth	32
11.	Close-Up View of Auxiliary Pumping System Attachment for EM6 Electron Microscope	32
12.	Electron Microscope Sample Holder	33
13.	CVD Microchamber	34
14.	Nuclei of $A\ell$ during <u>In Situ</u> PVD Growth after (a) 30 sec, (b) 60 sec, and (c) 210 sec of Deposition	36
15.	$(10\bar{1}4)$ $A\ell_2O_3$ Wafer Ion-Beam Etched at Low Angle	38
16.	Variation of Hall Mobility with Growth Temperature for $Si/A\ell_2O_3$ Films Having Net Donor Carrier Concentration of 1-5 x 10^{16} cm^{-3}	48
17.	Variation of Net Donor Carrier Concentration with Growth Temperature for $Si/A\ell_2O_3$ Films Grown at ~2 μm/min with Constant Dopant-Gas Flow Rate	50
18.	Variation of Hall Mobility with Growth Rate for N-Type $Si/A\ell_2O_3$ Films Grown at 1075 C	50
19.	Variation of Net Donor Carrier Concentration with Growth Rate for $Si/A\ell_2O_3$ Films Grown at 1975 C with Constant Dopant-Gas Flow Rate	51

ILLUSTRATIONS (Cont)

Figure		Page
20.	Variation of Net Donor Carrier Concentration with AsH_3 Flow Rate for Si/Al_2O_3 Films	51
21.	Variation of Net Acceptor Carrier Concentration Due to Al Autodoping as Function of Growth Temperature for Intentionally Undoped Si/Al_2O_3 Films	53
22.	Variation of Film Properties with Film Thickness for Thin N-Type Si/Al_2O_3 Films	59
23.	Variation of Hall Mobility with Film Thickness for Intentionally Undoped P-type Si/Al_2O_3 Films	61
24.	Variation of Net Acceptor Concentration with Film Thickness for Intentionally Undoped Si/Al_2O_3 Films	61
25.	Current vs Voltage for Photoemitted Electron Transport through Al_2O_3	64
26.	Current vs $(\text{Voltage})^{1/2}$ for Photoemitted Electron Transport through Al_2O_3	64
27.	Experimental Arrangement for Film Mobility Measurements at High Fields	65
28.	Current Density as Function of Electric Field for N-Type Si/Al_2O_3 Film	65
29.	Current Density as Function of Electric Field for P-Type Si/Al_2O_3 Film	66
30.	MOS Geometry for Carrier Lifetime Measurements	68
31.	Characteristics of MOS Capacitor in Si/Al_2O_3	69
32.	Schematic of C-V, C-t Measurement Instrumentation	71

TABLES

Table		Page
1.	Properties of Si Films Grown on $A\ell_2O_3$ by Pyrolysis of SiH_4 at Low Pressure	14
2.	Properties of Si Films Grown on $A\ell_2O_3$ by Pyrolysis of SiH_4 at Medium Pressures	15
3.	Electrical Properties of N-Type CVD Si Grown on $A\ell_2O_3$ and $MgA\ell_2O_4$ in He Atmosphere	17
4.	Electrical Properties of N-Type CVD Si Grown at 1025 C on (111) $MgA\ell_2O_4$ and $(01\bar{1}2)$ $A\ell_2O_3$ in He Atmosphere Using 200 ppm AsH_3-in-H_2 as Dopant (Total Flow Rate 6 lpm)	18
5.	Electrical Properties of N-Type CVD Si on $(011\bar{2})$ and ~$(11\bar{2}0)$ $A\ell_2O_3$ Substrates Grown at 1040 C at Rate ~2 μm/min. (Film Thickness ~2 μm)	43
6.	Electrical Properties of N-Type CVD Si on $(01\bar{1}2)$ and ~$(11\bar{2}0)$ $A\ell_2O_3$ Substrates Grown at 1060 C at Rate ~2 μm/min. (Film Thickness ~2 μm)	44
7.	Electrical Properties of N-Type CVD Si on $(01\bar{1}2)$ and ~$(11\bar{2}0)$ $A\ell_2O_3$ Substrates Grown at 1060 C at Rate of ~0.8 μm/min. (Film Thickness ~2 μm)	45
8.	Electrical Properties of ~2 μm-Thick N-Type CVD Si Films Grown on $A\ell_2O_3$ at 1075 C with Addition of Constant Dopant Concentration (0.22 ccpm AsH_3-in-H_2) as Influenced by Growth Rate	46
9.	Electrical Properties of ~2 μm-Thick N-Type CVD Si Films Grown on $A\ell_2O_3$ at 1100 C at Rate ~2 μm/min.	47
10.	Effect of Growth Temperature on Properties of ~2 μm-Thick N-Type (100) and (111) Si Films Grown at Rate of ~2 μm/min with Constant AsH_3-in-H_2 Dopant Flow (0.22 ccpm)	49
11.	Comparison of Electrical Properties of 2μm-Thick N-Type Si Films Grown on $A\ell_2O_3$ at 1125 C at Rate ~2μm/min.	52
12.	Effects of Extended O_2 and N_2 Anneals on Electrical Properties of Three As-Doped, ~2 μm-Thick Si/$A\ell_2O_3$ Films (Growth Temperature 1100 C)	54
13.	Effects on Film Properties of Order of Sequential Annealing Steps in O_2 and N_2 for ~2 μm-Thick As-Doped Si Films Grown at Various Temperatures on ~$(11\bar{2}0)$ $A\ell_2O_3$ at Rate of 2 μm/min.	55
14.	Properties of Si Films Grown at 1100 C at a Nominal Growth Rate of 2 μm/min. (Annealed and Unannealed samples)	57
15.	Properties of Thin Si Films Grown on $A\ell_2O_3$ at 1100 C as Function of Thickness (Nominal Growth Rate 2 μm/min)	58
16.	Interface Barrier Height and Work Function for Several Metals	62

SECTION I

INTRODUCTION

This is the third Semiannual Technical Report for this contract. It describes work carried out during the period 1 July - 31 December 1971. Earlier semiannual reports (Refs 1, 2) described work done in the first year of the program.

1. PROGRAM OBJECTIVES

The overall objective of the program, unchanged from that originally proposed, is to carry out a fundamental study of the nucleation and film growth mechanisms in heteroepitaxial semiconductor thin films, leading to new knowledge and understanding of these processes, and then to apply these results to the preparation of improved semiconductor thin films and thin-film devices on insulating substrates.

The specific technical objectives of the three-year program are the following:

1. Investigation of the many aspects of the mechanisms of heteroepitaxial film growth, to establish (through accumulation of basic knowledge) sets of technical guidelines for the preparation of better films which can then be applied to real situations.

2. Preparation of improved, high-quality, device-grade heteroepitaxial films of Si and GaAs on insulating substrates by chemical vapor deposition (CVD) methods.

3. Development of methods of characterizing heteroepitaxial films as to their suitability for subsequent device fabrication.

4. Design and fabrication of selected thin-film devices which take advantage of the unique properties of such films.

The general plan for accomplishing these objectives involves as the primary effort the study of the fundamentals of heteroepitaxial semiconductor film growth on insulating substrates, with specialized device fabrication used both as a means of evaluating certain properties of the films (and thus as a measure of film quality as the program progresses) and as a means of exploiting certain unique properties of heteroepitaxial semiconductor-insulator systems. The insight into the question of which fundamental mechanisms, properties, and processes to investigate in these studies comes from extensive background knowledge of epitaxy and its variety of problems of long standing and from the thin-film device difficulties repeatedly demonstrated over a period of several years in our own laboratories and those of others. The problems subjected to study are in no way restricted to those identified a priori; experimental (and theoretical) attention is shifted as needed as the program progresses, in order to achieve the goal of a better understanding of heteroepitaxial process and the resultant improvement in thin-film active semiconductor devices.

2. PROGRAM SCOPE

The program involves both theoretical and experimental investigation of the nucleation and growth mechanisms of heteroepitaxial films in semiconductor-insulator systems, the development of improved techniques for preparation of heteroepitaxial semiconductor films, and the fabrication of some devices utilizing these films, the latter primarily for the purpose of evaluating the heteroepitaxial film materials but also to exploit the special properties of the films.

The theoretical studies consist of two types of activity. First, there is direct interaction with the experimental program involving data analyses, suggestion of definitive experiments, and postulation of specific models to explain experimental observations. Second, there is development of original contributions to the theory of heteroepitaxial growth, the goal of which is the generation of significant advances in fundamental epitaxy theory.

The experimental investigations are also of two types. First, fundamental explorations are carried out to delineate mechanisms and general empirical principles of the heteroepitaxial growth process. Second, practical studies accompany the fundamental investigations so that useful developments can be immediately applied to the improvement of semiconductor films and thin-film devices on insulating substrates.

The work has emphasized the CVD method of growing semiconductor thin films because of its importance in the semiconductor industry. One of the unique aspects of the program is this emphasis on the study of fundamental mechanisms of CVD growth; most previous fundamental studies of epitaxy have concentrated upon physical vapor deposition (PVD) methods, partly because such studies are easier with PVD techniques.

The program emphasis is on films of Si and GaAs and substrates of sapphire ($A\ell_2O_3$) and spinel ($MgA\ell_2O_4$); nonstoichiometric spinel and beryllia (BeO) may also be included as substrate materials as the program progresses. The initial emphasis has been on the Si-on-$A\ell_2O_3$ system, with increasing attention being given to the Si-on-$MgA\ell_2O_4$ and GaAs-on-$A\ell_2O_3$ systems. Si and GaAs have been chosen because of the preeminence of the former in the semiconductory industry and the high-frequency and high-temperature attributes of the latter; in addition, they represent the elemental and compound semiconductors for which most comparative information exists. If further modifications in the semiconductor-insulator systems under study appear advisable as the work develops other materials will be introduced.

The program as described is carried on primarily at facilities of the Electronics Group of North American Rockwell Corporation (NR) by NR personnel. Parts of several of the subtasks (see below) are performed by personnel of the University of California at Los Angeles (UCLA), in the Department of Electrical Sciences and Engineering and in the Chemistry Department. The UCLA work is supported by a subcontract from NR.

3. PROGRAM DESCRIPTION BY SUBTASK

The three-year program was originally divided into nine subtasks - two theoretical and seven experimental (Refs 1, 2). However, at the start of the second year it was decided that, on the basis of the way in which the work of the first twelve months had developed, the contract work would be more accurately described in terms of seven main subtasks - one theoretical and six experimental.

The seven subtasks are as follows:

Subtask 1: Theory of Epitaxy and Heteroepitaxial Interfaces. Theoretical examination of CVD kinetics and the processes of nucleation, surface migration, and film growth with emphasis on crystallographic relationships between overgrowth and substrate to attempt to identify mechanisms and establish general principles of heteroepitaxial growth; theoretical modeling of the heteroepitaxial interface using appropriate potentials to determine surface configurations and interfacial binding energies in real and/or simplified systems.

Subtask 2: Deposition Studies and Film Preparation. Investigation of the effects of various experimental parameters upon the properties of deposited semiconductor films; investigation of the delivery kinetics of CVD processes, to improve the detailed understanding and control of the chemical reactions involved in the preparation of heteroepitaxial semiconductor films by CVD; preparation of films for use in other parts of the program.

Subtask 3: Analysis and Purification of CVD Reactants. Analysis of impurity content of reactant materials used in metalorganic-hydride and other CVD processes; preparation of research-sample quantities of improved-purity reactants for use in film growth experiments.

Subtask 4: Preparation and Characterization of Substrates. Preparation of substrate wafers and characterization of surfaces and impurity content of substrates used for semiconductor heteroepitaxy; development of reproducible new and/or improved substrate polishing, cleaning, and handling methods.

Subtask 5: Studies of in situ Film Growth in the Electron Microscope. In situ observation and study of the early stages of growth in CVD films in the electron microscope, to develop additional fundamental knowledge of the epitaxy process. Results of these experimental observations will be incorporated into the theoretical studies wherever possible.

Subtask 6: Evaluation of Film Properties. Measurement of the electrical, optical, crystallographic, and thermal properties of heteroepitaxial semiconductor films on insulators, by a variety of measurement techniques. Standard techniques will be employed and new methods developed where required for measurement of those film properties which appear best to characterize ultimate device performance.

Subtask 7: Design and Fabrication of Devices. Design and experimental fabrication of certain types of devices, using heteroepitaxial films produced in the above studies. Some devices will be used to evaluate material properties and others to exploit semiconductor film characteristics unique to heteroepitaxial systems.

These subtasks will be modified as needed as the program progresses.

The results obtained during the third six-month period of the contract are discussed, by subtask, in Section II. An outline of the work planned for the next six months is contained in Section III. A program summary is given in Section IV.

An appendix (Appendix A) is included at the end of this report summarizing the work done at UCLA on analysis and purification of CVD reactants (Subtask 3) through July 1971. In addition, Appendix B provides additional entries for the bibliography on *in situ* studies of film nucleation and growth in the electron microscope, first presented in the Second Semiannual Report (Ref 2).

SECTION II

RESULTS AND DISCUSSION

The work of the third six-month period of the contract is discussed in this section. The effort of each of the seven subtasks is described separately. However, because of the interrelationships among some of the subtasks the discussion in several instances necessarily involves activities and results which technically are part of another subtask.

1. SUBTASK 1: THEORY OF EPITAXY AND HETEROEPITAXIAL INTERFACES

Several possible approaches to the theoretical modeling of heteroepitaxial systems have been investigated over the course of the contract. The general criteria adopted for determining suitability of a given technique are that the theoretical treatment and calculation should (1) relate explicitly to heteroepitaxy; (2) be as nearly as possible a "first-principles" approach; (3) relate as closely as possible to an actual system such as $Si/A\ell_2O_3$; and (4) represent an original contribution to the theory of heteroepitaxy.

Attempting to meet these criteria is both difficult and ambitious. The criteria are, nonetheless, useful in that any results obtained in striving to fulfill them should be significant. Based on these criteria, the primary fault of theories and calculations available in the literature is simply that they do not relate sufficiently to actual systems. The emphasis has instead been on simple and unrealistic one- or two-dimensional cubic crystal lattices which cannot be meaningfully applied to practical film-substrate systems such as $Si/A\ell_2O_3$ or $GaAs/A\ell_2O_3$. Applicability to real systems is of paramount importance and is basic to the theoretical approaches which have now evolved from these studies.

Theoretical studies are in progress both at NR and at UCLA (Chemistry Department). Although the two approaches now being used are quite different, the goal is essentially the same in both attempts to model the heteroepitaxial interface. The two studies will be discussed in sequence, beginning with the work at NR.

a. Computer Simulation of Si Film Growth on $A\ell_2O_3$

Before the theoretical efforts of the third six-months of the program at NR are discussed in detail, the previous studies will be briefly summarized in order to give perspective and allow a coherent presentation of the current work. The theoretical investigations at NR began with a critical examination of existing theories of heteroepitaxy for possible application to actual systems such as $Si/A\ell_2O_3$. The classic Frank-Van der Merwe model (Ref 3) was examined first. This model is of considerable significance in that it qualitatively predicts misfit or interfacial dislocations. However, it was concluded that this model could not be generalized to three dimensions and to the $Si/A\ell_2O_3$ system. Similar but less severe criticism was also found applicable to the early models of Reiss (Ref 4) and Bettman (Ref 5) and these models were not pursued further.

The formal theoretical approach of Fletcher and Adamson (Ref 6) was investigated in some detail. In this technique the interfacial energy between film and substrate is

calculated. The theory is variational and in principle allows for general deformations and elastic strain energy. However, it appears that this theory could not, in practice, be implemented for anything other than very simple and unrealistic cases.

The feasibility of performing a Green's function/Wannier-basis calculation of the interfacial one-electron redistribution energy was also investigated, but this led to the conclusion that such a quasi-first-principles approach was not feasible for this work. A less quantum-mechanical and more phenomenological approach--the modeling of the film and substrate by atoms interacting via pairwise two-body potentials--was investigated next. In this approach the total energy of a given static atomic configuration can be obtained by computer summation over all atoms. By allowing some atoms to relax near the surface or interface, a minimum energy configuration can be determined. The major questions in such an approach concern the physical basis and the theoretical foundations for such potentials. Granting these points, the next major hurdle is the actual determination of appropriate potentials for complicated systems such as $Si/A\ell_2O_3$.

Considerable effort was devoted to these questions, and it was determined that such interatomic potentials are open to criticism on a number of theoretical grounds. In addition, for the heteroepitaxial case there is a compounding of practical problems associated with determination of $Si/A\ell_2O_3$ adatom potentials not derivable from bulk crystal properties. In view of these various aspects of potential modeling, work with this approach was temporarily set aside.

The possible application of the LCAO-MO (linear combination of atomic orbital-molecular orbital) technique for interfacial binding energy calculations was investigated next. Since a large number of atoms are involved in the heteroepitaxial case, the simplest such technique - the Extended Hückel Theory (EHT), which is a semiempirical molecular-orbital approach (Ref 7) – was employed. In this approach, the interface, including nearby film and substrate atoms, is treated as an extended molecule and calculations performed for the total energy of the cluster of atoms.

The defect molecule consisting of a cluster of atoms in the solid near the interface is not in free space but is instead in a crystalline environment. Thus, the molecular orbital calculation encompasses conceptual problems not present in ordinary molecular orbital calculations. The major features are clear, however. The boundary between atoms in the defect molecule and in the rest of the crystal is merely a consequence of the model chosen. Thus, it would appear that external constraints imposed on the molecule at its surface must be consistent with the crystalline environment. Some of these questions are rather subtle and had not been either investigated or resolved satisfactorily by the end of the first year of the program.

During the current reporting period theoretical efforts began with a more detailed investigation of the Extended Hückel Theory for the $Si/A\ell_2O_3$ application. Because of the crystalline environment questions of molecular charge distribution and fluctuations, overall charge neutrality, and boundary conditions at the surface of the molecule arise. Treating the interface as an extended molecule has introduced an artifact, the surface of the molecule. The associated dangling bonds or surface states must be saturated or otherwise constrained by boundary conditions.

This study has shown that the Extended Hückel Theory for such a defect crystalline molecule apparently yields spurious charge gradients and fluctuations.

It was originally hoped that these charge fluctuations were due to the boundary conditions at the surface of the molecule and thus subject to useful modification. However, it now appears that the charge fluctuations are fundamental results of the theoretical approach itself.

The charge fluctuations can be substantially reduced or eliminated by a more involved molecular orbital technique, the so-called CNDO (complete neglect of differential overlap) approach. Unfortunately, the attendant increase in labor required is quite large. This circumstance cast some doubt on the feasibility of the molecular orbital technique for the heteroepitaxial interface. The CNDO approach is, however, feasible and proper for a chemisorption calculation (Ref 8). Such a calculation for Si atoms adsorbed on $A\ell_2O_3$ would be of general interest but falls short in terms of the criterion for direct relevance to heteroepitaxy..

In view of these conclusions concerning the feasibility of molecular orbital methods for the heteroepitaxial problem, the interatomic potential approach to heteroepitaxy appeared to be the technique most closely meeting the criteria stated earlier. These efforts have been reinstigated and now constitute the major theoretical effort on this problem at NR. This return to an interatomic potential approach was partially suggested by two major points on heteroepitaxy emerging from the 1971 Thin Films Gordon Research Conference (Ref 9): (1) Computer modeling (Refs 10, 11) with interatomic potentials for simple metals appeared to be regarded as worthwhile and significant for structural types of problems by most scientists in attendance. (2) There is at present no theory of epitaxy which makes it possible to predict the orientation of the overgrowth on the substrate for systems such as $Si/A\ell_2O_3$. The orientational aspects of heteroepitaxy can be treated fairly directly in terms of interatomic potentials.

Thus, the main theoretical effort is now the computer simulation of the growth of a Si film on an $A\ell_2O_3$ substrate using pairwise two-body potentials to model the interaction between atoms. The ultimate goal is to predict the Si overgrowth orientation with respect to the substrate. Such an effort has never before been attempted for actual systems such as $Si/A\ell_2O_3$ and will represent a fundamental contribution to the field when completed.

The modeling of heteroepitaxy with two-body interatomic potentials involves several distinct aspects. The first task is the determination of a set of Morse potentials which will model and simulate the $A\ell_2O_3$ structure. This has not been attempted before and is a formidable task because of the nature of the $A\ell_2O_3$ structure with 10 atoms per unit cell and two species of atoms.

A major requirement, and one which has required considerable effort, is the determination of stability conditions for such a collection of Morse potentials which yield a structure approximating that of $A\ell_2O_3$ and which is stable against transformation to other crystal structures. This is an important requirement if the computed surface and interfacial atomic relaxations are to be at all realistic. This determination turns out to be substantially more complicated for $A\ell_2O_3$ than for the (cubic) simple metals treated in the past by others.

A rigorous determination of stability for a given lattice or chemical phase would involve the calculation of the free energy and comparison of this free energy with that calculated for other crystal structures. This calculation would require solution of the lattice dynamics problem (for $A\ell_2O_3$ this would involve a 30 x 30 dynamical matrix) at

a sufficient number of points on the Brillouin zone to obtain the lattice energy. This is an exceedingly difficult task, with the required labor far exceeding either the value or the inherent accuracy of the result with present-day techniques.

The stability conditions determined for $A\ell_2O_3$ are macroscopic conditions based on the requirement that the strain energy be positive-definite. This places requirements on the elastic constants which in turn place constraints on the Morse interatomic potentials. For simple lattices, this macroscopic stability implies microscopic stability which relates to stability under an inhomogeneous deformation. The NR investigations of stability conditions have related to macroscopic (mechanical) stability, as have all other known lattice modeling efforts which are even remotely applicable.

The $A\ell_2O_3$ lattice, viewed as trigonal, contains 10 atoms per unit cell and can involve internal (unequal) displacements or strains of the various atoms in the unit cell. This internal strain complicates, by about an order of magnitude, the calculation of elastic constants and the strain energy. Therefore, the approximation in which the internal strain is neglected has been adopted as reasonable, in lieu of evidence to the contrary. Macroscopic conditions have been determined under this approximation, with a similar theoretical description being employed for the elastic constants.

This approach is believed adequate for the application, and at the very least is a reasonable first approximation. These stability conditions will later be augmented with numerical calculations of lattice energy and energy derivatives with respect to the various parameters of the lattice (lattice constant, angle and atomic positions) as a check on self consistency.

Computer programming of the lattice energy and elastic constants for the $A\ell_2O_3$ lattice has begun. The energy will be calculated as a function of the various lattice parameters for trial values of Morse potential parameters. Because of the large number of parameters, a straightforward determination is difficult and it is important to incorporate as much physical and empirical data as is possible.

The cohesive energy (the energy of formation) and the elastic constants for $A\ell_2O_3$ are known experimentally. Perhaps the most accurate recent data for the elastic constants is that given by Gieske and Barsch (Ref 12). These authors have noted that $A\ell_2O_3$ is somewhat unusual, compared with other oxides such as MgO, in that the Cauchy relations $C_{12} = C_{66}$ and $C_{23} = C_{44}$ are approximately fulfilled; although $A\ell_2O_3$ is trigonal (rhombohedral), the second-order elastic constant data indicate that deviation from pure hexagonal symmetry ($C_{14} = 0$) is small. ($C_{14} = -2.3 \times 10^{11}$ dyne/cm^2 and is about an order of magnitude smaller than the other elastic constants.) This suggests that the elastic properties of $A\ell_2O_3$ are primarily determined by the hcp oxygen framework. Anderson (Ref 13) had earlier expressed this same point of view - that the oxygen framework is dominant in determining the elastic properties of this oxide.

A number of trial Morse potentials are being tested, starting with first neighbors and working outward. The above discussion suggests that the second-neighbor oxygen-O-O interaction should be considered as equal to or more important than the first neighbor $A\ell$-O interaction, and trial potentials incorporating this concept are being tested. After tentative candidate lattice structures have been determined on the basis of cohesive energy and geometry, the elastic constants and stability conditions will be calculated and tested.

The second major task of modeling heteroepitaxy with two-body interatomic potentials is that of modeling Si with a Morse potential. This work has not yet begun. Swalin (Ref 14) has determined a Morse potential and employed it in Si vacancy calculations some years ago. The present work will start with this empirical potential and modify it as may be required for macroscopic stability

The next task required for the computer simulation of Si growth on $A\ell_2O_3$ is the determination of adatom potentials and will involve treating these interactions essentially as parameters; however, attempts will be made to incorporate the appropriate bond energies, where known approximately from other materials or from chemical reactions.

Following the completion of the above tasks, involving modeling of the Si and $A\ell_2O_3$ lattices, surface atom relaxation and surface reconstruction of $A\ell_2O_3$ will be investigated. The various components of the heteroepitaxial problem will then be combined and the computer simulation of Si growth on $A\ell_2O_3$ will be initiated. These computer growth studies represent the goal of this part of the theoretical subtask; their completion will bring the theoretical work at NR to fruition.

b. Application of Electron-on-Network Technique to Heteroepitaxy

The theoretical studies being carried on simultaneously at UCLA have now evolved into the application of the electron-on-network technique to develop a parameterized theory for the electronic properties of crystal surface states and eventually for the binding of one crystal to another as in heteroepitaxial systems.

The work of the past six months has been directed toward development of a relative theory. The latter term implies that the theory is quasi-empirical in the following sense: If the properties of some standard exposed surface on a crystal are measured, the theory should make it possible to predict the properties of any other surface (interface). In other words, a theory is sought which allows the approximate calculation of surface properties on any surface and which contains, at the most, a few parameters which can be determined through the measurement of properties on a standard surface.

Such theories are well known in the quantum mechanics of molecules. An example is the Hückel theory in which molecular wave functions (molecular orbitals) are approximated by linear combinations of atomic wave functions (orbitals), each centered at a known position of an atom in a molecule. In the Hückel theory, which has achieved considerable practical success in the treatment of conjugated aromatic molecules containing π electrons, there are two parameters which correspond to so-called overlap integrals. These are treated as empirical quantities which are determined, for example, by measuring the properties of one molecule. Thereafter, they are used to predict the properties of other molecules.

An alternative to the Hückel theory is the so-called "free-electron molecular orbital" (FEMO) theory. This method, which was pioneered by Kuhn and Rudenberg (Ref 15), assumes that the π electrons in a molecule are constrained to travel along the bonds (one-dimensional lines) connecting atoms. On these lines, however, the π electrons behave like free electrons in a box. The molecular problem is than reduced to a series of one-dimensional problems which, with proper consideration of boundary conditions and symmetry, allow the development of another parameterized theory (this time the only parameter is the bond length) which agrees very well with experiment. It appears that the FEMO method may also be used for metallic crystals like Na in which there is one valence electron per atom, sufficiently delocalized.

In related studies at UCLA in the past several months the theory has been applied to Na-like crystals of finite dimensions so that the Bloch theorem does not apply. The theory, however, must be modified so that the depth of the potential box within which the electrons move is not infinite, as in the π electron case, but finite and determined by the cohesive energy of the crystal (which becomes another parameter). In this way, the natural development of localized surface states has already been observed, and simple application of point group theory isolates those wave functions which transform under irreducible representations which correspond to various kinds of surface states, e.g., corners and edges.

Recently, Montroll and his coworkers (Ref 16) have extended the FEMO theory so that it is possible to locate potential wells at the site of every atom in the crystal (or in a molecule, for that matter). For infinite crystals in which translational symmetry exists, the Bloch theorem is applicable, and Montroll and coworkers have combined the Bloch theorem with the FEMO theory to develop analytical solutions for the electronic theory of metals. This becomes possible in view of the fact that again the entire problem reduces to a collection of one-dimensional problems. Montroll has also treated defects and surface states in this manner by using a Green's function technique (the Green's functions are involved in the solution of difference equations), which he developed in connection with certain lattice dynamics problems. The Montroll technique by itself is not immediately applicable to the problem of heteroepitaxial interfaces because it assigns to atoms on and near surfaces the same potential well as is assigned to bulk atoms. This technique is being modified (with what amounts to the introduction of still another parameter) so that it will be applicable to the insulating crystals of interest in this program.

There appears to be no reason why the technique cannot be formally extended to a complicated real crystal such as $A\ell_2O_3$ without increased difficulty. The question remains, however, as to how precise a relative theory this method will lead to in the case of $A\ell_2O_3$. It is intended that this question will be answered during the next six months.

When sufficient familiarity with the free surface problem has been acquired, attention will be directed to the ultimate goal of studying heteroepitaxial interfaces. Again, there is no obvious reason why the technique cannot be extended in this manner. The only question that will remain will concern its validity in the sense that a good relative theory will result.

It now appears that a truly first-principles theory of electronic surface and interface properties is far in the future and, in fact, may never be possible. Research aimed at developing a first-principles theory is therefore inappropriate to the practical mission of the contract program. On the other hand, an empirical, parameterized, relative theory seems possible, and it is in this direction that present efforts are aimed.

In recent work based on this rationale, normalized eigenvectors have been developed which can serve as a basis for a secular equation whose solution is fundamental to the total solution. Matrix elements corresponding to surface states can be block diagonalized into local regions of the determinant. Thus far, only free surfaces have been considered. Based on the network model, it is planned to express the properties of surface states on any exposed surface in terms of those conceivably measurable on a standard surface. After this stage of the work is completed the attack on interfaces will be started.

2. SUBTASK 2: DEPOSITION STUDIES AND FILM PREPARATION

During the first year of the program the emphasis in this subtask was placed on determining the effect of experimental growth parameters on the quality of Si epitaxial films grown by the CVD method of pyrolysis of SiH_4 on substrates of various orientations of $A\ell_2O_3$ and $MgA\ell_2O_4$. It was established for the growth system used that autodoping occurs in Si on $A\ell_2O_3$ at temperatures greater than about 1050 C, so a concerted study was made which considered the effects of such factors as growth temperature, growth rate, and nucleation phenomena at or below this temperature (Ref 2).

Much of this work was rendered invalid by a very important effect which had not previously been reported in the technical literature dealing with the properties of heteroepitaxial semiconductor films. It was found that the electrical properties of Si films on insulators with carrier concentrations $<10^{16}cm^{-3}$ are dominated by surface-state conduction. Consequently, further studies were made on n-type films doped to $>10^{16}cm^{-3}$. Simultaneous growth studies on substrates which produced (100) Si and (111) Si below the autodoping temperature revealed the electrical properties of the films to be very dependent on substrate orientation. Although (111) Si growth on $(10\bar{1}4)$ $A\ell_2O_3$ was found to be essentially equivalent electrically to (100) Si growth on $(01\bar{1}2)$ $A\ell_2O_3$ below the autodoping temperature, changing the substrate orientation to near the $(11\bar{2}0)$ $A\ell_2O_3$ plane (not previously used in epitaxy studies) increased the mobility of (111) Si films by about 20 percent for 2 μm-thick films and even more (~50 percent) for 5μm-thick films, for the 10^{16}-$10^{17}cm^{-3}$ carrier concentration range (Ref 2). It is possible that the better match of the thermal expansion coefficients for this $A\ell_2O_3$ orientation and for Si is responsible for the improvement but this has not been established.

Continuing studies during this reporting period have been directed toward the effect of temperature, gaseous atmosphere, growth rate, and annealing steps on Si film properties and are permitting development of optimum conditions for both (100) and (111) Si growth on $A\ell_2O_3$. These studies are also providing comparative data for Si films grown on $MgA\ell_2O_4$, an effort which will be expanded during the second six months of the second year of this program. The current effort is also being directed toward evaluating the effect of substrate misorientation on electrical properties of films; a study of nucleation phenomena as a function of temperature, growth rate, and film and substrate orientation; and a determination of the effect of substrate work damage on film properties. Deposition parameter studies in the GaAs/insulator system, begun toward the end of the first year, have been temporarily postponed to the third year of the program.

The results of the above deposition studies are discussed in the section on Subtask 6.

a. Effects of Reactor Configuration on Film Properties

As part of the study of the effects of various reactor geometries and gas flow patterns on the properties of Si films on $A\ell_2O_3$ substrates, experiments were undertaken late in the report period with a horizontal reactor system of the type commonly used in pilot-line or production facilities and by some other laboratories for the growth of epitaxial Si films. Although the growth rates employed were the same as

those often used in the vertical reactor (~1μm/min), the H_2 carrier-gas flows (~40 lpm) were increased substantially over those used in the vertical system. (The vertical system prevents use of such high flow rates due to the turbulence generated in the gas stream.) The higher flows are used in the horizontal system to minimize the transfer of $A\ell$ impurity from one $A\ell_2O_3$ substrate to those further downstream. The growth temperature was varied from 960 to 1100 C. However, the visual appearance of those films grown at the highest temperatures indicated a deterioration of film quality at temperatures over 1075 C. Only those grown in the range 960 to 1075 C were evaluated electrically. Two different orientations of substrates, the $(01\bar{1}2)$ and near the $(11\bar{2}0)$, were compared at most temperatures.

The electrical data on the resulting films, shown in Figure 1, indicate that the electron mobility increases uniformly with decreasing growth temperature (T_g) for the $(01\bar{1}2)$ $A\ell_2O_3$ orientation, to a maximum of approximately 600 cm^2/V-sec at 960 C. (Carrier concentrations were kept approximately constant at ~2-6x10^{16} cm^{-3}, and film thicknesses were maintained at ~1.0 - 1.4 μm.) For T_g values from 1050 to 1075 C obilities were about 350 cm^2/V-sec. The mobilities of films grown on $(11\bar{2}0)$ $A\ell_2O_3$, on the other hand, showed a maximum of over 600 cm^2/V-sec at T_g ~1050 C with a decrease at both higher and lower growth temperatures. These results are in contrast to the data obtained on films grown in the vertical reactor system and emphasize the hazards of comparing data from different laboratories. It is apparent that the determination of optimum film growth parameters must relate only to the growth apparatus being employed. Ideally, any study designed to produce an optimum heteroepitaxial film must therefore treat the apparatus as an additional growth parameter.

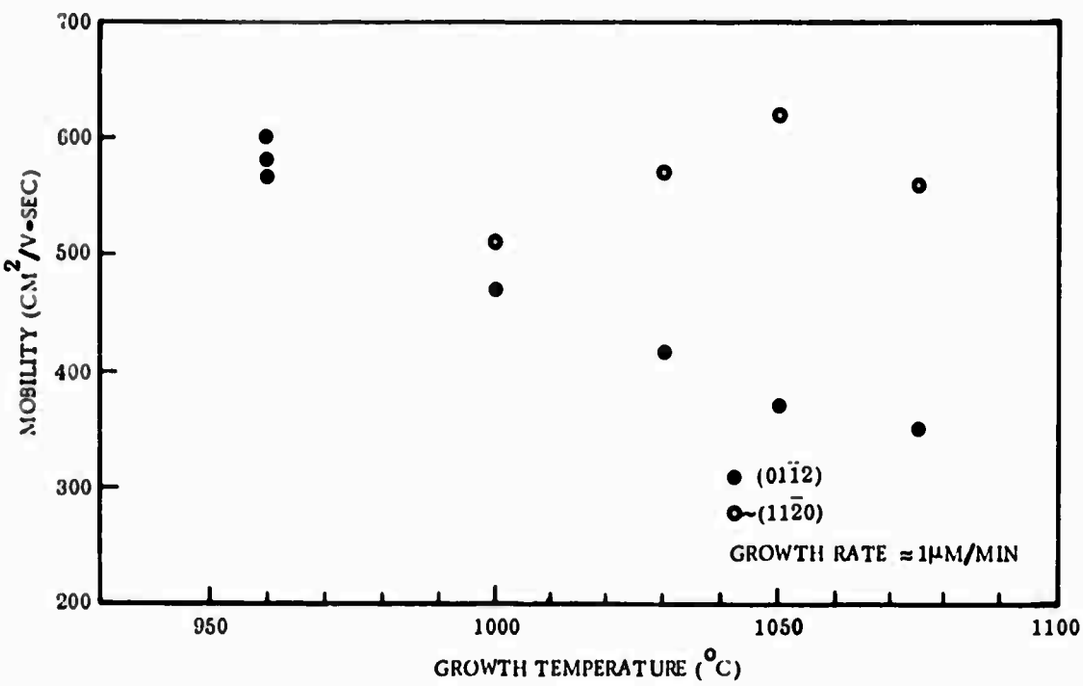

Figure 1. Variation of Hall Mobility with Growth Temperature for N-Type Si/$A\ell_2O_3$ Films Grown in Horizontal Reactor

b. Si Films Grown at Reduced Pressures

In preparation for the in situ CVD experiments in the electron microscope (Subtask 5) a series of experiments was carried out to demonstrate the formation of Si films by the pyrolysis of SiH_4 in H_2 at reduced total pressures in the range of 1 to 10 torr. Initial results at ~1 torr were encouraging, since Si deposits did form, but the first films were polycrystalline. These experiments indicated that further studies should be performed to examine the effect of growth rate, temperature, and other parameters on single-crystal Si growth at reduced pressures.

The full-scale reactor used for Si deposition work at atmospheric pressure was used for these experiments, except that a vacuum system connected directly to the outlet of the reactor chamber was used to evacuate the chamber prior to and during the introduction of the H_2 and/or SiH_4 into the apparatus for film growth. The amount of gas flow was controlled by adjustment of the flowmeter settings obtained by bleeding the gas into a low pressure environment until the flowmeter stabilized. The total pressures were read on a thermocouple gauge, adequate for the scope of the qualitative experiments performed. Except for two cases, the substrates were treated in H_2 for 15 min at 1300 C (or at 1100 C if $MgA\ell_2O_4$ was present) at atmospheric pressure prior to evacuation of the reactor. The H_2 flow was stabilized prior to the start of the SiH_4 flow. AsH_3-in-H_2 was added in some cases to produce n-type films for electrical measurements. In some instances it was added to the SiH_4; in others it was mixed with the H_2 flowing into the reactor. The experiments performed are summarized in Tables 1 and 2.

The evaluation of film crystal structures by reflection electron diffraction (RED) was made at the end of the series of preliminary experiments. The designation "fibrous" is used for patterns which displayed a nonrotating spot pattern when the sample was rotated in the electron beam; single-crystal structure is indicated by "SX," and includes those cases where spot-pattern and Kikucki-line rotation occurred with sample rotation. The term "poly" indicates that continuous rings were observed in the RED pattern, characteristic of polycrystalline structure.

These preliminary experiments revealed a number of interesting facts. They suggested strongly that single-crystal growth of Si could be obtained over a wide range of temperatures when growth conditions are optimized. The growth of a single-crystal film at low pressures and at the lowest temperature arbitrarily chosen for growth (885 C), particularly on ~$(11\bar{2}0)$ $A\ell_2O_3$ which in previous CVD growth experiments at atmospheric pressure had not supported epitaxy at low temperatures, is quite encouraging. In no previous experiment had such a very thin film grown as a single crystal. Since at 1100 C polycrystalline films were obtained in these experiments it suggests that the differences observed in crystalline structure are caused by the increased growth rate and/or temperature.

At medium pressures (see Table 2), single-crystal films were more readily obtained, particularly when an excess of H_2 was present when the SiH_4 was decomposed. The growth rate of Si was influenced by the H_2 concentration; it was decreased considerably when the H_2 pressure in the reactor was low or pure SiH_4 was decomposed. For a given set of SiH_4 and H_2 flowmeter settings (e.g., SiH_4 = 3.0 and H_2 = 7.0 (see Table 2)), the Si growth rate was essentially constant (~0.03-0.05 μm/min) over the temperature range studied (1000 to 1100 C), but when a relatively high concentration of AsH_3-in-H_2 (No. 607 flowmeter) was added, the Si growth rate decreased, a phenomenon previously reported by Farrow and Filby (Ref 17) for As-doped Si growth on Si. A low flow of AsH_3-in-H_2 did not seem to affect the Si growth rate on $A\ell_2O_3$.

Table 1. Properties of Si Films Grown on Al_2O_3 by Pyrolysis of SiH_4 at Low Pressure[a]

Substrate[b]	Growth Temp (°C)	Flowmeter Settings		Deposition Time (Min)	Film Thickness	Growth Rate	Film Crystal Structure[c]	Remarks**
		SiH_4*	H_2					
A	885	1.5	Low (see remarks)	68	250Å	3.7Å/min	Fibrous	T. P. ~400 μm; gold mirror; NHTH.
B	885	1.5		68	n.d.[d]	n.d.	SX[e]	
A	1045	5.0	None	106	0.89 μm	0.009μm/min	Poly over SX	Films gray; SiH_4 introduced into evac. reactor; gauge press. = 280 μm at start, dropped to 80 μm when SiH_4 passed through reactor.
B	1045	5.0	None	106	n.d.	n.d.	Poly	
A	1100	1.5	Low (see remarks)	60	2500Å	42A/min	Poly	T. P. ~400 μm; gold color; NHTH.
B	1100	1.5	Low (see remarks)	60	n.d.	n.d.	Poly	
A	1105	5.0	Low (see remarks)	60	0.66 μm	0.011 μm/min	Poly	Gray films; T. P. ~420 μm
B	1105	5.0	Low (see remarks)	60	0.75 μm	0.012 μm/min	Poly	
A	1105	5.0	Low (see remarks)	60	0.46 μm	0.008μm/min	Poly	T. P. ~800 μm; dropped to ~300 μm when SiH_4 + H_2 added to evac. reactor.
B	1105	5.0	Low (see remarks)	60	n.d.	n.d.	Poly over SX	

[a]Samples grouped together were grown in the same run

[b]A = $(01\bar{1}2)Al_2O_3$; B = $(11\bar{2}0)Al_2O_3$

[c]Determined by reflection electron diffraction

[d]n.d. = not determined

[e]SX = Single crystal

*Reading of pyrex ball in No. 600 (low-flow) flowmeter (Matheson)

**T. P. = Total pressure

NHTH = No high temperature H_2 treatment of surface

Table 2. Properties of Si Films Grown on Al_2O_3 by Pyrolysis of SiH_4 at Medium Pressures[a]

Substrate[b]	Growth Temp (°C)	Flowmeter Settings			Deposition Time (min)	Film Thickness[e] (μm)	Growth Rate (μm/min)	Film Crystal Structure[f]	Remarks
		SiH_4[c]	H_2[d]	AsH_3-in-H_2					
A	1000	3.0	7.0	-	60	2.14	0.036	Fibrous on SX[g]	Grsy film
B	1000	3.0		-	60	n.d.	n.d.	Fibrous and twinned	Gray film
A	1025	3.0	7.0	-	60	2.02	0.034	Fibrous	Gray film
B	1025	3.0	7.0	-	60	2.03	0.034	Fibrous	Gray film
C	1025	3.0	7.0	-	60	n.d.	n.d.	Twinned SX	Gray film
D	1025	3.0	7.0	-	60	n.d.	n.d.	Fibrous	Gray film
A	1030	3.0	7.0	1.0[c] (Added to H_2)	105	3.98	0.037	Fibrous on SX	Mirrored; $\rho = 0.04\ \Omega$-cm
B	1030	3.0	7.0	"	105	3.62	0.035	SX	Grsy:
C	1030	3.0	7.0	"	105	4.07	0.037	Fihrous on SX	Mirrored: $\rho = 0.05\ \Omega$-cm
D	1030	3.0	7.0	"	105	3.72	0.036	Fibrous on SX	Gray:
A	1045	3.0	6.0	1.0[d] (Added to H_2)	60	1.2	0.020	Fibrous on SX	Gray; $\rho = 0.02\ \Omega$-cm
B	1045	3.0	6.0	"	60	0.91	0.015	Fibrous	Mirrored: $\rho = 0.04\ \Omega$-cm
A	1050	3.0	7.0	-	60	2.20	0.036	Fibrous on SX	P-type; gray sheen
B	1050	3.0	7.0	-	60	1.94	0.032	Fibrous on SX	$\rho = 1\ \Omega$-cm; $n_p = 2.1 \times 10^{16}$ cm^{-3}, $\mu = 290$ cm^2/V-sec; grsy reflective
A	1055	3.0	7.0	1.0[c] (Added to H_2)	60	2.86	0.048	Oriented spots	$\rho = 0.17\ \Omega$-cm, as deposited
B	1055	3.0	7.0	"	60	2.44	0.040	SX + Kikuchi lines	$\rho = 0.13\ \Omega$-cm, ss deposited
C	1055	3.0	7.0	"	60	2.47	0.041	SX + Kikuchi lines + spots	$\rho = 0.09\ \Omega$-cm, ss deposited
D	1055	3.0	7.0	"	60	2.83	0.048	Oriented spots	$\rho = 0.10\ \Omega$-cm ss deposited
A	1060	3.0	3.0	3.0[d] (Added to SiH_4)	120	0.5	0.004	Fibrous on SX	$\rho = 0.04\ \Omega$-cm, as deposited
B	1060	3.0	3.0	"	120	0.5	0.004	Poly	$\rho = 0.04\ \Omega$-cm, ss deposited
A	1070	3.0	7.0	-	60	3.2	0.053	Poly	$SiH_4 + H_2$ into evacuated reactor
B	1070	3.0	7.0	-	60	n.d.	n.d.	Poly	
A	1075	3.0	7.0	1.0[c] (Added to SiH_4)	60	2.2	0.037	SX + Kikuchi lines	$\rho = 0.13\ \Omega$-cm; $n_s = 1.5 \times 10^{17}$ cm^{-3}; $\mu = 320$ cm^2/V-sec
C	1075	3.0	7.0	"	60	2.2	0.037	SX + Kikuchi lines	$\rho = 0.12\ \Omega$-cm; $n_a = 9.9 \times 10^{16}$ cm^{-3}; $\mu = 510$ cm^2/V-sec
A	1100	3.0	7.0	-	60	2.3	0.038	SX + Kikuchi lines; twins	Gray
B	1100	3.0	7.0	-	60	2.1	0.035	Fibrous on SX	p-type; reflective $\rho = 0.11\ \Omega$-cm; $n_p = 2.2 \times 10^{17}$ cm^{-3} $\mu = 230$ cm^2/V-sec

[a] Samples grouped together were grown in same run

[b] A = $(01\bar{1}2)$ Al_2O_3; B = ~$(11\bar{2}0)$ Al_2O_3; C = (111) Czochralski $MgAl_2O_4$ (polished by Union Carbide); D = (100) Czochralski $MgAl_2O_4$ (polished by Union Carbide).

[c] Reading of pyrex ball in No. 600 (low-flow) flowmeter (Matheson)

[d] Reading of pyrex ball in No. 607 (high-flow) flowmeter (Matheson)

[e] n.d. = Not determined

[f] Determined by reflection electron diffraction

[g] SX = Single crystal

It was encouraging to obtain reflective single-crystal growth on (111) $MgA\ell_2O_4$ as well as on $(01\bar{1}2)$ $A\ell_2O_3$ and ~$(11\bar{2}0)$ $A\ell_2O_3$. In all cases the (111) Si growths appeared to possess better electrical properties than the (100) Si growths. As indicated in Table 2, a Si film 2μm thick grown on (111)-oriented Czochralski-grown $MgA\ell_2O_4$ at 1075 C exhibited a mobility of ~510 cm^2/V-sec compared with a mobility of 320 cm^2/V-sec measured for (100) Si growth on $(01\bar{1}2)$ $A\ell_2O_3$, for carrier concentrations ~1 x 10^{17} cm^{-3}. The reproducible growth of good quality Si on $MgA\ell_2O_4$ has been elusive at atmospheric pressure, and the results obtained in these preliminary studies suggest that additional experiments using low-pressure growth conditions should be performed. These would probably take place during the third-year of the program, since they represent a relatively new approach to obtaining Si growth on insulators and would require some additions and changes in equipment in order to perform the most significant experimental studies.

c. Si Heteroepitaxy on $A\ell_2O_3$ and $MgA\ell_2O_4$ in He Atmosphere

A preliminary investigation of the growth of Si films on $A\ell_2O_3$ and $MgA\ell_2O_4$ substrates using He as the growth atmosphere and as the carrier gas for both the SiH_4 and the AsH_3 dopant was carried out during this report period. The results obtained in this limited study are summarized in Tables 3 and 4.

Copious quantities of yellow-brown residue deposited on the reactor walls, and the growth rates of Si on the substrates were found to be considerably reduced from those found in H_2 and were strongly dependent upon temperature and total flow rate. Dopant gas flows also had to be increased considerably to obtain equivalent carrier concentrations. For example, Si growth rates in H_2 were ~4-8 times larger than those obtained in a He atmosphere, and n-type films with carrier concentrations ~$10^{16}cm^{-3}$ required ~35 ccpm of nominally 200 ppm AsH_3-in-He flow but only ~0.1 ccpm of 200 ppm AsH_3-in-H_2 flow in a H_2 growth atmosphere.

The most highly reflective films were measured electrically; little difference in properties was found before and after a 1-hr O_2 anneal, presumably due to the minimized outodoping at low growth temperatures. Since many films had carrier concentrations <$16^{16}cm^{-3}$, and hence may exhibit electrical properties strongly influenced by surface-state conduction, it was difficult to draw conclusions from the data. The (111)Si films did appear to posses fewer active donors than (100)Si films. Relatively high mobilities (~500 cm^2/V-sec) were measured in (100)Si films grown over a wide temperature range.

The addition of a small amount of H_2 to the reactor chamber, accomplished by switching from AsH_3-in-He to AsH_3-in-H_2 as the dopant, caused a noticeable change in both the amount of wall deposit and the dopant flow rate required to obtain a given donor concentration (see Table 4). The first effect suggests that Si growth studies of the effect on film properties of controlled additions of H_2 to a He atmosphere are warranted. The second effect could be caused by a lack of stability of AsH_3 in He carrier gas after storage for extended periods of time, thus leading to dopant concentrations far different from the nominal value of 200 ppm. This latter point can be determined experimentally or by chemical analysis. Again because of problems associated with surface conduction, only part of the data in Table 4 lends itself to interpretation. In addition, since it was found after film growth and removal that the $MgA\ell_2O_4$ substrates had very deep surface and subsurface damage, conclusions relative to Si growth on $MgA\ell_2O_4$ based on these experiments would be unjustified. Additional experiments are in progress.

Table 3. Electrical Properties of N-type CVD Si Grown on $A\ell_2O_3$ and $MgA\ell_2O_4$ in He Atmosphere[a]

Nominal Growth Temperature (°C)	Substrate[b]	SiH_4 Flow Rate (ccpm)	Si Growth Rate (μm/min)	Film Thickness (μm)	AsH_3-in-He Flow (ccpm)	Resistivity (ohm-cm)	Carrier Conc (cm^{-3})	Mobility (cm^2/V-sec)	Total Gas Flow (ℓpm)
950	A	25	0.43	2.3	35	0.12	1.3×10^{17}	390	1
	B	25	0.46	2.3	35	0.18	9.1×10^{16}	390	1
	L	25	0.45	2.3	35	0.27	9.4×10^{16}	250	1
1000	A	170	4.0	4.0	35	0.32	3.4×10^{16}	580	1
	B	170	3.5	3.5	35	43	$\sim 6 \times 10^{15}$	25*	1
1030	A	170	2.8	2.8	35	0.50	2.6×10^{16}	490	1
	B	170	2.3	2.3	35	3.3	7.7×10^{15}	240*	1
1035	A	250	1.5	3.0	3	3.3	3.9×10^{15}	490*	6
1040	A	250	1.0	2.0	15	14.0	1.0×10^{16}	410*	3
1040	A	150	1.7	3.4	15	13	9.2×10^{14}	520*	1
1040	A	95	1.0	2.0	35	0.88	1.5×10^{16}	460	1
1060	A	150	1.2	2.5	35	1.7	7.4×10^{15}	490*	1
	B	150	1.3	2.5	35	2.4	4.1×10^{15}	650*	1
	L	150	1.2	2.6	35	55	$\sim 3 \times 10^{15}$	~40*	1

[a]Samples grouped together were grown in the same run

[b]A = $(01\bar{1}2)$ $A\ell_2O_3$; B = $\sim(11\bar{2}0)A\ell_2O_3$; L = (111) Czochralski $MgA\ell_2O_4$ grown and polished by Union Carbide

*Samples with $n<10^{16}$ cm^{-3} appear to be dominated by surface conduction

Table 4. Electrical Properties of N-Type CVD Si Grown at 1025 C on (111) $MgA\ell_2O_4$ and $(01\bar{1}2)$ $A\ell_2O_3$ in He Atmosphere Using 200 ppm AsH_3-in-H_2 as Dopant (Total Flow Rate 6 ℓpm)[a]

Substrate[b]	Growth Rate (μm/min)	Thickness (μm)	AsH_3-in-H_2 Flow (ccpm)	Resistivity (ohm-cm)	Carrier Conc (cm^{-3})	Mobility (cm^2/V-sec)
A	0.28	2.0	0.60	0.21	7.7×10^{16}	390
K	0.23	1.6	0.60	3.9	2.3×10^{16}	69
L	0.23	1.6	0.60	0.88	2.5×10^{16}	290
M	0.27	1.9	0.60	5.1	2.7×10^{16}	46
N	0.29	2.2	0.60	0.62	3.7×10^{16}	270
A	0.26	1.8	0.06	1.1	1.3×10^{16}	430
L	0.23	1.6	0.06	2.2	5.3×10^{15}	530*
M	0.26	1.8	0.06	120.0	$\sim 4 \times 10^{15}$	~15*
N	0.27	1.9	0.06	11.5	4.6×10^{15}	130
A	0.17	1.2	0.06	4.7	6.0×10^{15}	220*
L	0.13	0.9	0.06	7.9	2.7×10^{15}	290*
N	0.14	1.0	0.06	7.5	2.8×10^{15}	300*

[a]Samples grouped together were grown in the same run

[b]A = $(01\bar{1}2)A\ell_2O_3$, K = (111) Czochralski $MgA\ell_2O_4$ from Union Carbide polished at NR; L = (111) Czochralski $MgA\ell_2O_4$ grown and polished by UC; M = (111) Czochralski $MgA\ell_2O_4$ grown and polished by Crystal Technology; N = (111) Czochralski $MgA\ell_2O_4$ grown by Crystal Technology and polished by NR.

* Samples with $n < 10^{16}$ cm^{-3} cm appear to be dominated by surface conduction.

3. SUBTASK 3. ANALYSIS AND PURIFICATION OF CVD REACTANTS

The work of this subtask has been carried out at a much-reduced level of effort during this report period because the UCLA personnel who were involved in the work are no longer available. An interim summary of the work carried out to date in the UCLA Chemistry Department is included in this report in Appendix A.

In addition to the analytical studies performed at UCLA, mass spectrometric techniques have been employed to analyze for trace impurities two samples of SiH_4 and the remaining portion of a trimethylgallium (TMG) sample previously used for GaAs deposition experiments with $A\ell_2O_3$ substrates. The first tank of 100 percent SiH_4 examined was found to contain only a few impurities in the concentration range greater than 2 ppm; disilane was found in a concentration of 9 ppm and trimethylsilane at 23 ppm. The latter impurity is of concern, since the pyrolysis of trimethylsilane could produce silicon carbide. A second tank, which is presently in use for Si growth, was found to be free of trimethylsilane. The impurity analysis revealed 115 ppm of H_2, 195 ppm disilane, 26 ppm $A\ell$, and 1 ppm each of H_2O and hydrocarbons (as butane). The first tank was returned to the vendor (Scientific Gas Products) for replacement, but the new material has not yet been received.

The analysis of the residual gases in the TMG bubbler indicated 25 ppm dimethylchlorogallium, 0.14 mole percent of a material with a mass spectrum peak suggesting it to be hexamethyldigallium, and ~2 ppm of unidentified boron-containing compounds. Further analyses are to be performed to determine the quality of the materials in use during various stages of the continuing experimental studies.

A new 136 gm batch of trimethylgallium (TMG) received from Texas Alkyls was used for epitaxial GaAs growth on $A\ell_2O_3$ with and without H_2S as a dopant. The use test revealed the TMG to be as high in quality as any that had been previously received. A 36.2 μm-thick film on (0001) $A\ell_2O_3$ showed the following properties: resistivity, 8.5 (±20 percent) ohm-cm; carrier concentration, $3.9 \times 10^{14} cm^{-3}$; mobility, 1900 (±20 percent) cm^2/V-sec. An 8.6μm-thick high-resistivity interface layer was found, consistent with the above properties. With this TMG, a 34.1μm-thick S-doped GaAs film was grown with a mobility of 6000 cm^2/V-sec at a measured carrier concentration of $7.4 \times 10^{15} cm^{-3}$.

As has been indicated in the monthly technical and the quarterly management reports for this contract, several alternative arrangements are under consideration for the conduct of the work of this subtask for the balance of the second year of the program. In any event, analyses of the reactants used in the CVD experiments will be continued, primarily (but not exclusively) by mass spectrometric techniques with the assistance of external analytical service laboratories.

4. SUBTASK 4. PREPARATION AND CHARACTERIZATION OF SUBSTRATES

During this six-month period additional effort has been expended on developing reproducible techniques for polishing $A\ell_2O_3$ and $MgA\ell_2O_4$ substrate wafers to provide surfaces for Si and for GaAs heteroepitaxy. Gas-phase etching/polishing techniques first examined during the second six months of the program (Ref 2), have been further developed and exploited as a means of evaluating substrate surface quality. Only a small amount of additional work has been done with liquid-phase etching methods, however.

Routine characterization of substrate surfaces at various stages of preparation for use in heteroepitaxial growth experiments has continued, using techniques of X-ray and electron diffraction analyses, optical and electron microcopy, and (at the end of the report period) charged-particle backscattering measurements.

The planned study of film nucleation behavior and its relationship to resulting film quality and to the type and density of defects in the substrate surface has been delayed to the second half of the year. In addition, it was determined that the absorption and diffusion of surface monolayers of stearic acid, as monitored by total internal reflectance techniques (Ref 2), as an indicator of the surface texture (i.e., microscopic roughness) of $A\ell_2O_3$ and $MgA\ell_2O_4$ does not appear to be a practical technique at this time.*

a. Mechanical Polishing of $A\ell_2O_3$ and $MgA\ell_2O_4$

The polishing techniques used for preparing $A\ell_2O_3$ substrates of various orientations for heteroepitaxy of Si and GaAs have remained largely as described in previous reports (Ref 2). Exceptions are for $(10\bar{1}4)$ $A\ell_2O_3$ and $MgA\ell_2O_4$. In the former instance considerable difficulty has been experienced in the past in developing reproducible polishing procedures which result in sufficiently little subsurface damage. for the substrates to be acceptable for heteroepitaxy use. For the case of $MgA\ell_2O_4$ a previously developed technique has been used in this program with fairly consistent success, although reproducibility and surface quality are not as good as is desired and attempts to improve the procedure are continuing.

During the past six months a much improved technique for polishing $(10\bar{1}4)$ $A\ell_2O_3$ has gradually evolved; excellent surfaces in this orientation are now being obtained. Two groups of such substrates have recently been polished to provide surfaces of epitaxy quality. With both of these groups it was found that each wafer required that

---

* This decision was reached after consultation with Prof. Gary Haller (Yale University), who has developed and utilized the technique on $A\ell_2O_3$ surfaces for other measurements (Ref 18).

the edge be beveled at its point of intersection with each face of the wafer so that no sharp edges remained after mounting to serve as starting points for chipping or more extensive breakage. Earlier observations had indicated repeatedly that this type of edge breakage during lapping and polishing operations was probably responsible for much of the damage produced on the wafer surface. The edge beveling has greatly reduced this problem.

The $A\ell_2O_3$ surfaces of this orientation are typically mounted, after beveling, in groups of four or five on a single holder. The samples are then lapping using three specially designed cast-iron laps in sequence. The laps are charged with slurries of synthetic diamond abrasive of particle sizes 5, 3, and 1μm, respectively. A typical surface of $(10\bar{1}4)$ $A\ell_2O_3$ after the 1μm lapping step is shown in Figure 2. Numerous scratches are readily visible. Following the 1μm step, another specially designed lap (in this case brass) is charged with 0.5μm synthetic diamond abrasive and is used in a last polishing process on the optical polisher, prior to transferring the mounted samples (on the holder) to a vibratory polisher for the final polishing. The surface of a $(10\bar{1}4)$ $A\ell_2O_3$ wafer after the brass-lap polishing step with 0.5μm diamond is shown in Figure 3a.

One of the above groups of $(10\bar{1}4)$ wafers was polished on the vibratory polisher with a nylon cloth providing the polishing surface and the carrier for a slurry of synthetic diamond abrasive of 0.25μm particle size. The second group of samples was also polished on the vibratory polisher with 0.25μm synthetic diamond, but the polishing surface in this instance was a Pellon cloth. The latter cloth appears to give more rapid polishing action than nylon, although the finish obtained appears to be equally good in the two cases. Figure 3b shows the same region of the $A\ell_2O_3$ wafer shown in Figure 3a, but after 66 hr of polishing time on the vibratory polisher with nylon cloth and 0.25μm diamond.

This technique for preparing the $(10\bar{1}4)$ surface of $A\ell_2O_3$ substrates now appears to provide a finish which is acceptable for heteroepitaxial experiments. It has been adopted as the standard mechanical polishing procedure for this orientation.

The procedure used for preparing (111) and (110) $MgA\ell_2O_4$ substrate wafers for Si and GaAs growth is as follows. As-cut $MgA\ell_2O_4$ slices are mounted on appropriate polishing jigs with wax, using standard techniques. The wafers are lapped on a vibratory polisher, first with 12μm and then with 5μm SiC abrasive, to remove surface damage caused by the sawing operation and to provide a smooth flat surface for subsequent processing. The lapped wafers are then pre-polished with a slurry of Linde "A" (0.3μm-particle-size $A\ell_2O_3$) on nylon cloth in the vibratory polisher. Typical time for this step is ~26 hr, with at least two changes of the abrasive slurry required. Observation of the substrate surface following this step, using the Nomarski interference-contrast objective on the microscope, shows that very shallow scratches remain in the surface.

To remove the Linde "A" scratches an additional polishing step using a slurry of Linde "B" (0.05μm-particle-size $A\ell_2O_3$) on nylon cloth is employed, resulting in moderate overall improvement of the surface finish, with much finer scratches still present. Although other polishing cloths have been used in the Linde "B" step, the best results so far have been obtained with nylon.

There is still some indication of possible filling-in of remaining polishing scratches with polishing debris, as has been observed previously with $A\ell_2O_3$ (Ref 2). Further processing of such $MgA\ell_2O_4$ wafers by polishing with Cab-o-Sil (0.05μm SiO_2) abrasive on the vibratory polisher still leaves evidence of fine scratches in the surface. It is not yet certain whether these scratches were previously formed and then filled in with polishing debris or are newly created by the Cab-o-Sil itself. Attempts to clarify this remaining uncertainty are still being made.

Recently, a group of several $MgA\ell_2O_4$ slices was processed as indicated above and then final-polished with a small amount of H_3PO_4 mixed in with the Linde "B" slurry. Preliminary experiments with Si films grown on these substrates appear encouraging, although electrical measurements on the films have not been completed. This chemical-mechanical polishing technique is being further evaluated.

b. Gas-Phase Etching of $A\ell_2O_3$

Gas-phase etching with Freon has been used during this report period for several purposes: (1) as a means for thinning $A\ell_2O_3$ substrates to thicknesses the order of 1 mil; (2) to evaluate the effect of slow but prolonged etching on ~$(11\bar{2}0)$, $(01\bar{1}2)$ and (0001) $A\ell_2O_3$; and (3) to assess the subsurface damage, if any, caused by new and improved polishing procedures, specifically that for $(10\bar{1}4)$ $A\ell_2O_3$. These will be described in turn.

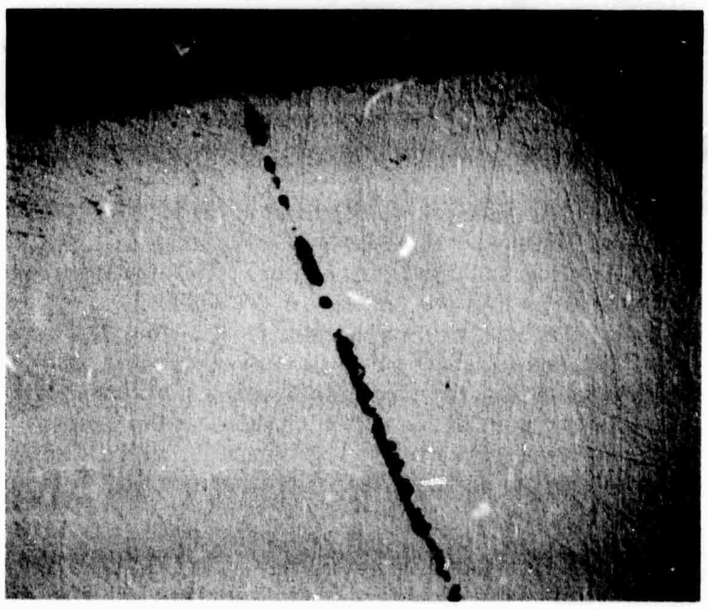

Figure 2. Typical Surface Finish Obtained on $(10\bar{1}4)$ $A\ell_2O_3$ Substrate with Special Cast Iron Laps with Slurry of 1 μm Synthetic Diamond on Optical Polisher. (94X)

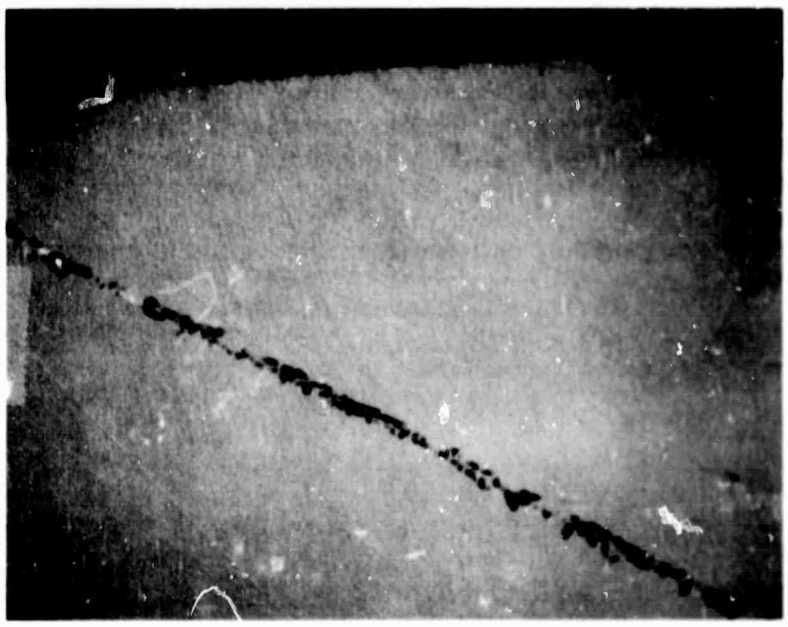

(a)

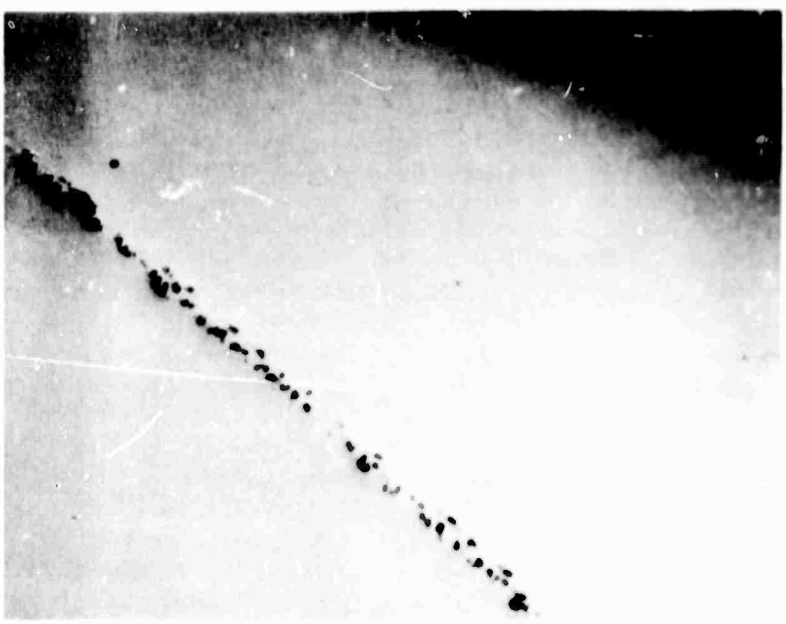

(b)

Figure 3. a. Surface Finish on $(10\bar{1}4)$ $A\ell_2O_3$ Substrate after Using Special Brass Lap with Slurry of 0.5 μm Synthetic Diamond on Optical Polisher. b. Same Area after 66 Hr Polishing on Vibratory Polisher Using 0.25 μm Synthetic Diamond on Nylon Cloth. (94X)

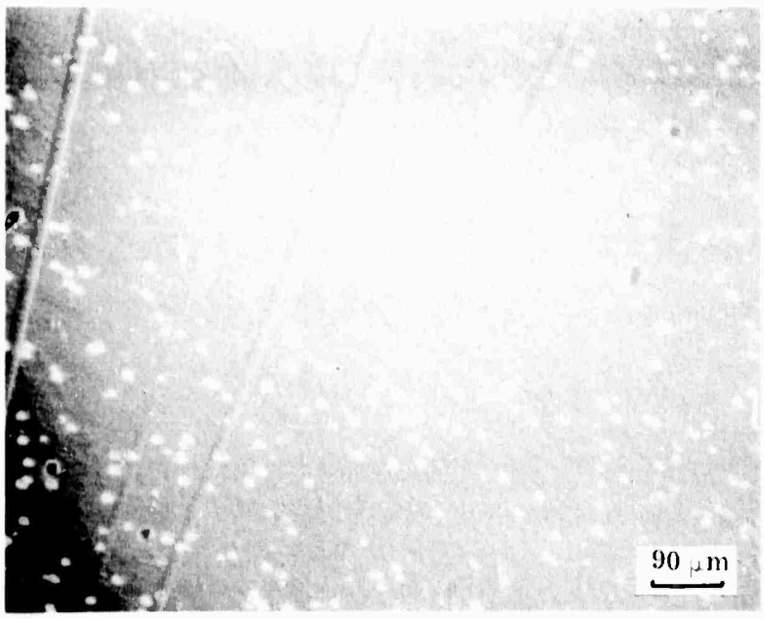

NOT REPRODUCIBLE

Figure 4. Surface Structure of $(10\bar{1}4)$ $A\ell_2O_3$ after Removal ~7 μm of $A\ell_2O_3$ by Freon Etch at 1550 C (Etch Rate ~0.1 μm/min)

(1) $A\ell_2O_3$ Thinning Studies

A $(10\bar{1}4)$-oriented mechanically polished substrate, initially treated with Freon at 1550 C for 60 min at a low etch rate (~0.1μm/min) to remove ~7μm of material, displayed the etch-pit density and scratch structure shown in Figure 4. At 110X magnification, the surface defect density as shown in Figure 4a is quite high, but at 450X magnification (Figure 4b) it can be observed that the space between etch-pits is quite smooth; it can be assumed that these surfaces of low dislocation $A\ell_2O_3$ after Freon etching would be usable for epitaxy. However, in order to use this method as a practical thinning technique, greater etch rates are necessary; etching at a nominal rate of 0.6μm/min for ~3 hr resulted in extreme deepening of the dislocation etch pits and a general severe faceting of the entire surface, as shown in Figure 5. Thus, Freon etching at high rates does not appear satisfactory for thinning and producing smooth surfaces on $(10\bar{1}4)$-oriented $A\ell_2O_3$.

(2) Effects of Prolonged Etching

$A\ell_2O_3$ substrates oriented in the ~$(11\bar{2}0)$, $(01\bar{1}2)$, and (0001) planes were treated with Freon for 25 min periods using those etch-polishing conditions which seem to be less orientation dependent (see data reported in last semiannual report (Ref 2)). The results are depicted in the accompanying photomicrographs, which were obtained with a Nomarski interference contrast attachment on a metallurgical microscope.

Figure 5. The Surface of Verneuil-Grown $(10\bar{1}4)$ $A\ell_2O_3$ after Etching with Freon at 1500 C for ~3 Hr at Nominal Rate of 0.6 μm/min. Several Deep Large Etch Pits (as in Center) were Randomly Distributed on Surface.

Figure 6 shows that gas-phase etching of Czochralski-grown $(01\bar{1}2)$ $A\ell_2O_3$ can produce considerable etching of the crystal planes, but the structure changes in character with etching time with the surface apparently becoming smoother as a stable surface is found by the etching action. Etching of good quality $A\ell_2O_3$ oriented to ~$(11\bar{2}0)$ (Figure 7) seems to reveal only the work damage due to polishing the substrate; however, some areas of the Verneuil-grown substrates did possess a relatively high density of diamond-shaped etch pits (not shown in the figure).

The same set of etch-polish conditions proved to be helpful in preparing smooth surfaces on (0001) $A\ell_2O_3$, shown in Figure 8. After 25 min of etching, scratches were still visible. After 50 min the scratches were essentially gone, and the surface remained smooth after 75 and 100 min of etching. However, a number of hexogonal etch pits are evident; these may be characteristic of the substrate or caused by reaction of impurities in the etchant and etching atmosphere with the substrate. Figure 8c is included to show the sensitivity of the gas-phase etching process to certain types of defect structure present in these substrates cut from Verneuil-grown $A\ell_2O_3$.

(3) Evaluation of Mechanical Polishing Procedures

As indicated in the last semiannual report (Ref 2), the $(10\bar{1}4)$ $A\ell_2O_3$ orientation has been found to be particularly difficult to polish properly for semiconductor epitaxy; subsequent mechanical polishing at NR of vendor-polished material has always brought out greater surface and subsurface damage than had been expected. Light polishing of vendor-polished substrates at NR apparently removes polishing debris which, when packed into the scratches, gives the impression that the surface is of high quality when this is simply not the case.

Such surfaces after a light gas-phase etch show even more indication of the damage introduced during the mechanical polishing, and the technique of using gas-phase etching for such evaluation is being used extensively. Figure 9 represents the surface of a $(10\bar{1}4)$ $A\ell_2O_3$ substrate wafer after being polished in NR laboratories by the method described in the preceding sections. The major defect shown was mechanically introduced to act as a point of reference for examination during the polishing and etching process. Before gas-phase etching but after mechanical polishing the surface was very smooth and displayed essentially no character (Figure 9a), but after 10 min (~0.2μm material removed) and 30 min of etching (~0.6 μm removed) some subsurface damage was revealed (Figures 9b and c). However, the amount of damage was only a small fraction of that found in vendor-polished material, and the data offer evidence that considerable progress has been made in polishing $(10\bar{1}4)$ $A\ell_2O_3$, a significant achievement.

Application of the technique of ion-beam sputter-etching to the polishing of $(10\bar{1}4)$ $A\ell_2O_3$ surfaces is described under Section 5, in the next section.

Figure 6 shows that gas-phase etching of Czochralski-grown $(01\bar{1}2)$ $A\ell_2O_3$ can produce considerable etching of the crystal planes, but the structure changes in character with etching time with the surface apparently becoming smoother as a stable surface is found by the etching action. Etching of good quality $A\ell_2O_3$ oriented to ~$(11\bar{2}0)$ (Figure 7) seems to reveal only the work damage due to polishing the substrate; however, some areas of the Verneuil-grown substrates did possess a relatively high density of diamond-shaped etch pits (not shown in the figure).

The same set of etch-polish conditions proved to be helpful in preparing smooth surfaces on (0001) $A\ell_2O_3$, shown in Figure 8. After 25 min of etching, scratches were still visible. After 50 min the scratches were essentially gone, and the surface remained smooth after 75 and 100 min of etching. However, a number of hexogonal etch pits are evident; these may be characteristic of the substrate or caused by reaction of impurities in the etchant and etching atmosphere with the substrate. Figure 8c is included to show the sensitivity of the gas-phase etching process to certain types of defect structure present in these substrates cut from Verneuil-grown $A\ell_2O_3$.

(3) Evaluation of Mechanical Polishing Procedures

As indicated in the last semiannual report (Ref 2), the $(10\bar{1}4)$ $A\ell_2O_3$ orientation has been found to be particularly difficult to polish properly for semiconductor epitaxy; subsequent mechanical polishing at NR of vendor-polished material has always brought out greater surface and subsurface damage than had been expected. Light polishing of vendor-polished substrates at NR apparently removes polishing debris which, when packed into the scratches, gives the impression that the surface is of high quality when this is simply not the case.

Such surfaces after a light gas-phase etch show even more indication of the damage introduced during the mechanical polishing, and the technique of using gas-phase etching for such evaluation is being used extensively. Figure 9 represents the surface of a $(10\bar{1}4)$ $A\ell_2O_3$ substrate wafer after being polished in NR laboratories by the method described in the preceding sections. The major defect shown was mechanically introduced to act as a point of reference for examination during the polishing and etching process. Before gas-phase etching but after mechanical polishing the surface was very smooth and displayed essentially no character (Figure 9a), but after 10 min (~0.2μm material removed) and 30 min of etching (~0.6 μm removed) some subsurface damage was revealed (Figures 9b and c). However, the amount of damage was only a small fraction of that found in vendor-polished material, and the data offer evidence that considerable progress has been made in polishing $(10\bar{1}4)$ $A\ell_2O_3$, a significant achievement.

Application of the technique of ion-beam sputter-etching to the polishing of $(10\bar{1}4)$ $A\ell_2O_3$ surfaces is described under Section 5, in the next section.

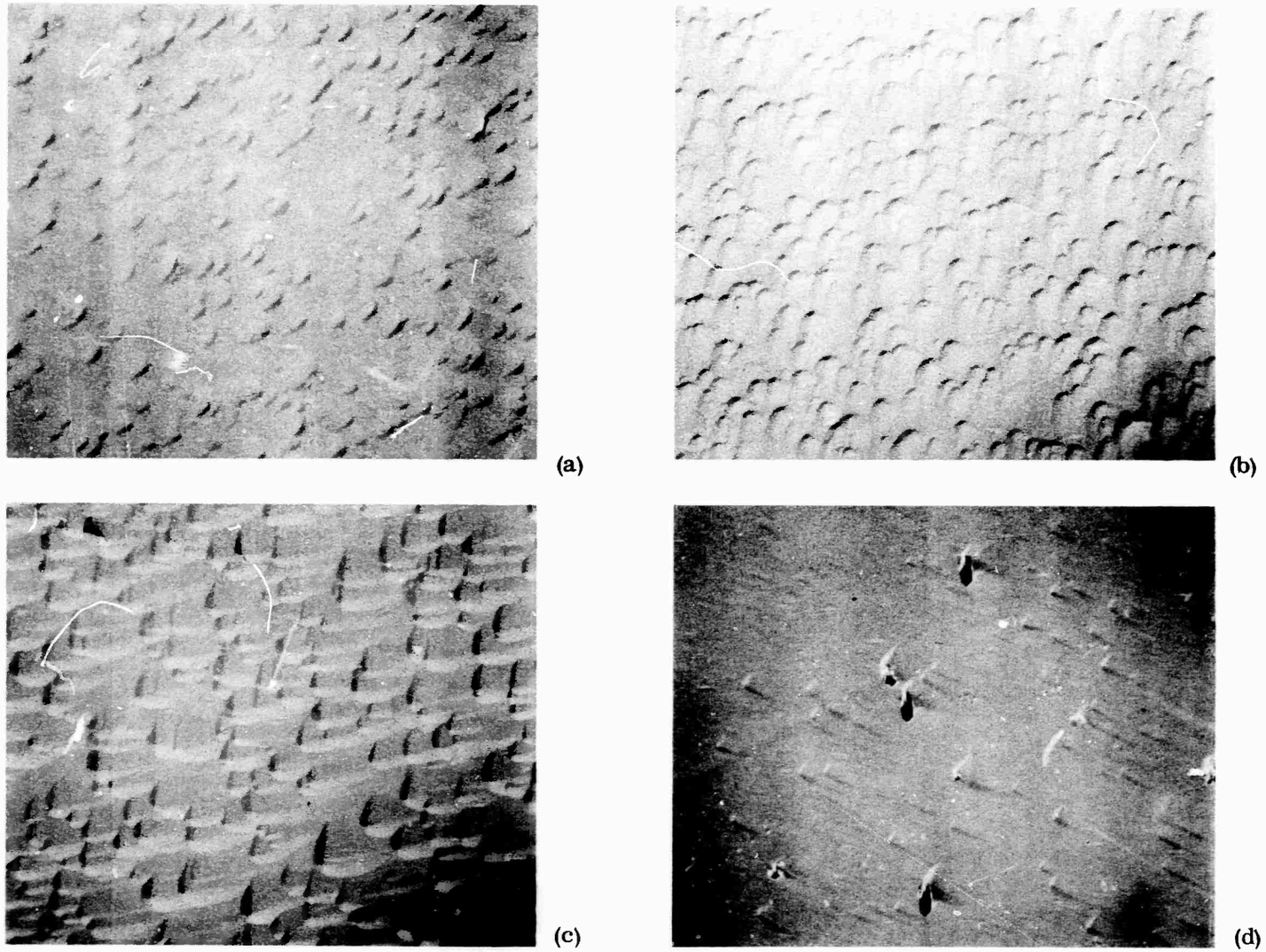

Figure 6. The Surface of Czochralski-Grown $(01\bar{1}2)$ $A\ell_2O_3$ after Etching at 1500C with Freon at a Flow Rate of 13 ccpm for (a) 25 min, (b) 50 min, (c) 75 min, and (d) 100 min. (All 110X)

NOT REPRODUCIBLE

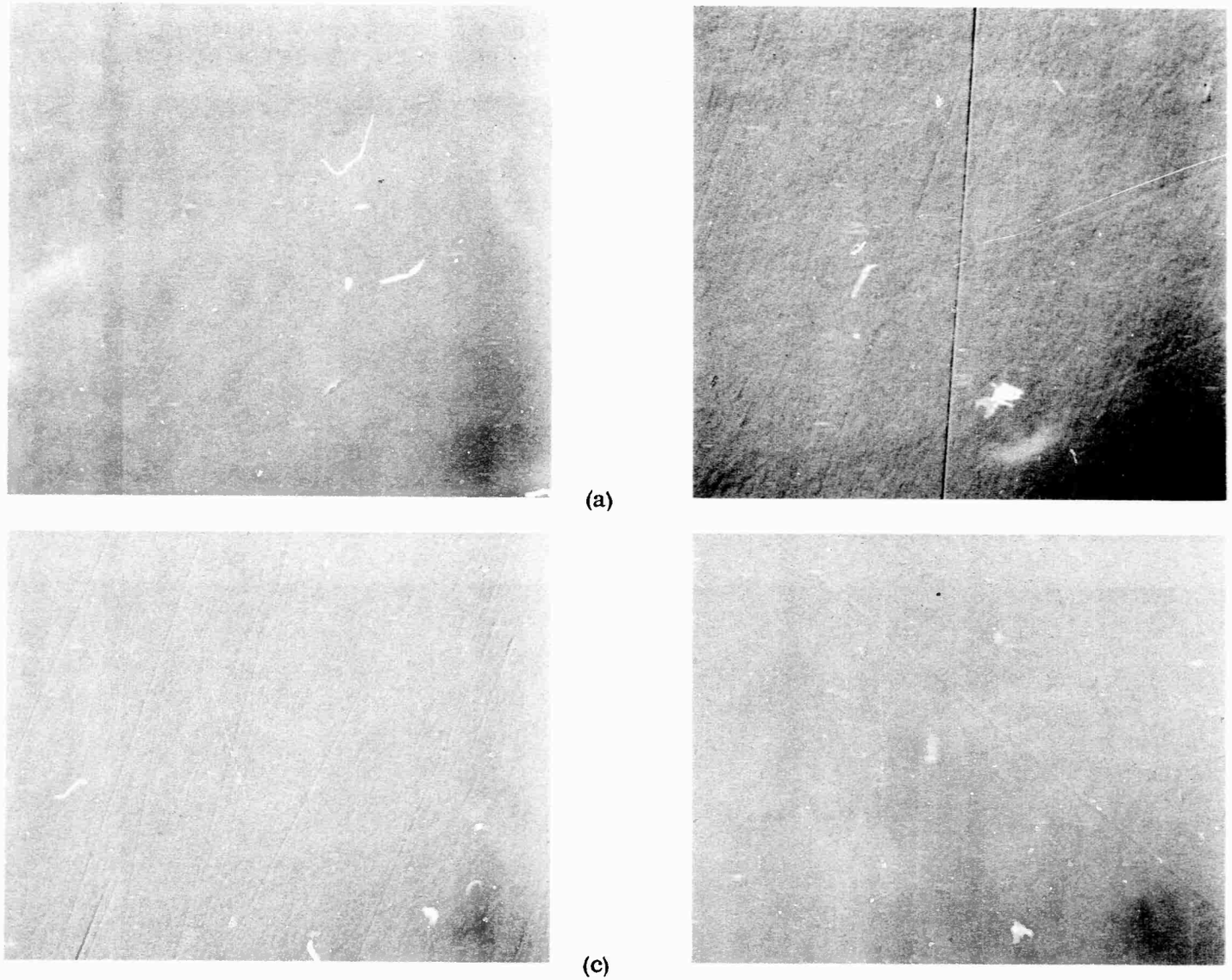

Figure 7. The Surface of Different Substrates of Verneuil-Grown ~$(11\bar{2}0)$ $A\ell_2O_3$ after Etching at 1500C with Freon at a Flow Rate of 13 ccpm for (a) 25 min, (b) 50 min, (c) 75 min, and (d) 100 min.

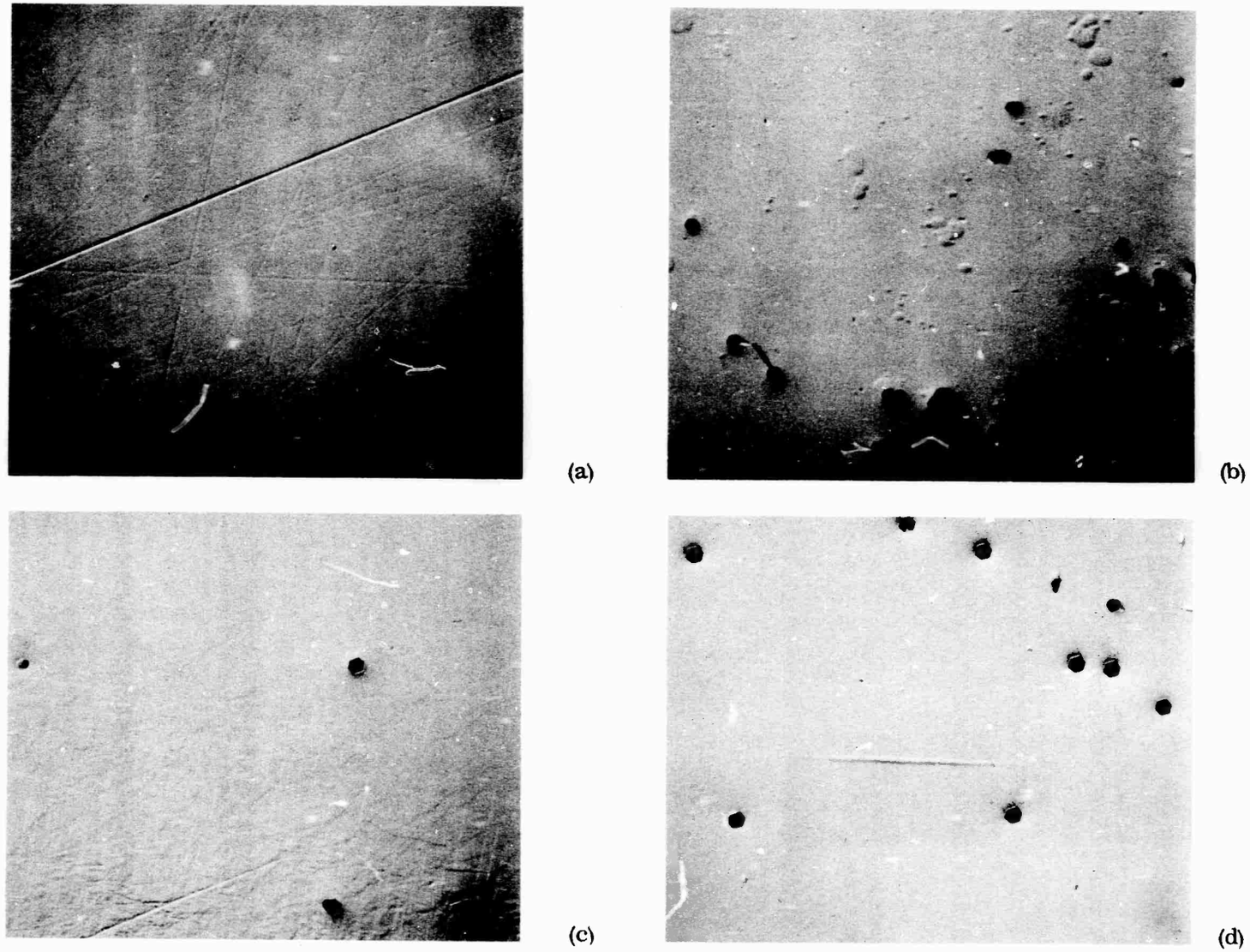

Figure 8. The Surface of (0001) $A\ell_2O_3$ after Etching at 1500C with Freon at a Flow Rate of 13 ccpm for (a) 25 min, (b) 50 min, (c) 75 min, and (d) 100 min

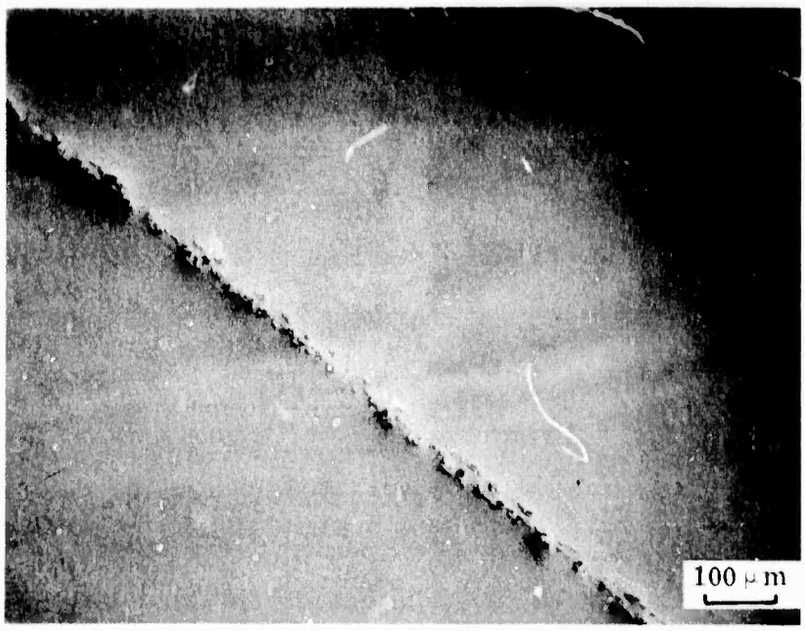

(a)

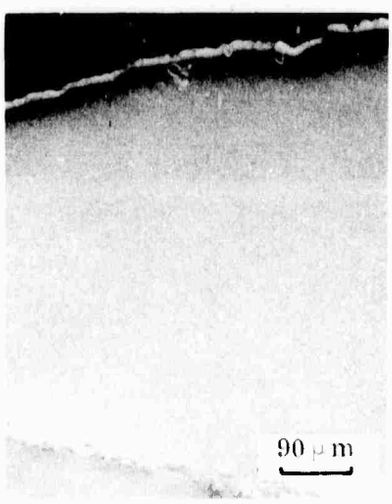

(b)

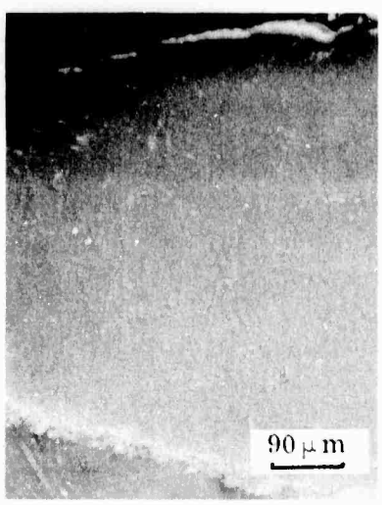

(c)

Figure 9. Surface of $(10\bar{1}4)$ $A\ell_2O_3$ (a) after Mechanical Polishing in the NR Laboratory: (b) after a 10 min Etch with Freon at 1400C; (c) after a 30 min Etch with Freon at 1400C (~0.6μm removed.)

5. SUBTASK 5: STUDIES OF IN SITU FILM GROWTH IN THE ELECTRON MICROSCOPE

Work has continued on the electron microscope modifications required for the in situ film growth studies. The auxiliary pumping system has been fabricated, installed, and tested. The CVD microchamber design has been completed, and fabrication is proceeding. The electron microscope itself has been improved, particularly with respect to the contamination rate and the operating pressure. Several physical vapor deposition (PVD) experiments have been completed, demonstrating the feasibility of performing in situ nucleation and growth studies in this equipment. The objective of performing the first in situ Si CVD experiment remains scheduled for the end of the second year, with preliminary experiments with simpler chemical processes to be initiated soon. Finally, in preparation for the CVD in situ experiments, which will require very thin (≤200Å) $A\ell_2O_3$ substrates to permit transmission of the electron beam, work has begun on evaluation of several alternative methods for thinning $A\ell_2O_3$ wafers.

A number of technical articles peripherally related to the present work are listed in Appendix B as addenda to the bibliography presented in the Second Semi-annual Report (Ref 2). In common with those previously reported, few are of direct value to these studies but they are collectively valuable for their experimental ideas and techniques.

a. Auxiliary Pumping System

The auxiliary pumping system for the specimen chamber* has been fabricated, installed, and tested. A general view of the EM6 electron microscope, showing the location at the auxiliary pumping system, is shown in Figure 10. The pumping system itself consists of a diffusion pump, liquid nitrogen trap, and isolation valve, and is shown in greater detail in the photograph of Figure 11. The system is connected to the specimen chamber through a vacuum tee and a special flexible metal bellows and adapter, visible near the center of Figure 11. An ionization gauge is mounted on the other side of the tee to record the pressure near the sample chamber. The present design has maintained the specimen airlock-exchange mechanism, so the microscope can also be used for routine electron microscopy with no time loss.

A second ionization gauge has been installed on a specially machined flange which temporarily replaces the right hand side of the specimen-exchange air lock. The base pressure of the system is $<1 \times 10^{-7}$ torr, but the best pressure to date has been 2×10^{-6} torr, limited by the poor quality of the O-ring sealing surfaces and the organic vapors present as contamination in the microscope. Installation (in the coming six months) of the pumping apertures** and associated shields in the beam deflector stage and objective lens (respectively above and below the specimen chamber) will permit true differential pumping of this portion of the microscope.

---

*The term specimen chamber refers to that portion of the electron microscope column containing the specimen holder (or CVD microchamber when installed), the specimen holder exchange and airlock mechanism, and the specimen holder stage with its associated control mechanisms for specimen rotation, tilt and translation.

**These pumping apertures should not be confused with the gas limiting apertures in in the CVD microchamber shown in Figure 13.

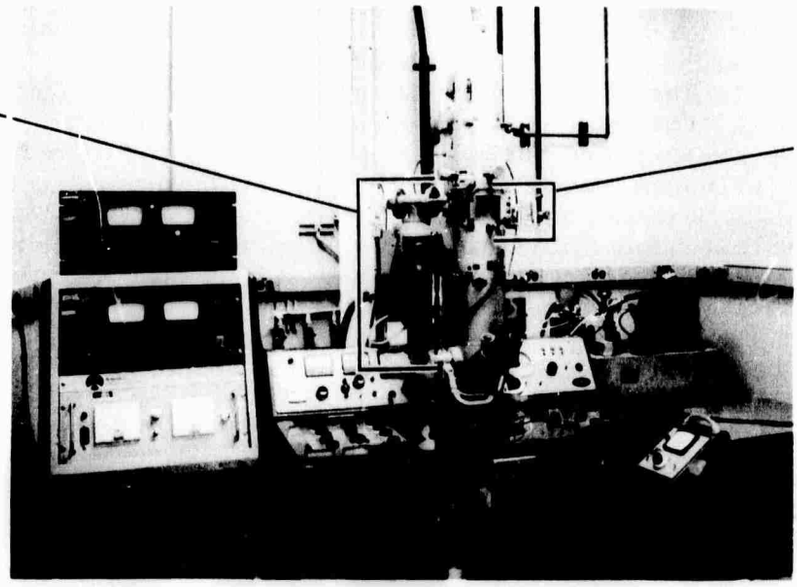

Figure 10. Overall View of EM6 Electron Microscope as Modified for *in situ* Film Growth

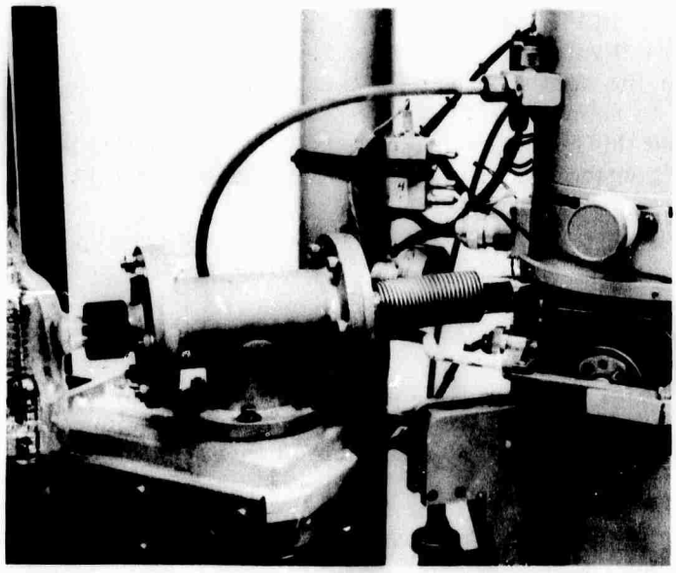

Figure 11. Close-Up View of Auxiliary Pumping System Attachment for EM6 Electron Microscope

b. CVD Microchamber

The design for the first CVD microchamber for the electron microscope has been completed. The present PVD specimen heater, although suitable for the PVD experiments, cannot be modified for use as a CVD microchamber. Instead, a standard specimen holder (Figure 12) will be modified as shown in the diagram of Figure 13.

The substrate will be heated by passing a current through a high-resistance tungsten grid (wavy line). The sides of the grid are insulated from the body of the specimen holder and bottom plate (+ and - electrodes, respectively) by two $A\ell_2O_3$ half rings, shown finely cross-hatched. Two apertures, provided to permit passage of the electron beam but reduce the gas outflow, are welded to the specimen holder body and bottom plate. A gas-tight seal is made possible at S by precision lapping of the $A\ell_2O_3$ insulator, shown cross-hatched. A gas inlet and outlet are installed as shown.

The design shown has the advantage of heating only a small area near the substrate specimen, but it will require close machining tolerances to allow minimum gas leakage and simultaneously to maintain the proper distance between the focusing and reference planes. The construction of the specimen microchamber is the most difficult project anticipated in this subtask so sufficient allowance has been made in the program plans for construction of a second design, if required.

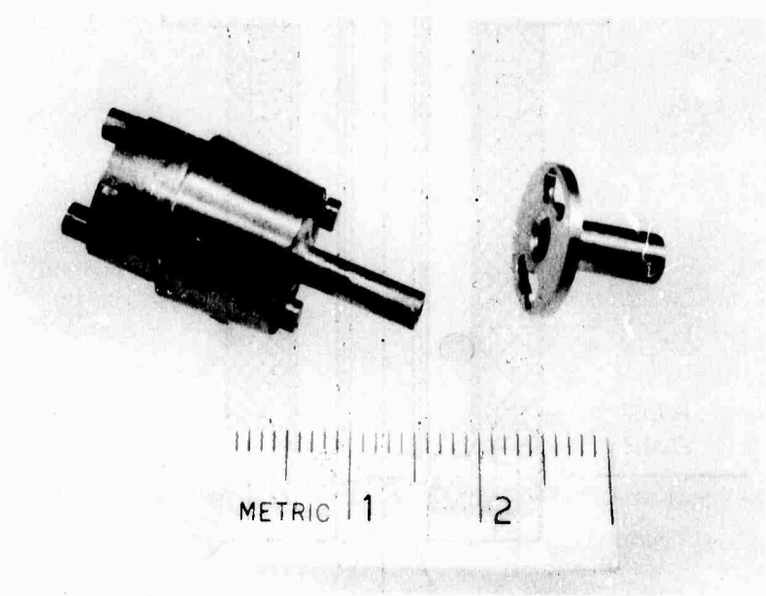

Figure 12. Electron Microscope Sample Holder

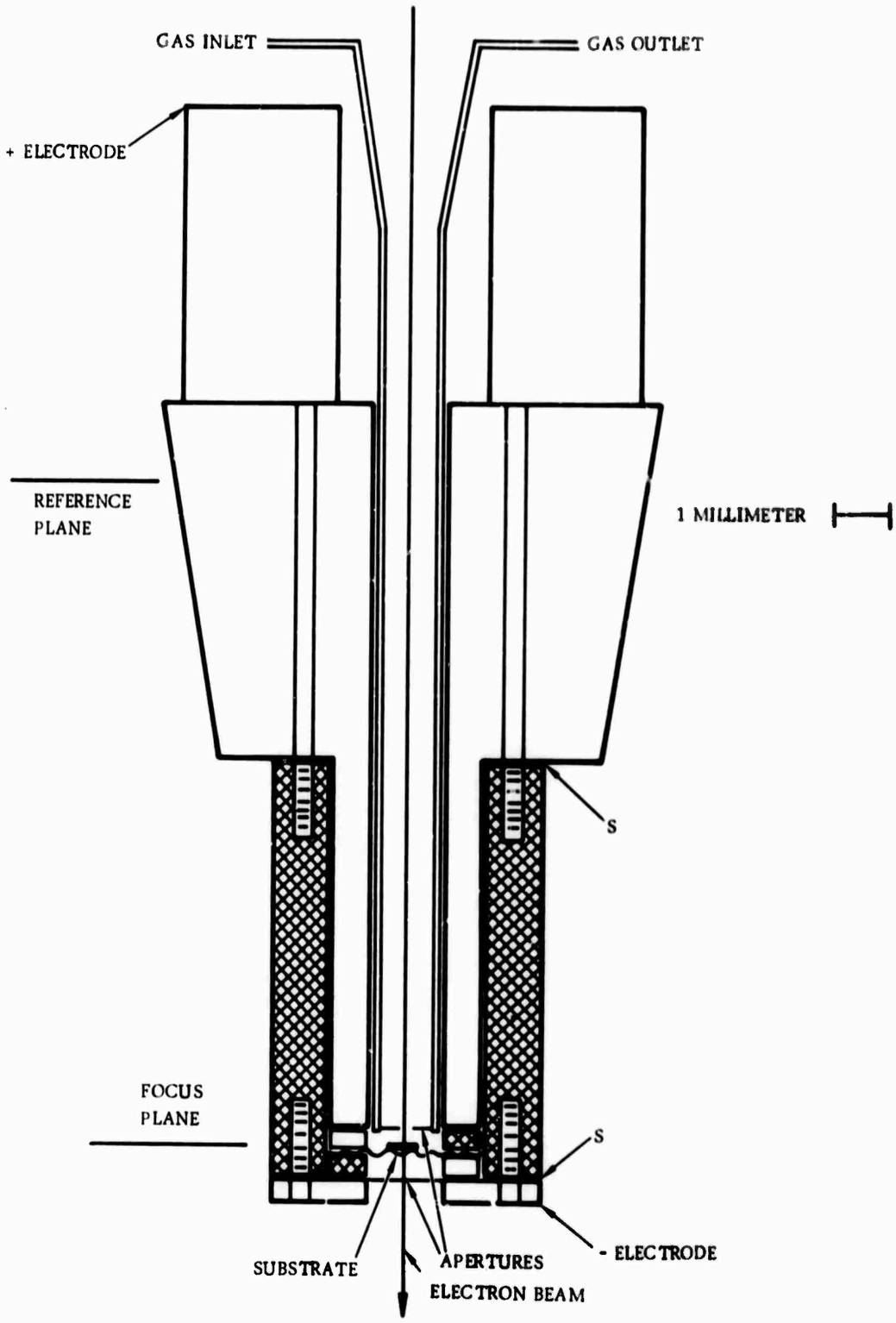

Figure 13. CVD Microchamber

c. Microscope Contamination Rate

Considerable effort has been expended in improving the vacuum performance of the basic electron microscope. Improvements have been made primarily by improving the polished finish on the O-ring sealing surfaces and by cleaning well the interior of the microscope. Approximately half of the 150 O-ring grooves in the microscope have been carefully inspected; the vast majority of these were adequate only for the normal operating vacuum of $\sim 5 \times 10^{-5}$ torr. Accordingly, the O-ring grooves in the high-vacuum valve, pumping manifold, and electron-gun region were polished to better than a 16-μin. finish. These portions of the microscope were thoroughly cleaned to remove traces of vacuum pump oil which had been condensed prior to installation of the thermoelectrically-cooled baffle.

The contamination rate measured after this cleaning and polishing, and using only the standard microscope pumping system, was less than 100 Å/min, which may be compared with the 240 Å/min reported in the Second Semiannual Report (Ref 2). Further improvement is anticipated as the O-ring grooves in the electron lenses and specimen chamber are polished and these regions similarly cleaned. This is planned for the time of CVD microchamber installation or at the yearly colum disassembly, whichever occurs first.

d. In situ PVD Experiments

Several in situ physical vapor deposition (PVD) nucleation and growth experiments have now been performed in the microscope. Vacuum-evaporated Aℓ has been deposited onto a carbon substrate heated to $\sim$300 C in these investigations. The experiments were sufficient to demonstrate the feasibility of in-situ film growth observations, but minor operational difficulties have repeatedly prevented recording the growth process on motion picture film.

The series of PVD experiments has twice been interrupted when the high-voltage cable on the electron microscope failed. Considerable microscope down-time has resulted from these incidents. The first demonstration motion pictures of film nucleation and growth, scheduled for completion in January, will now be completed in March. However, there has been very little net loss to the overall subtask timeline because effort was transferred to other required projects of the subtask.

A sequence of electron micrographs taken in one of the preliminary PVD experiments is shown in Figure 14. Each micrograph is at the same magnification, with the bar representing a 1μm length. Despite the poor photographic definition, the micrographs were made during in situ deposition of Aℓ at times of 30, 60, and 210 sec after deposition had begun. Nucleation proceeded in a manner similar to that for other metal films: Aℓ atoms arriving singly from the vapor phase strike the C-film substrate and then diffuse about the surface until a number agglomerate to form small nuclei. Each three-dimensional nucleus grows by the atom-by-atom arrival of Aℓ, eventually coalescing with other nuclei to form larger nuclei. The coalescence process continues until a continuous thin film is formed (not shown).

Comparison of the same areas in Figures 14 a and b show the increased size of nuclei after growth has continued an additional 30 sec. In several locations, marked with arrows, two nuclei seen in Figure 14a have coalesced into a single nucleus in Figure 14b. The mechanism presumably involves surface diffusion of individual

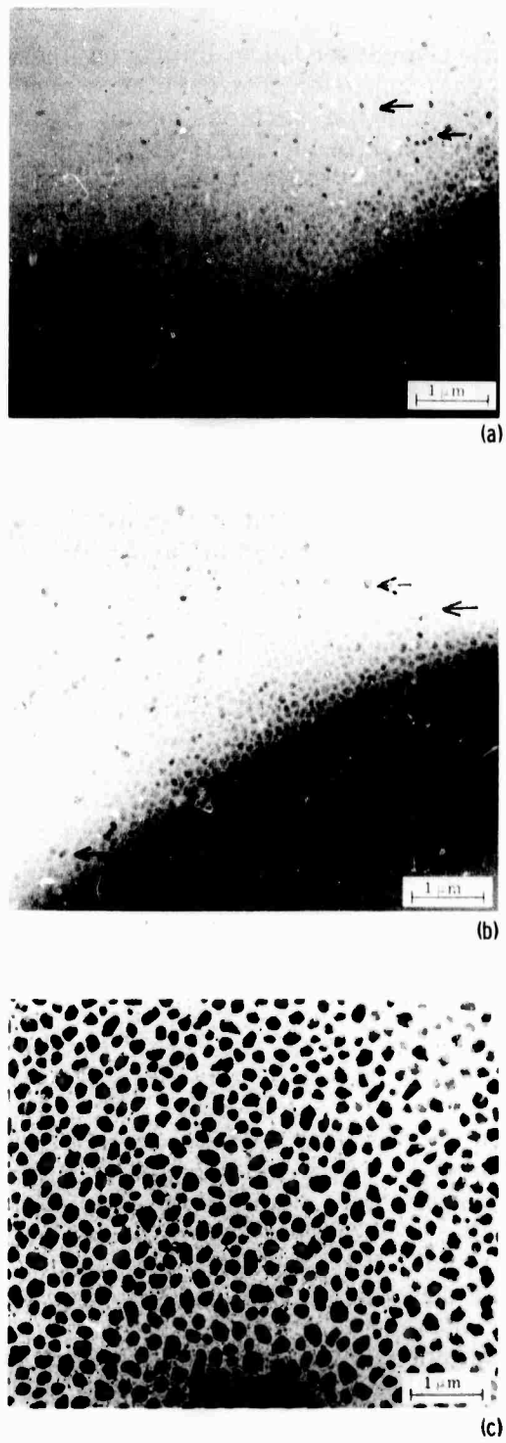

Figure 14. Nuclei of Aℓ during In-Situ PVD Growth after (a) 30 sec, (b) 60 sec, and (c) 210 sec of Deposition

atoms of the two nuclei, with the driving force being the reduction in total surface energy. As discussed by Pashley (Ref 19), movement of the two nuclei as a whole is unlikely.

Figure 14c, although not of the identical area, is representative of the growth after 210 sec of deposition, at which time deposition was terminated. The nuclei are larger, and the internal defect structure resulting from coalescence of several nuclei into one is now apparent. In addition, the phenomenon of secondary nucleation is visible. Areas of substrate left bare by the coalescence of two nuclei have served as nucleation points for secondary nuclei formed from the continually arriving stream of $A\ell$ atoms from the vapor.

Additional experiments of this type are in progress as an important preliminary step to undertaking the first simplified in situ CVD experiments.

e. Preparation of Thinned $A\ell_2O_3$ Substrates

Efforts have begun to prepare the thin (≤200 Å) $A\ell_2O_3$ wafers required as substrates for the in situ film growth studies. Various mechanical lapping techniques using a vibratory polisher and 400 to 1000-grit boron carbide were unsuccessful in reducing $(10\bar{1}4)$-oriented samples to less than 0.008 in. before cracking. An alternate technique using a standard optical polishing machine has yielded crack-free samples ~0.003 in. thick. These samples were then cut into small discs, and will be thinned by the ion-beam method to the required 200 Å.

Special apparatus for controlled ion-beam sputter-etching has been acquired late in the present reporting period and is now fully operational. With this apparatus, $A\ell_2O_3$ wafers originally 0.002 to 0.003 in. thick can be thinned to a few hundred Å in thickness by sputtering effects from two beams of 5 to 10 KV argon ions directed at a 5 to 15 deg angle to the substrate surface. The sample is normally rotated about an axis perpendicular to its surface during the sputtering process. The thinning is uniform over an area of ~0.2 in.^{2} and proceeds at a slow but controllable rate, typically 0.1 to 1.0 μm/hr.

As an initial instrument performance test, the equipment was used to ion-etch the surface of a mechanically polished $(10\bar{1}4)$-oriented $A\ell_2O_3$ wafer. Evidence of scratches originally present on the polished surface remained after removing more than 9 μm of material. The results after successive removal of a total of <0.1, 2.7, 7, and 9.6 μm of $A\ell_2O_3$ are shown in Figure 15. In all of the photomicrographs the irregular line at the extreme top right is the edge of the sample; the area immediately next to it was untouched by the ion beam during the etching process and represents the original condition of the $A\ell_2O_3$ surface. Only the area in the lower left portion of each photomicrograph represents the region of the crystal which had been fully etched by the ion beam; the remaining intermediate areas were only partially etched.

Comparison of the etched and unetched regions of the sample as shown in Figure 15a reveals that the light ion-etching (<0.1 μm) enhanced the visibility of the original scratches. This effect, previously noted with Freon etching (see Subtask 2), is attributed to the removal of polishing debris which had filled-in the scratches. Further ion-etching, sufficient to remove 2.7 and 7 μm as shown in Figures 15b and c, respectively, began to produce a smoother surface, although the original scratches remain clearly visible.

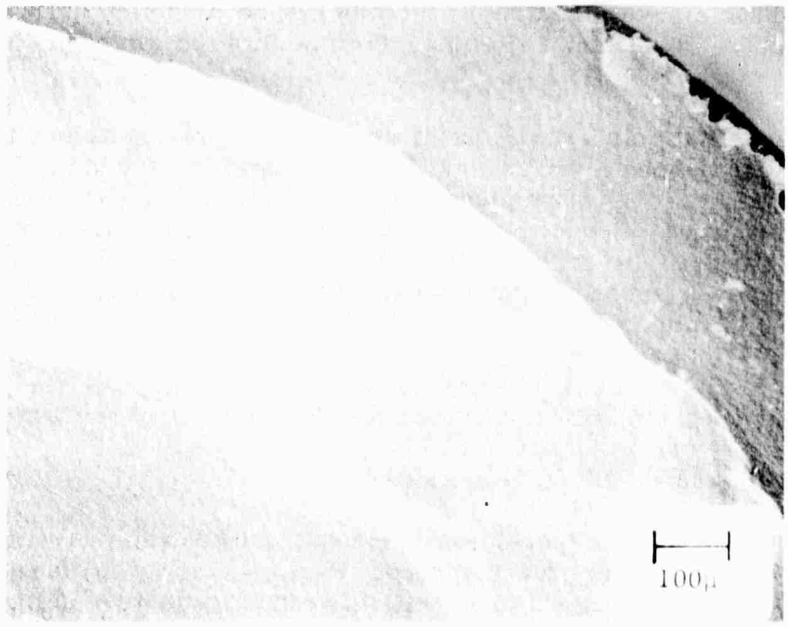

(a)

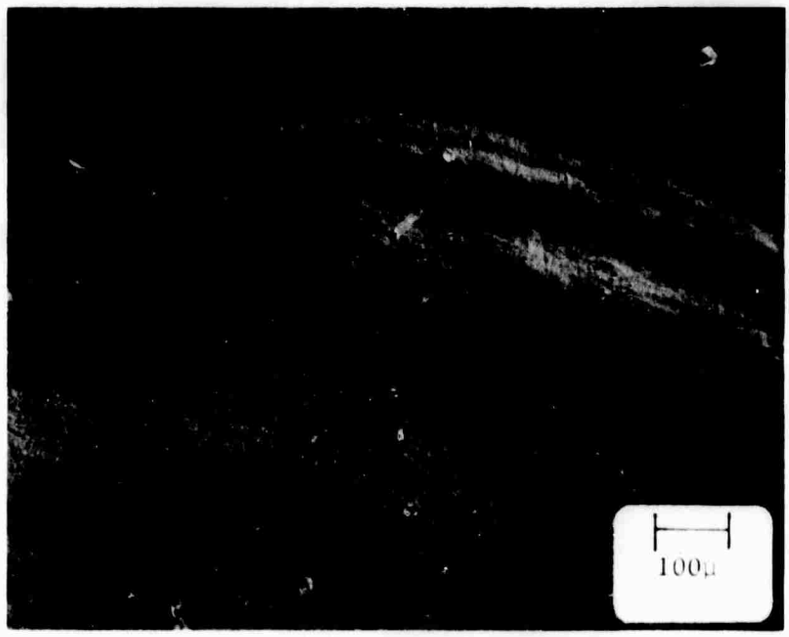

(b)

Figure 15. $(10\bar{1}4)$ $A\ell_2O_3$ Wafer Ion-Beam Etched at Low Angle to Remove (a) <0.1 μm. (b) 2.7 μm

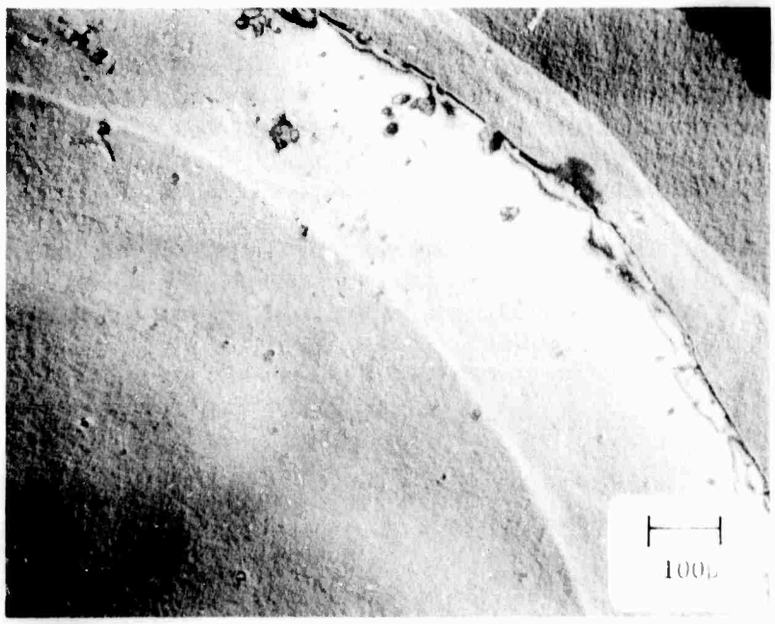

(c)

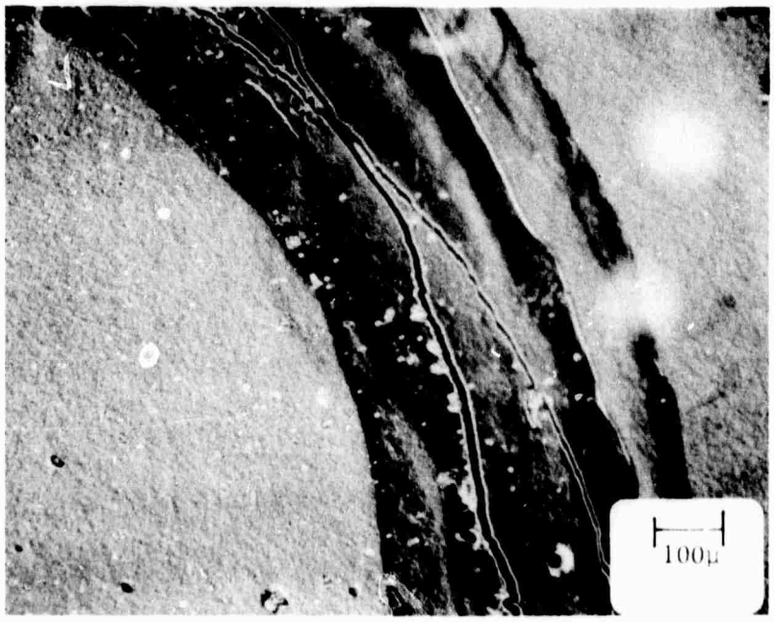

(d)

Figure 15. $(10\bar{1}4)$ $A\ell_2O_3$ Wafer Ion-Beam Etched at Low Angle to Remove (c) 7 μm; (d) 9.6 μm

After removal of 9.6 μm of $A\ell_2O_3$ (Figure 15d) the surface appears significantly improved, yet traces of the original scratches are still present. Although the scratches themselves were not 9.6 μm deep prior to the start of the ion-etching process, it does appear that the damaged regions below the scratches may have extended at least this deep into the original polished crystal surface, causing a preferential etching effect until the damaged regions are completely removed.

This initial experiment suggests the possibility of producing smooth substrate surfaces by ion-etching large crystals, then subsequently depositing Si by CVD in the normal manner. Since the ion-etching is both a polishing and a cleaning process, it is anticipated that it may be possible to grow a higher quality Si film on such a treated substrate. Experiments to evaluate this prospect are presently in progress.

6. SUBTASK 6: EVALUATION OF FILM PROPERTIES

Evaluation of the structural and electrical properties of thin heteroepitaxial films on $A\ell_2O_3$ and $MgA\ell_2O_4$ substrates continued during the past six months; results of these studies are described in this section as well as in Section II-2.

The measurements of photoemission of electrons from heteroepitaxial semiconductor films and transport of electrons in $A\ell_2O_3$ have been carried further and are discussed below. Further use of channeling and Rutherford backscattering of charged-particle beams in the heteroepitaxial films, which was previously demonstrated to be a feasible and useful method for establishing the density and location of defects in the films (Ref 2), was postponed temporarily but has now been resumed midway into the second-year program. The planned investigations of film microstructure in the interface region by means of X-ray techniques have not yet been initiated; it is expected that this work will be under way early in the forthcoming report period.

In the studies of the effects of changes in deposition parameters on $Si/A\ell_2O_3$ film properties the emphasis has been placed on comparison of the growth of (100) Si with (111) Si, over a wide range of growth temperatures and growth rates. Changes in reactor geometry have also been shown to be a significant factor in the determination of film properties, as was discussed in Section II-2. The effects of $A\ell$ autodoping on film characteristics have been examined in more detail, and additional studies of the effects of annealing to stabilize film properties have been completed. The variation in film properties with film thickness has been further explored in stabilized (i.e., annealed) Si films on $A\ell_2O_3$.

a. Precision of Measurements of Electrical Properties

Various experimentally measured quantities are required for the determination of the electrical characteristics of thin semiconductor films. These include, for example, voltages, currents, magnetic field strengths, and geometrical properties (i.e., dimensions) of the semiconductor samples. The accuracy of the values quoted for resistivity (ρ), carrier concentration (n) and mobility (μ) can therefore be estimated, based on estimates of the error in the measured quantitites.

Typically, for $Si/A\ell_2O_3$ films, the largest source of error in the determination of ρ and n is the film thickness, leading to relative errors of approximately ±5 percent, with an absolute error estimated to be about ±10 percent. Since the other important parameters (width of "Hall bridge," voltage, current) are each known to be approximately ±0.5 percent or bet' r, the overall relative error in ρ and n is estimated to be ~±7 percent. The mobility (μ) is independent of thickness as a measured parameter and is therefore measured to an accuracy of approximately ±2-3 percent.

However, there are other factors which may influence the accuracy of the quoted values of electrical properties of the heteroepitaxial films. The influence of surface conduction is minimized by intentional doping of films to carrier concentrations of $\sim 10^{16}$ cm $^{-3}$ or higher, but even in this range the surface effects may lead to errors in all electrical parameters of approximately ±10 percent. This error is, of course, much smaller for higher carrier concentrations and is probably insignificant compared with measurement errors for values of n $> 10^{17}$ cm^{-3}.

Considering all of the above sources of error, the values of ρ and n typically reported in these studies are estimated to be accurate to approximately ±15 percent (for samples with n in the low and middle 10^{16} cm^{-3} range), and the corresponding mobilities have approximately ±10 percent accuracy.

The van der Pauw (Ref 20) method, which has occasionally been used for measuring the electrical properties of semiconductor films, has been examined to determine the accuracy of the technique when applied to the evaluation of $Si/A\ell_2O_3$ films. Several samples were measured by this technique by applying contacts at the periphery of films approximately 1/2 in. in diameter. The electrical data obtained were compared with those found with the standard Hall bridge-type samples subsequently etched into each of the films. In most cases the resistivity found by the two methods differed at most by less than 6 percent, with the bridge method always yielding the smaller value. The carrier concentrations had a wider range of variation, with the bridge value being an average of 12 percent smaller. The largest variation occurred in the Hall mobility; the bridge values were an average of 16 percent larger than those found by the van der Pauw technique. These differences between the two methods are similar to those previously established in the $GaAs/A\ell_2O_3$ system (Ref 21). As a consequence of these differences, the van der Pauw technique is not ordinarily used for data included in reports; if the method has been used out of some necessity the results so obtained are clearly identified.

b. Variation of Si Film Properties with Growth Parameters

A summary of the electrical properties of n-type $Si/A\ell_2O_3$ films 0.5 to 2.0 μm thick grown during the present report period is shown in Tables 5 through 9, in which the films have been tabulated according to growth temperature. Most of the data were obtained on films grown at a rate of ~2 μm/min, since lower growth rates tend to yield poorer quality films over most of the temperature range examined.

It is found that for a growth rate of ~2 μm/min the electron mobility in (100) Si/$(01\bar{1}2)$ $A\ell_2O_3$ is nearly independent of growth temperature for 1040 C ≤ Tg ≤ 1100 C. At both higher and lower growth temperatures the limited data available suggest that the mobility decreases. This is shown in Figure 16, where the mobilities of films grown on $(01\bar{1}2)$ and ~$(11\bar{2}0)$ $A\ell_2O_3$ substrates are plotted as a function of growth temperature. At each temperature data for a number of films with net donor concentrations between 1 and 5 x 10^{16} cm^{-3} are averaged; the error bars indicate the range of mobilities over which the points are averaged (not the error in the data point itself), and the number next to the point indicates how many samples contributed to the average value plotted. All films were annealed at least one hour in O_2 at 1100 C to stabilize film properties.

Contrary to the case for the (100)Si growth on $(01\bar{1}2)$ $A\ell_2O_3$, the data for (111) Si growth on the $A\ell_2O_3$ orientation near the $(11\bar{2}0)$ plane show that a 2 μm/min growth rate yields films which appear to improve with increasing growth temperature and show a mobility maximum around 1075 - 1100 C.

The variation of carrier concentration with growth temperature for a constant dopant gas flow rate (0.22 ccpm AsH_3-H_2 mixture) and constant growth rate (~2 μm/min) was examined with the group of films listed in Table 10. The data are plotted in Figure 17 and indicate no definitive trend except for the slight decrease in carrier concentration at the highest growth temperatures.

Table 5. Electrical Properties of N-Type CVD Si on $(01\bar{1}2)$ and $\sim(11\bar{2}0)$ $A\ell_2O_3$ Substrates Grown at 1040 C at Rate ~2 μm/min. (Film Thickness ~2 μm)[a]

Substrate Orientation[b]	AsH_3-in-H_2 Flow (ccpm)	Resistivity (ohm-cm)	Carrier Concentration (cm^{-3})	Mobility (cm^2/V-sec)
A	0.056	1.7	5.5×10^{15}	660*
B	"	4.0	2.8×10^{15}	550*
A	0.11	0.36	3.0×10^{16}	580
B	"	0.67	2.0×10^{16}	470
A	0.22	0.19	6.0×10^{16}	540
B	"	1.7	2.8×10^{16}	130
A	0.45	0.095	1.4×10^{17}	480
B	"	0.59	5.6×10^{16}	190
A	0.90	0.056	2.8×10^{17}	400
B	"	0.081	1.8×10^{17}	440
A	1.2	0.059	2.8×10^{17}	380
B	"	0.091	1.9×10^{17}	360

a Samples grouped together were grown in the same run

b A = $(01\bar{1}2)$ $A\ell_2O_3$; B = $\sim(11\bar{2}0)$ $A\ell_2O_3$

* Samples with $n < \sim10^{16}$ cm^{-3} appear to be dominated by surface conduction

Data for films grown at a lower growth rate of ~0.8 μm/min (Table 7) show that the mobilities of films on $(01\bar{1}2)$ $A\ell_2O_3$ remain fairly high at temperatures up to 1060 C and are nearly equivalent to those grown at 2 μm/min at 1060 C (Table 6).

Higher growth rates can improve mobilities for Si films grown on the $(01\bar{1}2)$ orientation at higher temperatures. The effects of growth rate on the mobility of films on $(01\bar{1}2)$ and also on $\sim(11\bar{2}0)$ $A\ell_2O_3$ are shown in Table 8 and in the corresponding data plotted in Figure 18 (for growth at 1075 C). The mobility data indicate that high growth rates are necessary to produce optimized film properties at this (and presumably higher) temperature on $(01\bar{1}2)$ $A\ell_2O_3$; for 1075 C the mobility maximum occurs at a growth rate of about 4 μm/min for the $(01\bar{1}2)$ orientation and about 2 μm/min for the orientation near the $(11\bar{2}0)$. These films were grown under conditions of constant dopant gas flow. However, the measured carrier concentration is found to vary with growth rate as shown in Figure 19. The nearly linear behavior shown in Figure 19 suggests an exponential relationship between growth rate and carrier concentration. These data point out the importance of growth rate as well as growth temperature in determining the quality of Si films grown on $A\ell_2O_3$ substrates.

Table 6. Electrical Properties of N-Type CVD Si on $(01\bar{1}2)$ and $\sim(11\bar{2}0)$ $A\ell_2O_3$ Substrates Grown at 1060 C at Rate ~2 μm/min. (Film Thickness ~2 μm)[a]

Substrate Orientation[b]	AsH_3-in-H_2 Flow (ccpm)	Resistivity (ohm-cm)	Carrier Concentration (cm^{-3})	Mobility (cm^2/V-sec)
B	0.006	6.6	1.8×10^{15}	530*
A	0.014	1.9	5.7×10^{15}	590*
B	"	$\sim 7 \times 10^3$	---	---
A	0.021	3.0	8.0×10^{15}	260*
B	"	1.9	9.0×10^{15}	360*
A	0.028	1.1	9.2×10^{15}	600
B	"	2.3	5.3×10^{15}	510*
A	0.056	0.80	1.5×10^{16}	520
B	"	2.4	6.3×10^{15}	410*
A	0.11	0.67	1.8×10^{16}	530
B	"	0.96	1.1×10^{16}	620
A	0.45	0.10	1.4×10^{17}	440
B	"	0.13	8.0×10^{16}	600
A	1.2	0.070	2.5×10^{17}	370
B	"	0.062	2.1×10^{17}	490

[a] Samples grouped together were grown in the same run

[b] A = $(01\bar{1}2)$ $A\ell_2O_3$; B = $\sim(11\bar{2}0)$ $A\ell_2O_3$

* Samples with $n < \sim 10^{16}$ cm^{-3} appear to be dominated by surface conduction

Table 7. Electrical Properties of N-Type CVD Si on $(01\bar{1}2)$ and $\sim(11\bar{2}0)$ $A\ell_2O_3$ Substrates Grown at 1060 C at Rate of ~0.8 μm/min. (Film Thickness ~2 μm)[a]

Substrate Orientation[b]	AsH_3-in-H_2 Flow (ccpm)	Resistivity (ohm-cm)	Carrier Concentration (cm^{-3})	Mobility (cm^2/V-sec)
A	0.0056	0.26	4.4×10^{16}	550
B	"	0.49	2.1×10^{16}	600
A	0.014	0.65	1.7×10^{16}	570
B	"	2.7	5.7×10^{15}	400
A	0.028	0.72	1.9×10^{16}	460
B	"	5.1	5.3×10^{15}	230*
A	0.056	1.2	1.06×10^{16}	480
B	"	16.0	3.0×10^{15}	130*
A	0.22	0.16	9.9×10^{16}	400
B	"	0.18	6.0×10^{16}	570

[a] Samples grouped together were grown in the same run

[b] A = $(01\bar{1}2)$ $A\ell_2O_3$; B = $\sim(11\bar{2}0)$ $A\ell_2O_3$

*Samples with $n < \sim 10^{16}$ cm^{-3} appear to be dominated by surface conduction

Table 8. Electrical Properties of ~2 μm-Thick N-Type CVD Si Films Grown on $A\ell_2O_3$ at 1075 C with Addition of Constant Dopant Concentration (0.22 ccpm AsH_3-in-H_2) as Influenced by Growth Rate[a]

Substrate Orientation[b]	Growth Rate (μm/min)	Resistivity (ohm-cm)	Carrier Concentration (cm^{-3})	Mobility (cm^2/V-sec)
A	0.2	0.085	1.9×10^{17}	380
B	0.2	0.084	1.4×10^{17}	520
A	0.46	0.08	2.2×10^{17}	370
B	0.47	0.10	1.4×10^{17}	450
A	0.66	0.08	2.2×10^{17}	360
B	0.70	0.13	1.2×10^{17}	410
A	0.95	0.12	1.3×10^{17}	420
B	0.90	0.16	7.4×10^{16}	520
A	1.7	0.18	7.2×10^{16}	500
B	1.7	0.19	5.2×10^{16}	620
A	3.1	0.29	3.6×10^{16}	600
B	3.0	0.47	2.5×10^{16}	520
C	3.0	0.38	3.6×10^{16}	470
A	4.4	0.30	3.2×10^{16}	660
B	3.9	0.58	1.9×10^{16}	560
C	4.2	0.47	3.2×10^{16}	420
A	5.0	0.79	1.4×10^{16}	630
B	5.0	1.5	9.0×10^{15}	495
C	5.0	1.2	1.1×10^{16}	480
A	5.7	0.66	1.6×10^{16}	580
B	5.3	3.1	5.6×10^{15}	360*

[a] Samples grouped together were grown in the same run

[b] A = $(01\bar{1}2)$ $A\ell_2O_3$; B = ~$(11\bar{2}0)$ $A\ell_2O_3$; C = $(11\bar{2}2)$ $A\ell_2O_3$

* Samples with n < ~10^{16} cm^{-3} appear to be dominated by surface conduction

Table 9. Electrical Properties of ~2 μm-Thick N-Type CVD Si Films Grown on $A\ell_2O_3$ at 1100 C at Rate ~2 μm/min.[a]

Substrate Orientation[b]	AsH_3-in-H_2 Flow (ccpm)	Resistivity (ohm-cm)	Carrier Concentration (cm^{-3})	Mobility (cm^2/V-sec)
A	0.11	1.1	9.6×10^{15}	590
A	0.11	0.76	1.8×10^{16}	460
B	0.17	0.57	1.7×10^{16}	660
B	0.22	0.24	3.8×10^{16}	700
B	0.22	0.49	2.3×10^{16}	570
B	0.22	0.28	3.3×10^{16}	670
A	0.22	0.34	3.7×10^{16}	490
B	0.22	0.36	2.5×10^{16}	680
B	0.22	0.28	3.1×10^{16}	730
A	0.22	0.28	4.6×10^{16}	480
B	0.22	0.22	3.6×10^{16}	780
A	0.22	0.29	5.8×10^{16}	370
B	0.22	0.35	2.9×10^{16}	610
D	0.22	0.32	3.3×10^{16}	590
D	0.22	0.73	2.0×10^{16}	425
C	0.22	0.52	1.8×10^{16}	680
E	0.22	1.0	1.3×10^{16}	470

[a] Samples grouped together were grown in the same run

[b] A = $(01\bar{1}2)$ $A\ell_2O_3$; B = $(11\bar{2}0)$ $A\ell_2O_3$; C = $(11\bar{2}2)$ $A\ell_2O_3$; D = $(10\bar{1}4)$ $A\ell_2O_3$; E = $(11\bar{2}3)$ $A\ell_2O_3$

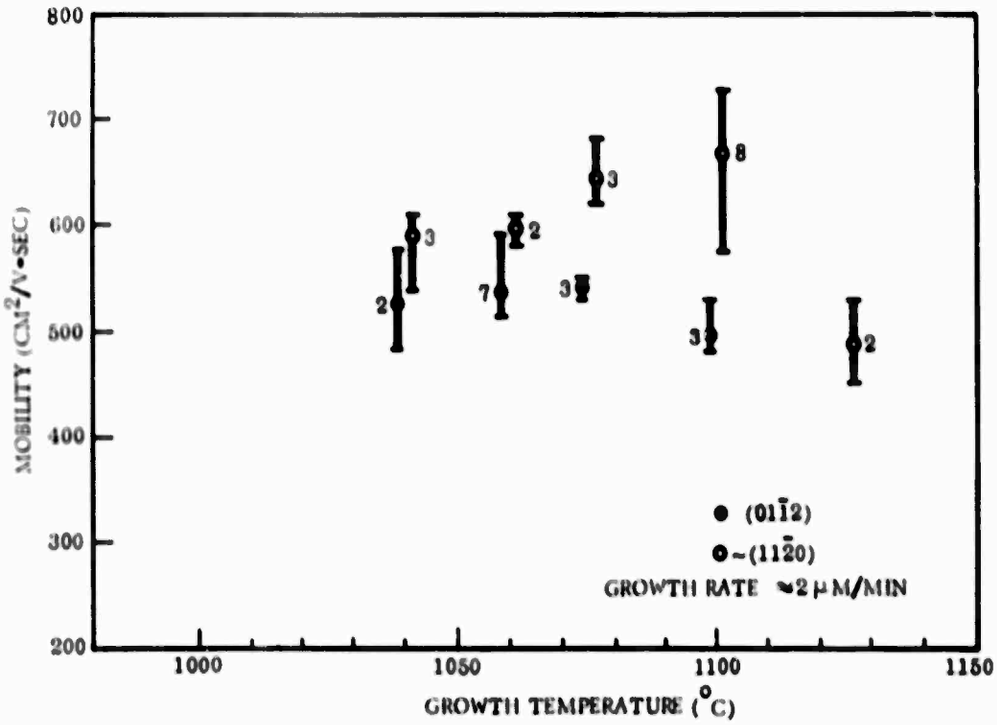

Figure 16. Variation of Hall Mobility with Growth Temperature for Si/$A\ell_2O_3$ Films Having Net Donor Carrier Concentration of 1-5 x 10^{16} cm^{-3}.

At constant growth rate the carrier concentration is related to the dopant gas flow (Table 5) as shown in Figure 20. (Included in Figure 20 are some data taken prior to the present report period.) The data are seen to agree with the dashed curve, representing a linear relationship between the two parameters, as would be expected. It is interesting to note that the carrier concentrations found in films on ~(11$\bar{2}$0) $A\ell_2O_3$ are consistently lower than those grown simultaneously on (01$\bar{1}$2) $A\ell_2O_3$. This fact suggests that the dopant is incorporated less easily into the (111)-oriented Si lattice.

Growth of Si on various other $A\ell_2O_3$ orientations at high growth temperatures was also examined recently. This study was stimulated by the observation that the quality of (111) Si appears to be quite high at 1100 C, and that some other orientations produce very reflective films at high temperatures. The (10$\bar{1}$4), (11$\bar{2}$2), and (11$\bar{2}$3) $A\ell_2O_3$ orientations were used as substrates for Si growth at temperatures from 1075 to 1150 C (Tables 8, 9, and 11). For film thicknesses of 1.5 to 1.9 μm and carrier concentrations of 1-2 x 10^{16} cm^{-3}, the (10$\bar{1}$4) and (11$\bar{2}$3) orientations yielded films with mobilities of ~400 - 500 cm^2/V-sec over the whole temperature range. The (11$\bar{2}$2) orientation gave (221)-oriented Si films with surprisingly high mobilities—up to 770 cm^2/V-sec in a 1.5 μm thick film—suggesting that this orientation may be superior to those so far examined. Further studies over a wider range of temperature and growth rate are clearly indicated.

Table 10. Effect of Growth Temperature on Properties of ~2μm- Thick N-Type (100) and (111) Si Films Grown at Rate of ~2μm/min with Constant AsH_3-in-H_2 Dopant Flow (0.22 ccpm)[a]

Nominal Growth Temperature(°C)	Substrate Orientation[b]	Resistivity (ohm-cm)	Carrier Concentration (cm^{-3})	Mobility (cm^2/V-sec)
1040	A	0.19	6.0×10^{16}	540
	B	1.7	2.8×10^{16}	130
1045[c]	A	0.21	5.7×10^{16}	520
	B	0.28	3.7×10^{16}	610
1060[d]	A	0.15	7.6×10^{16}	540
	B	0.22	4.9×10^{16}	580
1075	A	0.18	7.2×10^{16}	500
	B	0.19	5.2×10^{16}	620
1100	A	0.34	3.7×10^{16}	490
	B	0.36	2.5×10^{16}	680
	B	0.28	3.1×10^{16}	730
	A	0.28	4.6×10^{16}	480
	B	0.22	3.6×10^{16}	780
	B	0.24	3.8×10^{16}	700
	B	0.49	2.3×10^{16}	570
	B	0.28	3.3×10^{16}	670
	A	0.29	5.8×10^{16}	370
	B	0.35	2.9×10^{16}	610
	D	0.32	3.3×10^{16}	590
1125	A	0.97	2.5×10^{16}	260
	B	0.64	1.8×10^{16}	530
	C	0.80	1.0×10^{16}	770
	D	1.4	9.4×10^{15}	470
1150	C	0.51	1.8×10^{16}	690
	D	1.7×10^3	--	--
	E	0.93	1.5×10^{16}	460

[a]Samples grouped together were grown in same run

[b]A = $(01\bar{1}2)$ $A\ell_2O_3$; B = ~$(11\bar{2}0)$ $A\ell_2O_3$; C = $(11\bar{2}2)$ $A\ell_2O_3$; D = $(10\bar{1}4)$ $A\ell_2O_3$;

E = $(11\bar{2}3)$ $A\ell_2O_3$

A results in (100) Si growth; B, D, and E result in ~(111) Si growth; C results in ~(221) Si growth

[c]From Table IV, Ref 2. AsH_3-in-H_2 flow 0.15 ccpm

[d]From Table IV, Ref 2

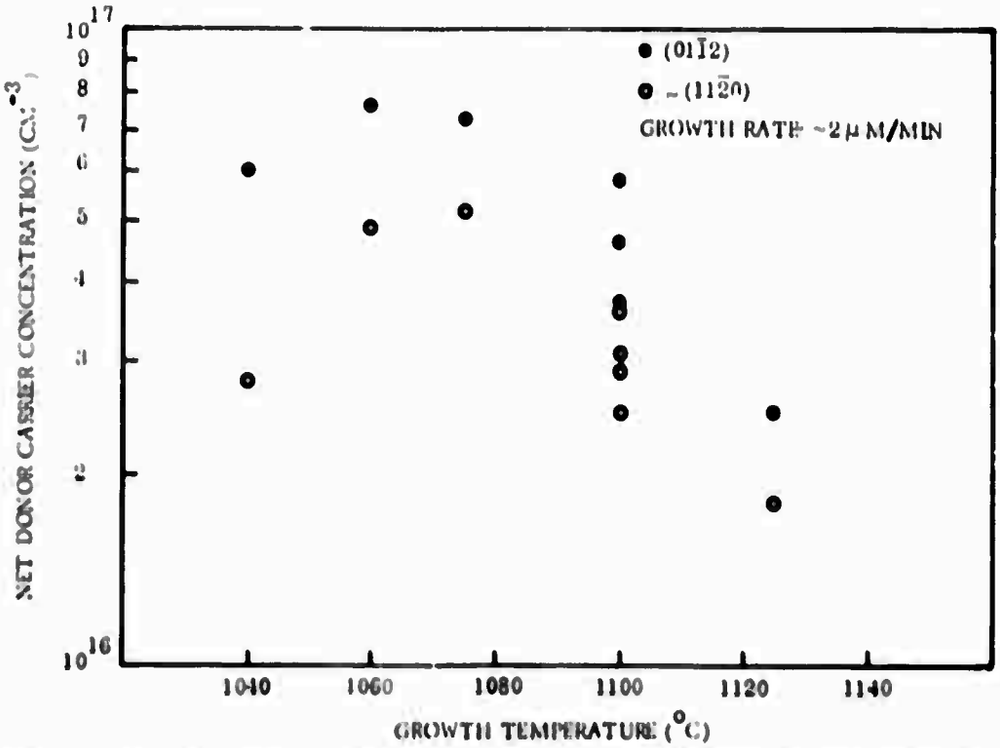

Figure 17. Variation of Net Donor Carrier Concentration with Growth Temperature for Si/Al_2O_3 Films Grown at ~2 μm/min. with Constant Dopant-Gas Flow Rate.

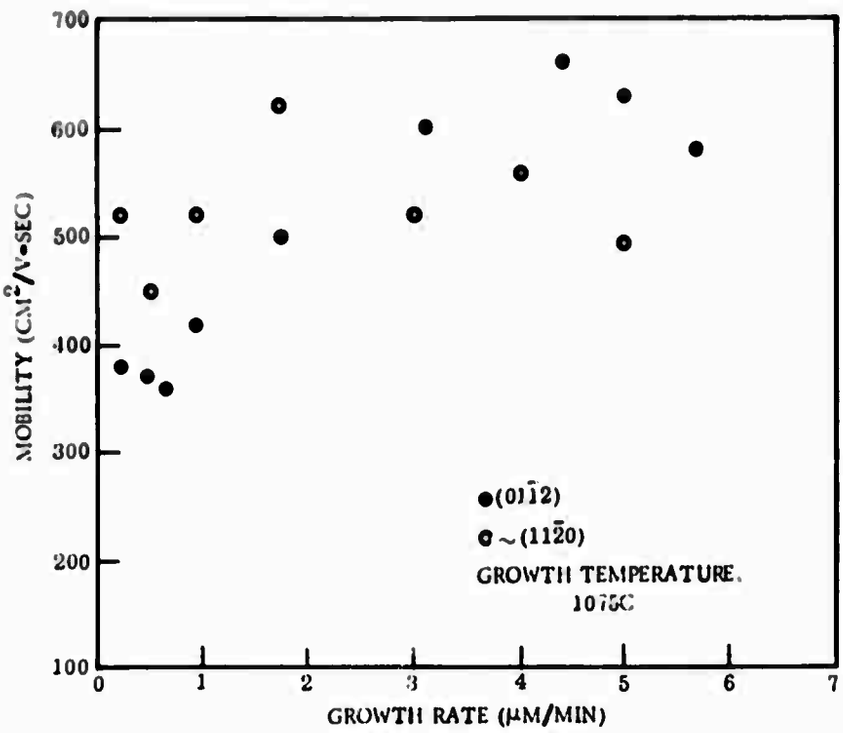

Figure 18. Variation of Hall Mobility with Growth Rate for N-Type Si/Al_2O_3 Films Grown at 1075 C.

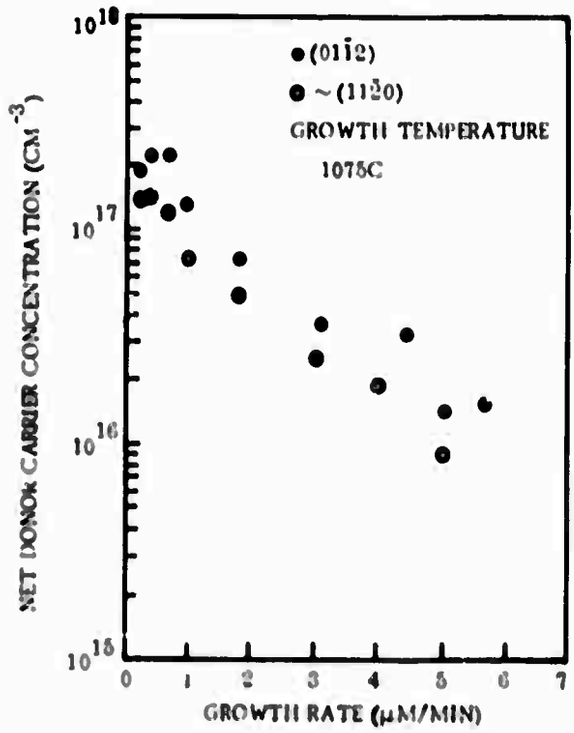

Figure 19. Variation of Net Donor Carrier Concentration with Growth Rate for Si/Al_2O_3 Films Grown at 1075 C with Constant Dopant-Gas Flow Rate.

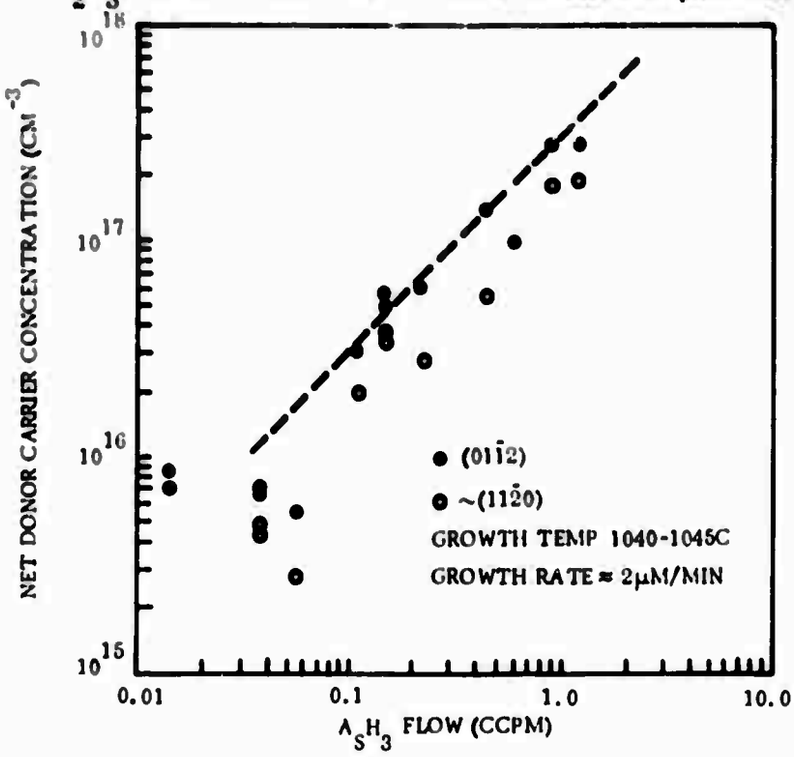

Figure 20. Variation of Net Donor Carrier Concentration with AsH_3 Flow Rate for Si/Al_2O_3 Films.

Table 11. Comparison of Electrical Properties of 2μm-Thick N-type Si Films Grown on $A\ell_2O_3$ at 1125 and 1150 C at Rate ~2μm/min.[a]

Temp. (°C)	Substrate Orientation[b]	AsH_3-in-H_2 Flow (ccpm)	Resistivity (ohm-cm)	Carrier Concen. (cm^{-3})	Mobility (cm^2/V-sec)
1125	A	0.22	0.97	2.5×10^{16}	260
	B	0.22	0.64	1.8×10^{16}	530
1125	C	0.22	0.80	1.0×10^{16}	770
	D	0.22	1.4	9.4×10^{15}	470
1125	A	0.45	0.20	8.1×10^{16}	390
	B	0.45	0.41	3.4×10^{16}	450
	D	0.45	0.34	4.1×10^{16}	450
1125*	A	0.45	0.27	6.6×10^{16}	360
	B	0.45	0.19	6.0×10^{16}	540
1125	A	0.90	0.12	1.4×10^{17}	360
	B	0.90	0.12	1.0×10^{17}	530
	D	0.90	0.14	9.6×10^{16}	460
1125	A	1.8	0.07	2.5×10^{17}	360
	B	1.8	0.10	$\sim 1.3 \times 10^{17}$	~480
1150	C	0.22	0.51	1.8×10^{16}	690
	D	0.22	1.7×10^{3}	-	-
	E	0.22	0.93	1.5×10^{16}	460

[a] Samples grouped together were grown in same run

[b] A = $(01\bar{1}2)$ $A\ell_2O_3$; B = $\sim(11\bar{2}0)$ $A\ell_2O_3$; C = $(11\bar{2}2)$ $A\ell_2O_3$; D = $(10\bar{1}4)$ $A\ell_2O_3$; E = $(11\bar{2}3)$ $A\ell_2O_3$

* Growth rate ~0.8 μm/min.

c. Study of Autodoping in $Si/A\ell_2O_3$ Films

As discussed in a previous report (Ref 2) $A\ell$ autodoping from the $A\ell_2O_3$ substrates has been shown to cause appreciable doping of an epitaxial Si film at temperatures greater than ~1050 C. In order to determine more precisely the extent of this doping, a number of films not intentionally doped were grown as a function of temperature from 1050 to 1150 C. The average acceptor concentrations measured in these films are shown plotted versus growth temperature in Figure 21 for ~2 μm-thick films grown at a rate of approximately 2 μm/min. Each data point represents an average value for data obtained from 1 to 3 samples. It is clear that slight changes in growth temperature can appreciably alter the extent of $A\ell$ doping, since the acceptor concentration varies by over two orders of magnitude for growth temperature changes of just 100 C.

These experiments raise the question of the extent to which autodoping affects the quality of the Si films and the devices formed in such films. As will be discussed in the next section, annealing sequences can apparently deactivate, i.e., electrically neutralize, the Si films in such a way as to minimize the effects of autodoping on electrical properties. From the data presented earlier, it is apparent that some of the best films, in terms of electron mobility, have been grown at temperatures where autodoping is most severe. The extent to which autodoping affects device performance will be the subject of subsequent studies in this program.

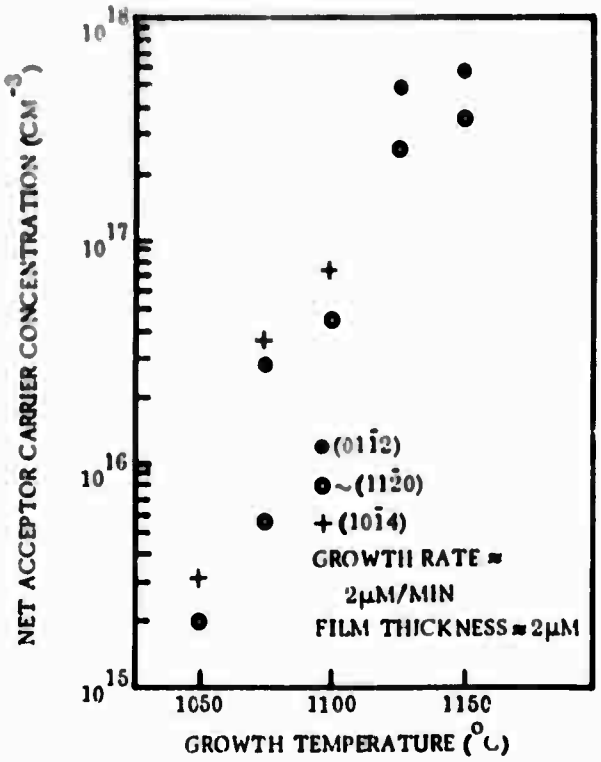

Figure 21. Variation of Net Acceptor Carrier Concentration Due to $A\ell$ Autodoping as Function of Growth Temperature for Intentionally Undoped $Si/A\ell_2O_3$ Films. (Data points are averaged values)

d. Effects of Annealing Sequences on Film Properties

Detailed studies of the effects of annealing $Si/A\ell_2O_3$ films have been continued during the present six-month period. (See Second Semiannual Report (Ref 2) for preliminary results.)

The effects of an anneal in an inert gas after previous extended O_2 anneals are shown in Table 12. This table indicates the relative stability of $Si/A\ell_2O_3$ film properties to both O_2 and N_2 anneals after initial annealing totaling 2 hours in O_2.

Table 12. Effects of Extended O_2 and N_2 Anneals on Electrical Properties of Three As-Doped, ~2 μm-Thick $Si/A\ell_2O_3$ Films (Growth Temperature 1100 C)

$A\ell_2O_3$ Substrate Orientation	Annealing Treatment	Si Film Resistivity (ohm-cm)	Carrier Concentration (cm^{-3})	Mobility (cm^2/V-sec)
$(10\bar{1}4)$	$1100/O_2$/1 hr	0.45	2.7×10^{16}	520
	+$1100/O_2$/1 hr	0.35	3.2×10^{16}	560
	+$1100/O_2$/1 hr	0.32	3.3×10^{16}	590
	+$1100/O_2$/30 min+			
	$1100/N_2$/4 hours	0.33	3.1×10^{16}	610
$-(11\bar{2}0)$	$1100/O_2$/1 hr	0.61	1.9×10^{16}	550
	+$1100/O_2$/1 hr	0.44	2.6×10^{16}	560
	+$1100/O_2$/1 hr	0.35	2.9×10^{16}	610
	+$1100/O_2$/30 min+			
	$1100/N_2$/4 hours	0.37	2.8×10^{16}	620
$(01\bar{1}2)$	$1100/O_2$/1 hr	0.46	3.5×10^{16}	390
	+$1100/O_2$/1 hr	0.30	5.1×10^{16}	410
	+$1100/O_2$/1 hr	0.29	5.8×10^{16}	370
	+$1100/O_2$/30 min+			
	$1100/N_2$/4 hours	0.31	4.9×10^{16}	410

In order to determine whether a N_2 anneal is as effective as an O_2 anneal for the deactivation of electrically-active Aℓ, several As-doped Si films were subjected to a N_2 anneal followed by an O_2 anneal. Identical control samples were annealed only in O_2. The resistivity was measured after each step with a 4-point probe, and the conductivity type was determined with a thermoelectric probe. The results are shown in Table 13, and strongly suggest that the mechanism of Aℓ deactivation is not primarily oxide gettering.

Table 13. Effects on Film Properties of Order of Sequential Annealing Steps in O_2 and N_2 for ~2 μm-Thick As-Doped Si Films Grown at Various Temperatures on -(11$\bar{2}$0) $A\ell_2O_3$ at Rate of 2 μm/min.

Growth Temp (C)	Substrate Designation	Annealing Treatment	Resistivity (ohm-cm)	Conductivity Type
1150	LM-27A	As grown	0.095	P
		1100/N_2/2 hours	3.1	P
		+1100/N_2/2 hours	3.4	N
		+1100/O_2/1 hour	3.2	N
1150	LM-27B (Control)	As grown	0.095	P
		1100/O_2/1 hour	1.0	N
1125	LM-33A	As grown	0.26	P
		1100/N_2/2 hours	6.0	N
		+1100/N_2/2 hours	~10 (est.)	N
		+1100/O_2/1 hour	~10 (est.)	N
1125	LM-33B (Control)	As grown	0.41	P
		1100/O_2/1 hour	0.74	N
1100	LM-32A	As grown	0.52	P
		1100/N_2/2 hours	2.1	N
		+1100/N_2/2 hours	1.7	N
		+1100/O_2/1 hour	1.3	N
1100	LM-32B (Control)	As grown	0.73	P
		1100/O_2/1 hour	0.53	N

A significant fraction of Aℓ is found to become electrically inactive after extended N_2 anneals. This suggests that most of the Aℓ remains in the film and probably complexes with defects and/or other impurities to form neutral centers. Subsequent O_2 anneals have little additional effect on film properties. If the film is initially treated with O_2 prior to the N_2 anneal a lower resistivity n-type film results, indicating that O_2 is slightly more effective in reducing the effect of Aℓ. These data imply that oxide gettering plays a significant but lesser role in reducing the active Aℓ content.

The effects of N_2 anneals on the electrical properties of intentionally undoped p-type films were also examined. In most cases, a reduction in net acceptor concentration by approximately a factor of two was found after a two-hour anneal at 1100 C. An additional two-hour anneal usually produced little additional change in acceptor concentration, with but slight decreases in Hall mobility. A subsequent O_2 anneal produced little additional change, just as in the case of the As-doped films.

A technique has been suggested in the literature (Ref 22) to improve the lifetime and carrier mobilities of $Si/Aℓ_2O_3$ films. The technique involves annealing the films in a $HCℓ$-O_2 mixture, which supposedly results in removal of many of those impurities which can deleteriously affect the carrier lifetime. Preliminary experiments in this program to determine the effects upon film mobility have proved negative; i.e., no improvement in film quality was achieved. These experiments will be repeated in the coming months to determine the effects upon lifetime and device performance.

A number of experiments have also been performed to determine the effects of annealing on the properties of relatively thin Si films after and/or during stepwise film growth. The data are summarized in Table 14 for the various annealing conditions shown.

The results indicate that 60-min anneals in H_2 at 1100 C deteriorate the quality of Si films ~0.25-0.5 μm thick, presumably by introducing additional defects and/or Aℓ as an impurity. A 20-min anneal does not improve the electrical properties of a ~0.5 μm-thick film but may affect a film 0.3 μm thick. However, a 20-minute anneal at 1100 C of a film ~0.15 μm thick seemed to improve the quality of subsequent growth on it; an electron mobility of 460 cm^2/V-sec was measured in the final 0.54 μm-thick growth. In all cases reflection electron diffraction (RED) showed the films to be single crystal, even though the long anneals resulted in partially gray-looking overgrowths for the (111) Si films. These studies are to be continued and the results are to be related to growth and annealing temperatures for films less than 1 μm thick.

e. Uniformity of Si Film Properties

The electrical properties of As-doped n-type (100) $Si/(01\bar{1}2)$ $Aℓ_2O_3$ films grown at 1100 C have been examined in detail as a function of film thickness. Measurements of as-grown films with thicknesses from 0.2 to 1.2 μm indicate that a considerably higher acceptor concentration exists near the interface than farther away, as evidenced by a net donor concentration which increases with film thickness.

Table 14. Properties of Si Films Grown at 1100 C at a Nominal Growth Rate of 2 μm/min. (Annealed and unannealed samples)

Film Orientation	Total Thickness (μm)	Resistivity (ohm-cm)	Carrier Concentration (cm^{-3})	Mobility (cm^2/V-sec)	Remarks
100	0.33	0.19	1.3×10^{17}	265	No H_2 anneal
111	0.38	0.61	3.5×10^{16}	300	
100	0.29	0.40	5.7×10^{16}	275	Anneal in H_2 at 1100 C
111	0.29	1.3	3.6×10^{16}	140	20 min after growth
100	0.25	~90	$\sim 5.8 \times 10^{14}$	~60	Anneal in H_2 at 1100 C for
111	0.24	1.5	$\sim 3.9 \times 10^{16}$	110	60 min after growth
100	0.62	0.45	3.9×10^{16}	360	No H_2 anneal
111	0.56	0.84	2.3×10^{16}	330	
100	0.53	0.35	5.4×10^{16}	330	Anneal in H_2 at 1100 C
111	0.51	0.60	2.5×10^{16}	370	for 20 min after growth
100	0.50	1.2	2.3×10^{16}	230	Two step growth. Anneal in
111	0.54	0.61	2.2×10^{16}	460	H_2 at 1100 C for 20 min after growth of ~1/3 of film
100	0.41	0.73	2.9×10^{16}	210	Two step growth. Anneal in
111	0.48	1.0	2.8×10^{16}	220	H_2 at 1100 C for 60 min after growth of ~1/3 of film

After a one-hour anneal in O_2 considerably less variation of film properties with thickness is apparent, as illustrated in Table 15 and in Figure 22. (Included in Figure 22 are data for several films grown on ~$(11\bar{2}0)$ $A\ell_2O_3$, also.) The carrier concentrations remained relatively constant, decreasing only slightly for thinner films, but the mobilities showed a steady decrease with decreasing film thickness, for both orientations.

When the films on $(01\bar{1}2)$ $A\ell_2O_3$ were reduced stepwise in thickness by polishing and then remeasured electrically, the average mobility showed the same general thickness dependence as that exhibited in Figure 22. The carrier concentrations, however, appeared to vary even less with thickness than the slight change indicated in the plot in Figure 22.

Table 15. Properties of Thin Si Films Grown on $A\ell_2O_3$ at 1100 C as Function of Thickness (Nominal Growth Rate 2 μm/min)[a]

Substrate[b]	Film Thickness (μm)	Resistivity (ohm-cm)	Carrier Concentration (cm^{-3})	Mobility (cm^2/V-sec)
A	0.19	1.6	2.6×10^{16}	160
A	0.24	1.7	2.0×10^{16}	180
A	0.35	0.75	3.2×10^{16}	260
A	0.49	0.47	4.4×10^{16}	300
A	0.56	0.56	3.6×10^{16}	310
A	0.90	0.32	4.8×10^{16}	400
B	0.18	5.1	1.3×10^{16}	95
B	0.37	1.1	1.5×10^{16}	370
B	0.83	0.84	1.7×10^{16}	430

[a] AsH_3-in-H_2 flow = 0.22 ccpm

[b] A = $(01\bar{1}2)$ $A\ell_2O_3$; B = ~$(11\bar{2}0)$ $A\ell_2O_3$

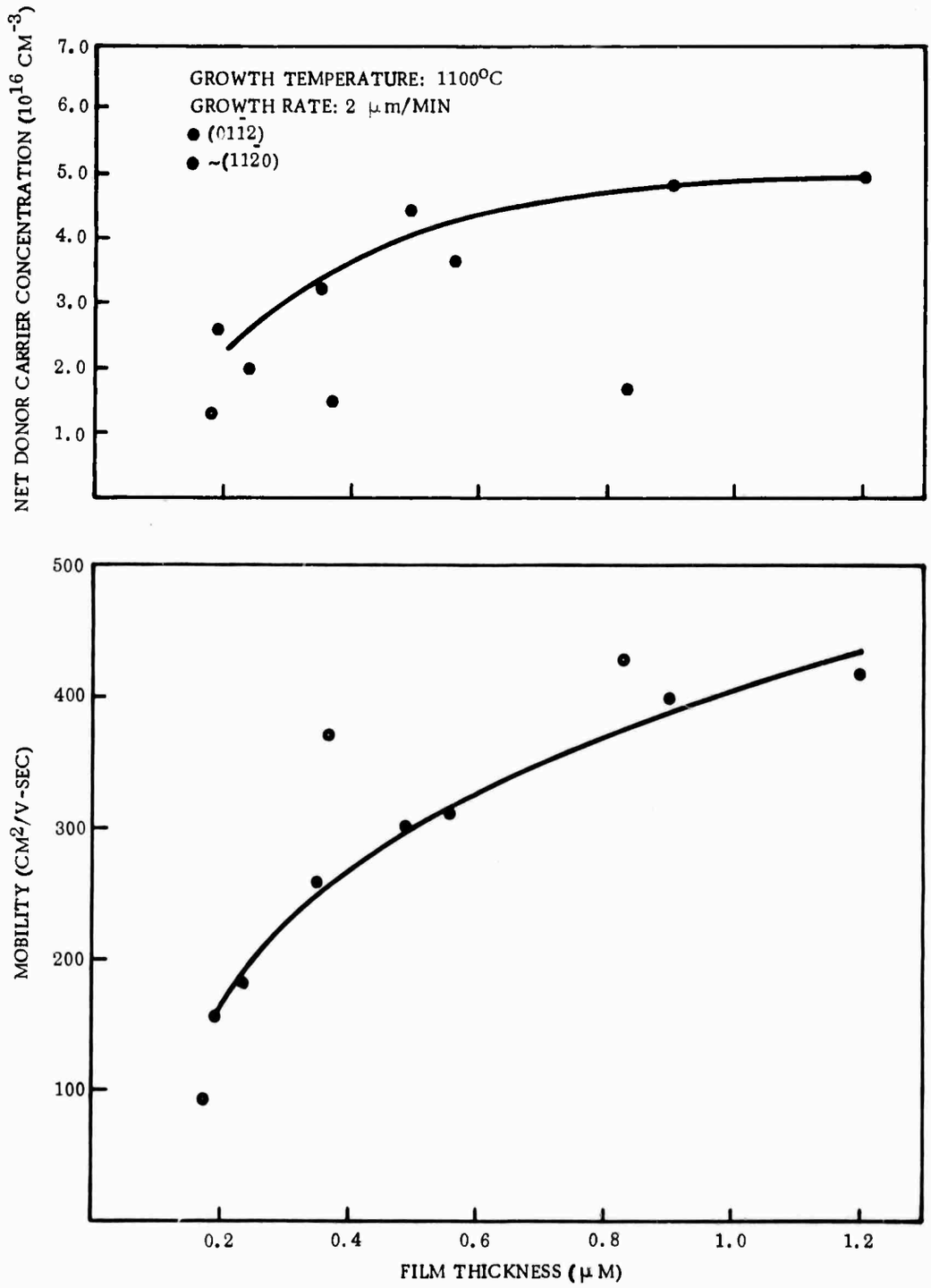

Figure 22. Variation of Film Properties with Film Thickness for Thin N-Type $Si/A\ell_2O_3$ Films. (All films annealed after growth for 1-hour in O_2 at 1100C.)

Although these results indicated that $A\ell$ autodoping appears to be much heavier near the Si-$A\ell_2O_3$ interface, particularly in the first 1 μm of growth, profiling studies of intentionally undoped p-type films ~5 μm thick indicate a nearly uniform concentration of $A\ell$ at thicknesses greater than 1 μm. For these measurements, films were grown on $(01\bar{1}2)$, ~$(11\bar{2}0)$, and $(10\bar{1}4)$ $A\ell_2O_3$ substrates at 1100 C, and then reduced stepwise in thickness.

The results of electrical measurements made after each step are shown in Figures 23 and 24. Although the $A\ell$ concentration appears to be relatively constant over the range of thicknesses investigated, it is interesting to note that the hole mobility appears to be steadily increasing with film thickness. The mobilities found in the films on $(10\bar{1}4)$ and ~$(11\bar{2}0)$ substrates are nearly equivalent to that of bulk Si.

The uniformity in properties of Si films was also recently investigated by examining the variation in electrical properties over the surface of a typical n-type Si/$A\ell_2O_3$ film. Three Hall bridges were etched at various positions on each of several films, and results of measurements on these bridges were compared after annealing at 1100 C in O_2 for one hour. Differences in electrical properties between bridges of ~20 percent or less were not considered to be significant, since the error in determination of bridge width and film thickness can easily lead to errors of ±10 percent. Out of 10 samples examined (with three bridges on each), two samples showed differences in resistivity among bridges of nearly a factor of two, while one showed a difference of 50 percent and another a difference of 25 percent. The remaining films all showed a resistivity spread of 20 percent or less.

The degree of uniformity of film properties does not appear to be completely or exclusively related to film growth conditions and is probably strongly dependent upon details of substrate surface preparation. This study does clearly indicate that conclusions regarding such things as optimum growth conditions and optimum substrate species or orientation based on electrical data for only a few samples may be erroneous, and that a sufficiently large group of samples must be used in order to draw meaningful conclusions.

f. Measurements of Photoelectric Effects in Heteroepitaxial Films

The measurements of photoemission of electrons from films of Si and GaAs on $A\ell_2O_3$ substrates and of electron transport through single-crystal $A\ell_2O_3$ have been continued during this reporting period.* The results of the first measurements were given in the Second Semiannual Report (Ref 2), and some additional results have since been reported (Ref 23).

---

* This work has been carried out at UCLA in the Department of Electrical Sciences and Engineering.

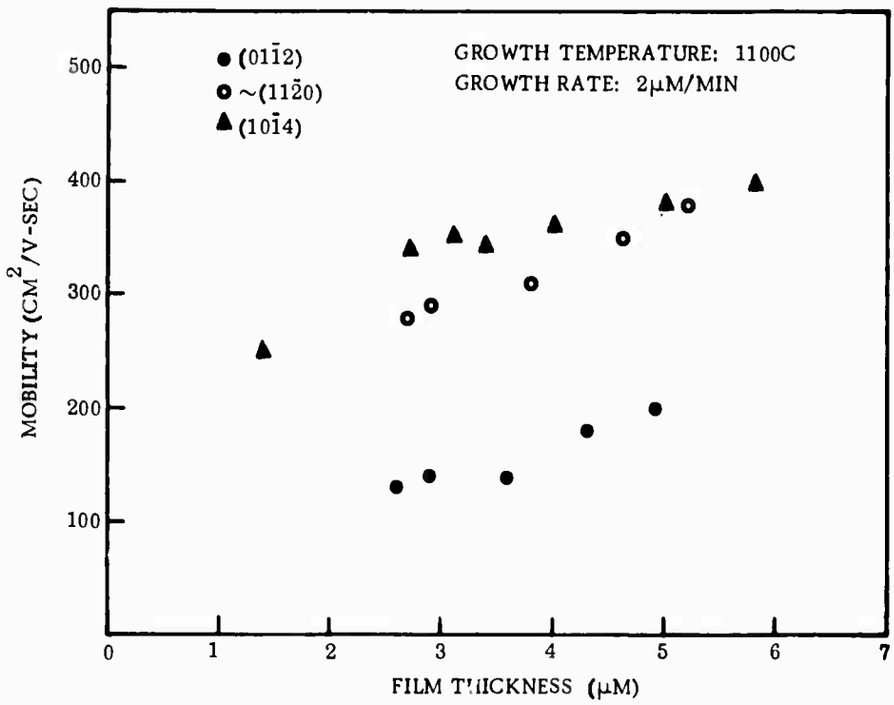

Figure 23. Variation of Hall Mobility with Film Thickness for Intentionally Undoped P-type Si/Aℓ_2O_3 Films

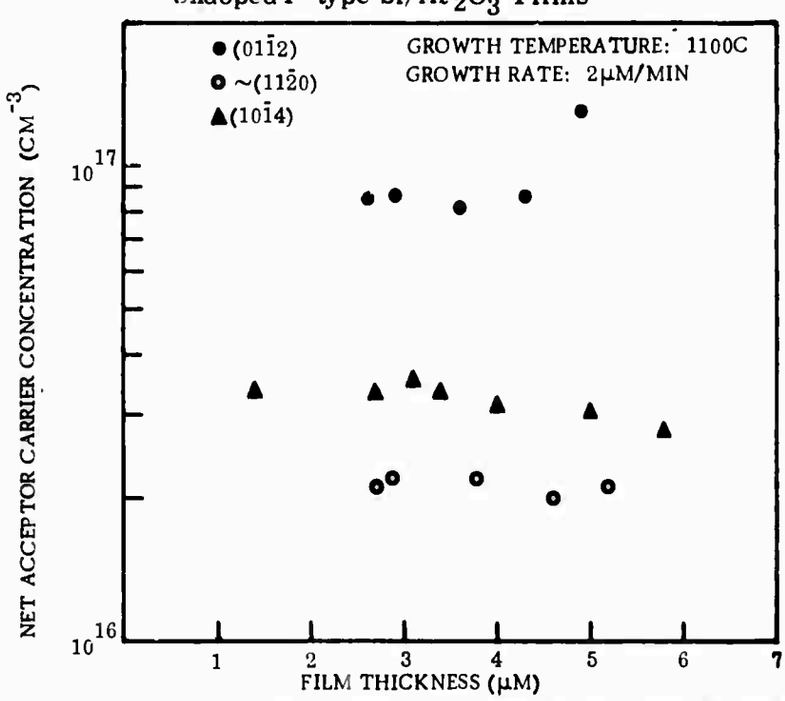

Figure 24. Variation of Net Acceptor Concentration with Film Thickness for Intentionally Undoped Si/Aℓ_2O_3 Films

In the initially-reported work values of the interface barrier height were obtained for several metals deposited onto the $A\ell_2O_3$ substrates. Similar measurements have now been made for other metals — viz., Ta, Hf and In — and the results are given in Table 16.

Table 16. Interface Barrier Height and Work Function for Several Metals

Metal	Interface Barrier Height ($h\nu_o$) (eV)	Electron Affinity (χ) of $A\ell_2O_3$ (eV)	Work Function $\Phi_m = h\nu_o + \chi$ (eV)
Ta	4.65	0.42	5.07
Hf	4.6	0.42	5.02
In	4.52	0.42	4.94

In order to understand the mechanism of current flow in single-crystal $A\ell_2O_3$ substrates, the photocurrent has been studied as a function of time by chopping the light beam. As soon as the light beam is switched on, the photocurrent quickly rises to a maximum and then slowly decays to a steady-state value. The rapid initial rise can be understood by the following argument: As soon as an electron is injected into the $A\ell_2O_3$ substrate the current due to the electron moving with a velocity v is $\frac{ev}{W}$, where W is the thickness of the insulator. The total current at time t after the light is switched on is

$$i(t) = A \int_0^{vt} \frac{nevdx}{W} = \frac{Anev^2t}{W} . \qquad (1)$$

The current will continue to rise until the electrons injected initially at t = 0 reach the far surface of the insulator. The peak of the current will be reached at time $t = \tau$, where $W = v\tau$; the magnitude of the peak current is Anev. It will retain this value as long as the light is incident on the surface, except for the effects of trapping of electrons. The trapped electrons produce a retarding field and the current decays to a steady-state value. By measuring the linear portion of the initial rise of the photocurrent, it is possible to determine the velocity with which the injected electrons move in the insulator. These measurements are in progress.

The photocurrent was also measured as a function of the applied voltage across the insulator. Both the peak current and the steady-state values were measured as a function of the applied voltage and are plotted in Figure 25 as a function of V and in Figure 26 as a function of $V^{1/2}$.

In addition to the gross increase in current with applied voltage, it is found that a definite structure exists in the current characteristic. The applied voltage influences the photocurrent in two ways. First, it reduces the interface barrier height due to the Schottky effect, and therefore the photoinjection is increased. Second, it gives rise to a field in the insulator which will influence the transport of these electrons through the insulator.

In the next few months, it is expected that an understanding of the mechanism for transporting electrons through the insulator can be acquired by carrying out similar experiments at several temperatures and several thicknesses of the insulator.

g. Measurement of High-Field Transport Properties

As a part of the film evaluation procedures attempts have been made to determine the high-field transport properties of Si on $A\ell_2O_3$ substrates.*

Mobility measurements have been made on heteroepitaxial films as a function of electric field using the simple relationship between measured current and applied field, i.e., $I = ne\mu\epsilon$. However, since the sample is heated by the current flow and the temperature is no longer constant, a pulse technique has been used in which the voltage is applied in the form of a narrow pulse at a low repetition frequency and the current pulses are measured on an oscilloscope. A simple calculation indicated that a pulse width of 0.1 μsec at a repetition rate of less than 100/sec was sufficient to keep the temperature rise negligibly small. The block-schematic of the experimental arrangement is shown in Figure 27.

Using this apparatus, mobility measurements have been made on both n-type and p-type $Si/A\ell_2O_3$ samples. A typical (111)-oriented n-type sample had a resistivity of approximately 0.3 ohm-cm and was of dimensions 11.1 μm x 0.03 cm x 0.25 cm. A typical p-type sample had a resistivity of approximately 0.25 ohm-cm and was of dimensions 10.5 μm x 0.06 cm x 0.5 cm.

Figures 28 and 29 are plots of the measured values of current density as a function of field strength for these two samples. High-field effects were not noticeable because of limitations in the sample geometry. It is expected that smaller sample dimensions to be used in the future will make the attainment of higher fields possible.

---

* The measurements have been carried out at UCLA in the Department of Electrical Sciences and Engineering.

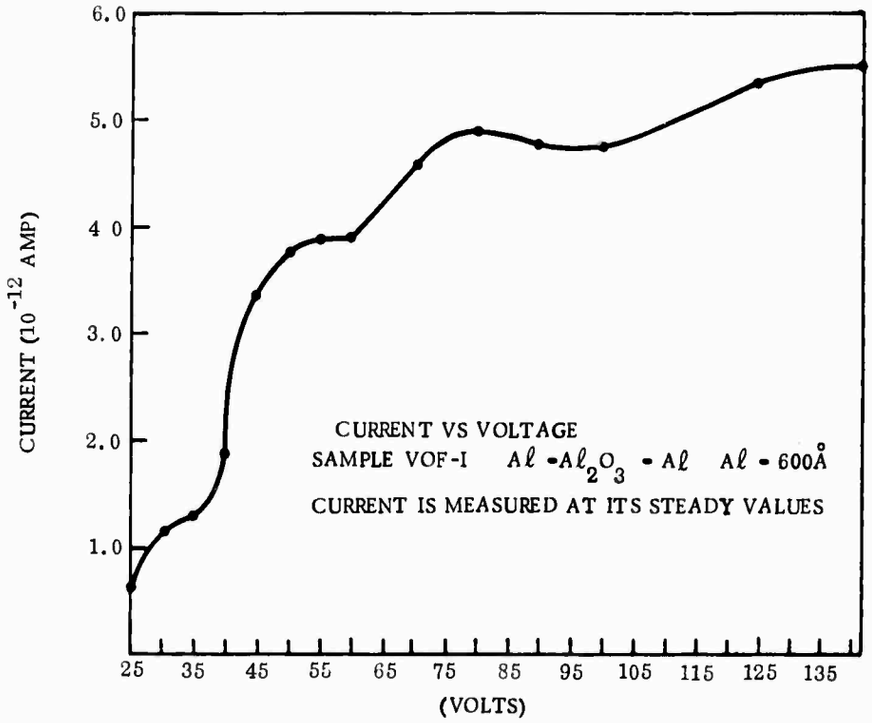

Figure 25. Current vs Voltage for Photoemitted Electron Transport through $A\ell_2O_3$ (Current is measured at its steady values)

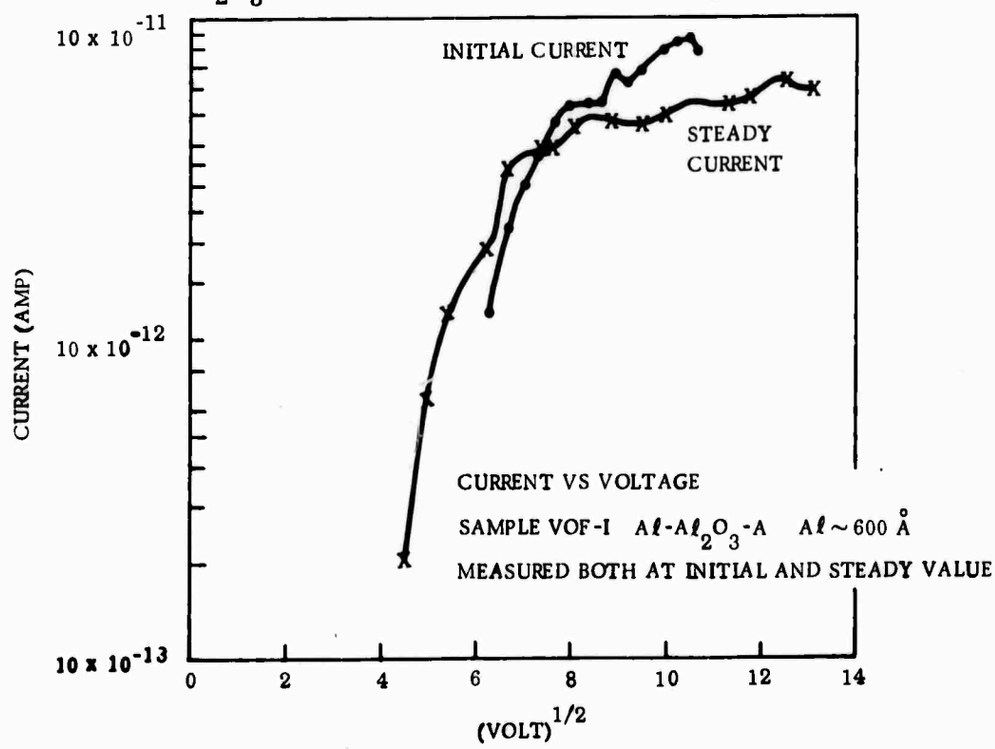

Figure 25. Current vs (Voltage)$^{1/2}$ for Photoemitted Electron Transport through $A\ell_2O_3$ (Current measured at both peak and steady value)

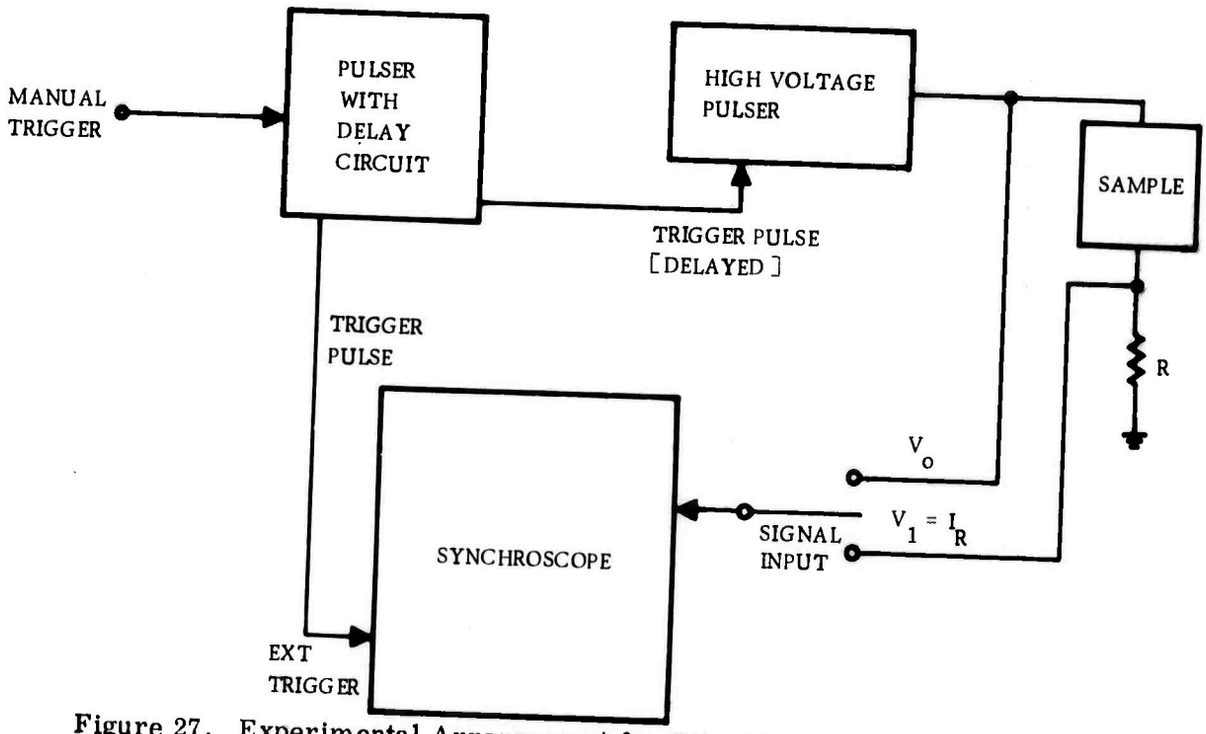

Figure 27. Experimental Arrangement for Film Mobility Measurements at High Fields

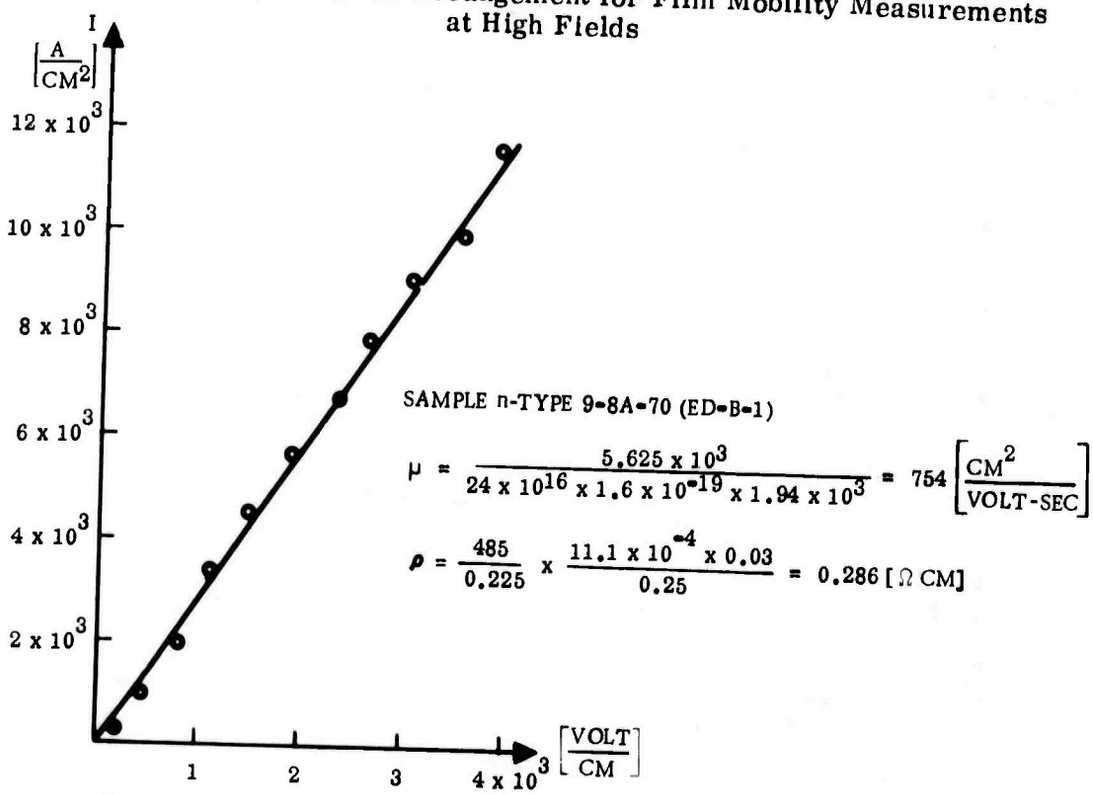

Figure 28. Current Density as Function of Electric Field for N-Type $Si/A\ell_2O_3$ Film

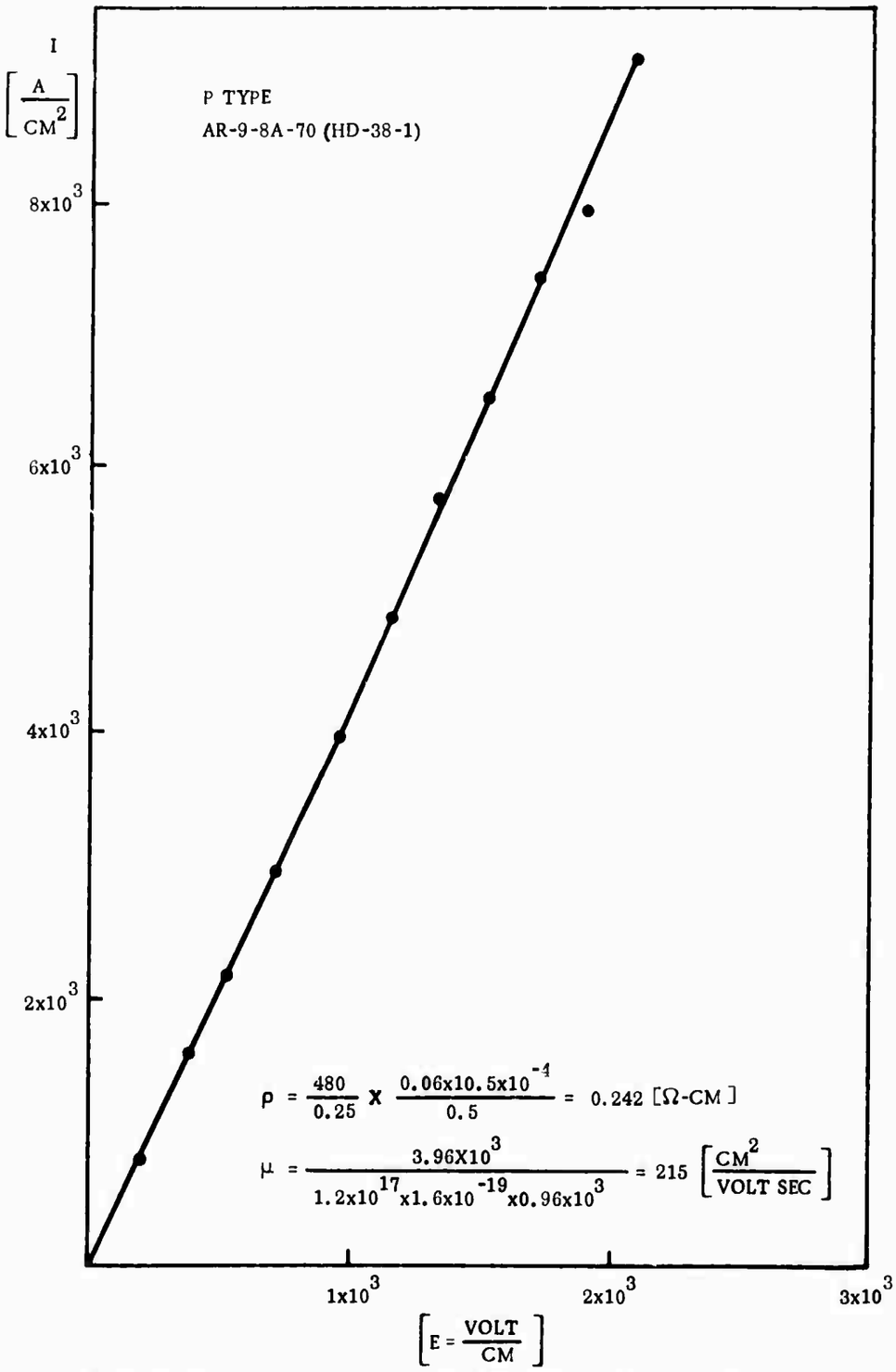

Figure 29. Current Density as Function of Electric Field for P-Type $Si/A\ell_2O_3$ Film

7. SUBTASK 7: DESIGN AND FABRICATION OF DEVICES

The measurement of carrier lifetimes in heteroepitaxial films has been initiated utilizing an MOS device structure, as suggested in the Second Semiannual Report (Ref 2). A Schottky-barrier FET has been designed for operation at 1 GHz in heteroepitaxial GaAs on $A\ell_2O_3$; the masks are being prepared and fabrication of experimental devices will commence early in the forthcoming report period.

a. Measurement of Bulk Generation Lifetime in Heteroepitaxial Films*

In earlier examination of several alternative methods of measuring carrier lifetime in Si and GaAs heteroepitaxial films it was determined that the most useful technique for the purpose is that involving pulsed capacitance-voltage measurements in an MOS structure (Ref 2). This method has now been put into use and results in $Si/A\ell_2O_3$ films have been obtained at the end of the present report period.

The object of the study has been to determine the dominant carrier recombination mechanisms in Si and GaAs films heteroepitaxially grown on $A\ell_2O_3$ substrates and to correlate measurements of bulk generation lifetime (τ_g) with film growth conditions and other film properties. The properties of interest are film resistivity, thickness and orientation. The very low lifetime ($\sim 10^{-9}$ sec) anticipated in thin heteroepitaxial samples has led to the choice of the pulsed MOS capacitance technique. This technique allows separation of bulk and surface components of lifetime.

MOS devices have been fabricated from bulk Si wafers and from $Si/A\ell_2O_3$ samples, and test equipment has been constructed to measure and automatically record capacitance-voltage (C-V), capacitance-time (C-t) and dC/dt-versus-t characteristics. The existing theory for the transient response of an MOS structure has been improved to include effects due to impurity redistribution during thermal oxidation of the Si and to variations in the surface recombination velocity across the depletion layer at the $Si\text{-}SiO_2$ interface.

(1) MOS Capacitor Used for Measurement of Bulk Generation Lifetime

In the MOS structure an insulating layer of SiO_2 is thermally grown onto a film (or wafer) of Si and a metal contact (gate electrode) is evaporated onto the top of the SiO_2. A metal ohmic contact is then made to the Si film (or bulk wafer). Figure 30 shows the MOS geometry used in this study for bulk Si wafers and for $Si/A\ell_2O_3$ films.

When a negative voltage pulse is applied to the gate electrode of a Si MOS structure majority carriers (electrons) will flow away from the SiO_2-Si interface and into the bulk Si, uncovering immobile ionized donor atoms. A space-charge region will be formed in a time interval the order of the dielectric relaxation time τ_d ($\sim 10^{-12}$ sec for 1 ohm-cm Si). Throughout the semiconductor, electron-hole pairs will be thermally generated at a constant rate g, dependent only on temperature and crystal parameters. Within the strong field of the space-charge region

* The lifetime investigations and the FET devide fabrication are being carried out at UCLA in the Department of Electrical Sciences and Engineering.

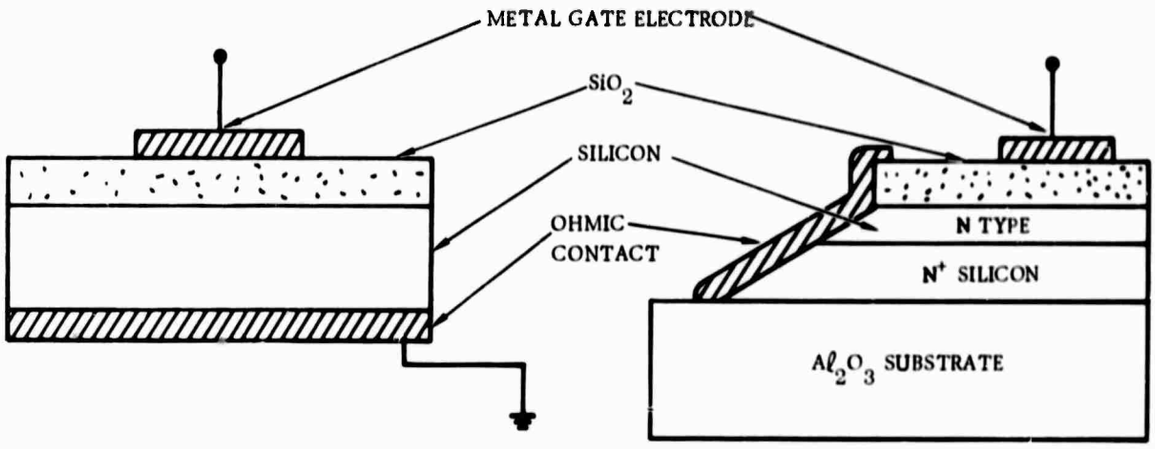

(a) MOS GEOMETRY FOR SILICON WAFERS

(b) MOS GEOMETRY USED FOR SOS SAMPLES

Figure 30. MOS Geometry for Carrier Lifetime Measurements

thermally generated holes will move toward the SiO_2-Si interface and electrons will move toward the bulk Si. Within a depletion layer of area A and width x(r) there will be Ag x dt electrons thermally generated between the times t and (t + dt). These electrons will drift to the edge of the depletion layer, neutralizing the space charge in a region dx containing AN_d dx immobile ionized donor atoms, where N_d is the donor doping concentration.

In a space-charge region the lifetime τ_g of the thermally generated carriers is related to the generation rate g by

$$g = \frac{n_i}{2\tau_g}, \tag{2}$$

where n_i is the intrinsic carrier concentration

Then,

$$AN_a\, dx = -Ag\, x\, dt = -A\frac{n_i}{2\tau_g}\, x\, dt. \tag{3}$$

Solving for x gives

$$x(t) = x(0)e^{-t/T}, \tag{4}$$

where

$$T = 2\tau_g \left(\frac{N_d}{n_i}\right).$$

At room temperature in Si $n_i \simeq 10^{10}$ cm^{-3} and N_d is typically 10^{15} to 10^{18} cm^{-3}. The MOS capacitor characteristic relaxation time T will be 5 to 8 orders of magnitude larger than the lifetime τ_g. In GaAs, $n_i \sim 10^7$ cm^{-3} so that T is 8 to 11 orders of magnitude larger than τ_g. If the capacitance C(t) is monitored as a function of time, from the characteristic shown in Figure 31 the anticipated lifetime values of 10^{-10} sec for heteroepitaxial films of Si and GaAs can be measured.

In a more rigorous analysis of the problem, Zerbst (Ref 24) has shown that a plot of $-\frac{d}{dt}\left(\frac{C_o}{C}\right)^2$ versus $\left(\frac{C_f}{C} - 1\right)$ yields a straight-line portion whose slope is related to the bulk generation lifetime τ_g and whose intercept on the $-d/dt\ (C_o/C)^2$ axis is related to the surface recombination velocity S. This analysis has been improved by a variety of workers to include surface effects more realistically but always for the case of an ideal MOS device, uniformly doped.

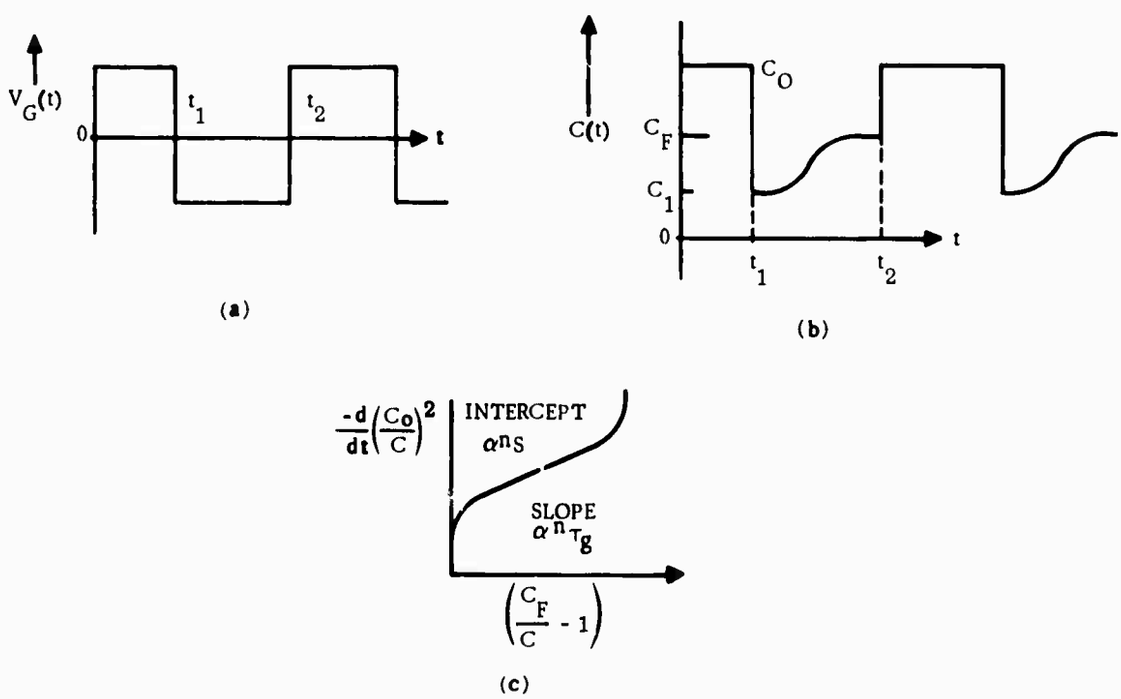

Figure 31. Characteristics of MOS Capacitor in Si/$A\ell_2O_3$. (a) Gate Voltage Pulse $V_G(t)$, (b) Resulting MOS Capacitance Transient Response, (c) Zerbst Plot for Capacitor.

When a Si film or wafer is subjected to a thermal oxidation cycle to create an SiO_2 layer it has been shown by Grove et al (Ref 25) that in a region the order of 1 μm into the Si adjoining the SiO_2-Si interface the doping concentration is redistributed. The surface impurity concentration may differ from that in the interior by a factor of from 2 to 7, depending upon the impurity and the SiO_2 growth conditions (temperature and ambient). Such doping variations have been explicitly incorporated in a calculation of the transient response; it is found that the measurement of both τ_g and S is markedly influenced — up to a factor of 5.

A further refinement in the theory of the MOS capacitor transient response is to consider the variation of S with energy-band bending. This is less important, however, since the effect of the surface can be minimized by using large, circular gate cletrodes.

(2) Fabrication of MOS Structures

SiO_2 films typically 1000 to 2000 Å thick were grown on Si wafers and $Si/A\ell_2O_3$ samples using a standard thermal oxidation system. This system is capable of producing dry, wet or steam-grown oxides at temperatures up to 1200 C. Since the surface recombination velocity for very small geometries can dominate the C-t response of an MOS device, particular attention was given to avoiding contamination of the samples during thermal oxidation. The SiO_2 layers grown on $Si/A\ell_2O_3$ samples were grown at temperatures below the Si film growth temperatures. Electrical contacts were formed by vacuum-deposited metallic films. Aℓ was used for the gate electrode on both p- and n-type devices. Aℓ deposited onto the back face of Si wafers served as an ohmic contact for p-type samples and Au/Sb deposited contacts served as ohmic contacts to n or n+ regions. In some cases the Au/Sb contacts were sintered at 500 C in a nitrogen furnace for 20 minutes to improve their ohmic behavior.

(3) Electrical Measurements

After the fabrication of an MOS device the DC electrical conductivity (between gate and ohmic contacts) was checked to ensure that a highly insulating oxide had been grown. The capacitance-voltage (C-V) characteristic was then automatically recorded on an x-y recorder (Figure 32). The capacitance-time (C-t) characteristic was then recorded, using either an x-y recorder for transients of the order of 5 sec or longer (typically bulk wafers) or a storage oscilloscope and camera for shorter capacitance transients. The test equipment is capable of measuring C-V characteristics from 1 to 10 pf (±0.2 pf) or ±2 percent from 10 to 3000 pf, and C-t transients of from 10^{-4} to 10^{3} sec. The capacitance monitoring equipment is also capable of displaying dC/dt versus t. This feature decreases the task of data reduction in an exact C-t analysis.

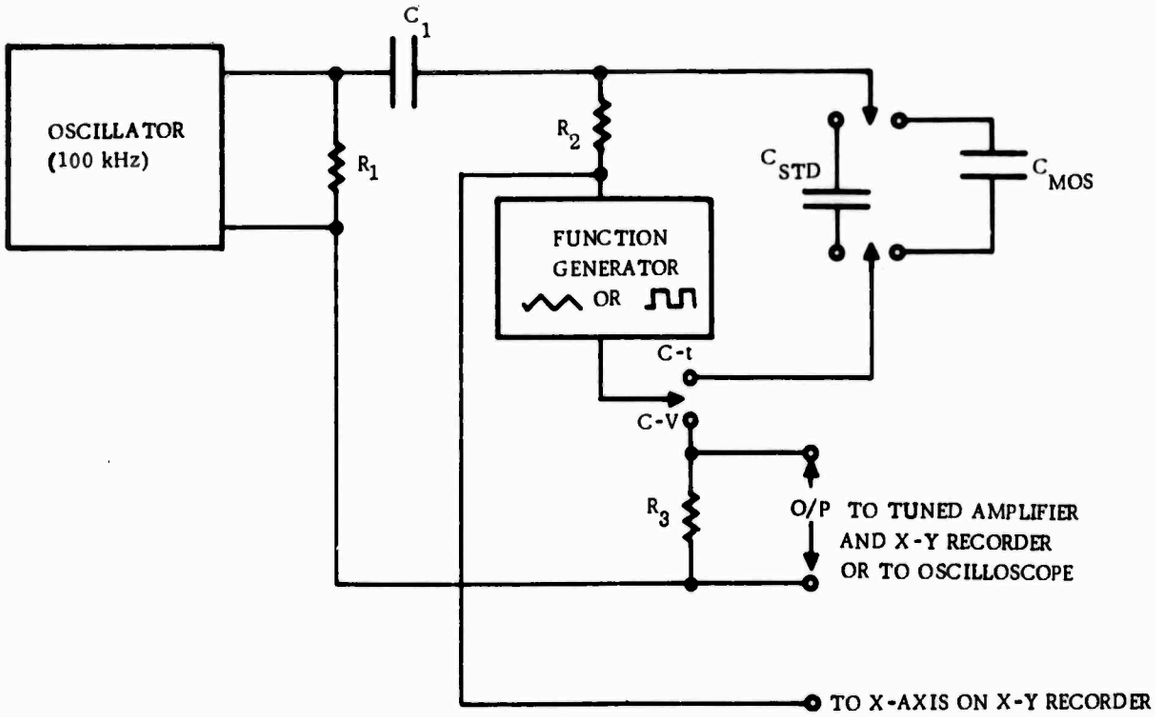

Figure 32. Schematic of C-V, C-t Measurement Instrumentation

Impurity redistribution studies are now being performed on bulk Si wafers. MOS structures have been fabricated from p-type (B-doped) and n-type (P-doped) wafers. Oxides have been grown in steam and dry oxygen at 1000 and 1100 C. This study suffered from erratic contamination in the oxide, which was finally discovered to be due to the gate electrode being excessively overheated during its formation in the evaporation process. This has been overcome simply by increasing the distance between the evaporator heating element and the Si wafers. Further MOS devices must be fabricated with oxides grown at 900 and 1200 C in steam and dry oxygen before comparative data is available.

SiO_2 films 1500 Å thick have been grown on $Si/A\ell_2O_3$ samples at 1000 C in steam, and successful MOS devices have been fabricated. In the study of the effect of film thickness on τ_g, measurements of C-V and C-t have been performed on several n-type samples which have consisted of about 3 μm of n-type Si on 10 to 15 μm of n^+ Si). The C-t responses were essentially exponential in character; using the simple theory outlined above yields τ_g values of 1.0 to 1.6 x 10^{-9} sec, respectively.

These lifetime values must be considered only as approximate, since the values of the doping concentrations were inferred from the Si film growth conditions. (No carrier concentration measurements were made after the film growth.) Future MOS devices on Si film samples will not require the n+ layer beneath the n-type Si film, and as such should provide more relevant data on film growth conditions.

SECTION III

WORK PLANNED FOR NEXT SIX MONTHS

Work on all seven subtasks will be in progress during the next si . months. The specific activities planned for this period will include the following.

1. SUBTASK 1: THEORY OF EPITAXY AND HETEROEPITAXIAL INTERFACES

The determination of a best-fit $A\ell_2O_3$ lattice modeled with Morse potentials taking account of equilibrium and stability conditions will be completed. Surface relaxation and reconstruction of $A\ell_2O_3$, using the previously determined potentials, will then be investigated. In addition, a Si lattice modeled with Morse potentials will be determined, and the computer simulation of Si growth on $A\ell_2O_3$ using previously determined lattices, surface reconstruction, and adatom potentials will be initiated. The major effort on and the completion of the last undertaking — the computer simulation of Si growth — will take place in the first half of the third contract year, at which time this theoretical investigation will come to fruition. The application of the electron-on-network technique to the case of heteroepitaxial systems will be further developed, with a preliminary theoretical model planned for completion midway through the report period.

2. SUBTASK 2: DEPOSITION STUDIES AND FILM PREPARATION

Initially, these studies will emphasize the investigation of effects of the cold-wall reactor on Si film growth processes and film properties. Examination of other reactor geometries and gas flow patterns and their effects on the properties of $Si/A\ell_2O_3$ films will be continued. Experiments with Si growth on $MgA\ell_2O_4$ will be extended to include a determination of the effect on film growth characteristics of H_2 additions to a He atmosphere, as a function of growth temperature and rate. This study will be directed toward identification of optimized CVD process parameters for Si growth on $MgA\ell_2O_4$, so that either $A\ell_2O_3$ or $MgA\ell_2O_4$ can be selected as the preferred substrate for obtaining the best electrical properties in heteroepitaxial Si films. Studies of film nucleation phenomena will also be resumed in the $Si/A\ell_2O_3$ system. Some additional Si CVD experiments at low pressures (~1 torr) will be carried out in preparation for the <u>in situ</u> CVD experiments in the electron microscope (Subtask 5). Deposition parameter studies in the GaAs/insulator system have been temporarily postponed into the third contract year.

3. SUBTASK 3: ANALYSIS AND PURIFICATION OF CVD REACTANTS

Mass spectrometric analyses of the impurity content of CVD reactants, including SiH_4, trimethylgallium, and AsH_3, will be continued. Attempts to persuade vendors to prepare and supply reactants of improved purity will also continue. As a means of impurity analysis for the reactants a series of Si and GaAs films will be analyzed for impurity content as a function of thickness (i.e., distance from the film-substrate interface) by means of localized mass spectrometric analysis and/or Rutherford backscattering analysis using charged particle beams. The possibility of initiating studies of the chemistry of the CVD reactions used for Si and GaAs film growth will also be investigated.

4. SUBTASK 4: PREPARATION AND CHARACTERIZATION OF SUBSTRATES

Further improvements in techniques for preparing the surfaces of $A\ell_2O_3$ and $MgA\ell_2O_4$ substrates for heteroepitaxy will be sought. Mechanical polishing methods involving combined vibratory and standard optical polishing techniques will be investigated further. An attachment for the vibratory polishers will be designed and fabricated for the purpose of producing improved sample rotation. Chemical-mechanical procedures will be examined, and liquid-phase etching procedures, both alone and in conjunction with various annealing cycles, will be investigated. Particular attention will be given to an examination of the effects of gas-phase etching on $MgA\ell_2O_4$ surfaces and to characterizing the surfaces so treated. The ion-beam sputtering technique will be developed further for producing very thin (~ 200 Å) $A\ell_2O_3$ substrates for the in situ CVD experiments of Subtask 5. This method will also be investigated for removing damaged substrate surface layers and for removing contaminants from substrate surfaces prior to heteroepitaxy experiments. The series of Si deposition experiments designed to establish correlations between Si film properties and the characteristics of $A\ell_2O_3$ substrate surfaces will be continued; replica electron microscopy, reflection electron diffraction, Rutherford backscattering of charged particle beams, X-ray diffraction techniques, and possibly gas adsorption measurement techniques will be used. Observations of film nucleation behavior (Subtask 2) will be correlated with the type and density of substrate surface defects. Finally, Auger electron spectroscopy will be evaluated as a means for characterizing the impurity content of surface regions of $A\ell_2O_3$ and $MgA\ell_2O_4$ substrates in special cases.

5. SUBTASK 5: STUDIES OF IN SITU FILM GROWTH IN THE ELECTRON MICROSCOPE

The planned series of PVD experiments will be completed and demonstration motion picture films made by the middle of the reporting period. The first simplified CVD experiment (the oxidation of Cu) will be carried out without use of the CVD microchamber. When the latter is completed and installed, the CVD experiment will be repeated inside the chamber. Following installation of the SiH_4 and H_2 gas lines and associated apparatus, the first Si CVD experiment will be undertaken. Using $A\ell_2O_3$ substrates thinned to ~200Å by the ion-beam sputtering technique, transmission electron microscopy of the thinned substrate will be undertaken, after which the Si-$A\ell_2O_3$ interface will be examined by transmission microscopy on samples in which the $A\ell_2O_3$ substrate has been ion-etched.

6. SUBTASK 6: EVALUATION OF FILM PROPERTIES

Emphasis will continue on routine evaluation of structural and electrical properties of Si and GaAs heteroepitaxial films using established methods of X-ray and electron diffraction analysis, metallographic analysis, and measurement of carrier transport properties. The study of the temperature variation of the electrical characteristics of n- and p-type Si films on $A\ell_2O_3$ and $MgA\ell_2O_4$ substrates will continue. Experiments with Rutherford backscattering of charged particle beams will be resumed as a means of establishing the density distribution of defects in heteroepitaxial films, particularly in the interface region. The results of these measurements will be correlated with substrate species, orientation, cleaning techniques, and annealing treatments. Additional experiments will be continued on the electron transport in $A\ell_2O_3$, particularly as a function of electric field; attempts will be made to establish fully the mechanisms of the transport processes involved.

Measurement of escape length in Si and in GaAs films will be completed. High field transport properties of both GaAs and Si films of various resistivities and orientations will be measured. An investigation of film microstructure will be undertaken to identify stress conditions as well as the type and concentration of defects, using various X-ray techniques. The comparative evaluation of Si films on $A\ell_2O_3$ and $MgA\ell_2O_4$ substrates will be extended to the point that selection of the preferred substrate species for obtaining optimized Si film properties can be accomplished.

7. SUBTASK 7: DESIGN AND FABRICATION OF DEVICES

Increasing emphasis will be placed on the use of device structures to characterize heteroepitaxial Si and GaAs films. The dependence of the characteristics of devices such as junction diodes, MOS structures, and FET's on film growth conditions for both Si and GaAs will be investigated. The measurement of carrier lifetime in Si and GaAs films on insulating substrates by the C-V technique in MOS structures will be continued, using samples having a range of resistivity and crystallographic orientation. A specially designed MOS structure will be used to determine channel conductance, high- and low-field transport properties, and other interface characteristics in Si and GaAs films. The Schottky-barrier FET, recently designed, will be fabricated in GaAs films on both $A\ell_2O_3$ and other insulating substrates. Attempts will be made to extend operation of the FET from its design frequency (1 GHz) into the microwave region (~30 GHz). Continued use will be made of arrays of MOS devices in Si films on various $A\ell_2O_3$ orientations as a means of characterizing film quality. Other special device structures, such as the photo-injected floating-gate MIS memory, will be designed for later fabrication in Si and GaAs films. Comparison device structures will be fabricated in Si films on $A\ell_2O_3$ and $MgA\ell_2O_4$ substrates for evaluation to assist in the selection of the preferred substrate for optimized film properties.

In addition to the activities described above, specific experiments and investigations prompted by various program developments will be carried out as required during the next six months.

SECTION IV

PROGRAM SUMMARY TO DATE

The overall objective of the program, for which this is the Third Semiannual Report, is unchanged from that originally proposed — to carry out a fundamental study of the nucleation and film growth mechanisms in heteroepitaxial semiconductor thin films, leading to new knowledge and understanding of these processes, and then to apply these results to the preparation of improved semiconductor thin films and thin-film devices on insulating substrates.

The specific technical objectives of the three-year program are the following:

1. Investigation of the many aspects of the mechanisms of heteroepitaxial film growth, to establish (through accumulation of basic knowledge) sets of technical guidelines for the preparation of better films which can then be applied to real situations.

2. Preparation of improved, high-quality, device-grade heteroepitaxial films of Si and GaAs on insulating substrates by chemical vapor deposition (CVD) methods.

3. Development of methods of characterizing heteroepitaxial films as to their suitability for subsequent device fabrication.

4. Design and fabrication of selected thin-film devices which take advantage of the unique properties of such films.

The general plan for accomplishing these objectives involves as the primary effort the study of the fundamentals of heteroepitaxial semiconductor film growth on insulating substrates, with specialized device fabrication used both as a means of evaluating certain properties of the films (and thus as a measure of film quality as the program progresses) and as a means of exploiting certain unique properties of heteroepitaxial semiconductor-insulator systems. The insight into the question of which fundamental mechanisms, properties, and processes to investigate in these studies comes from extensive background knowledge of epitaxy and its variety of problems of long standing and from the thin-film device difficulties demonstrated over a period of several years in many laboratories. The problems subjected to study are in no way restricted to those identified a priori; experimental (and theoretical) attention is shifted as needed as the program progresses, in order to achieve the goal of a better understanding of heteroepitaxial process and the resultant improvement in thin-film active semiconductor devices.

The program involves both theoretical and experimental investigation of the nucleation and growth mechanisms of heteroepitaxial films in semiconductor-insulator systems. The theoretical studies consist of two types of activity. First, there is direct interaction with the experimental program involving data analyses, suggestion of definitive experiments, and postulation of specific models to explain experimental observations. Second, there is development of original contributions to the theory of heteroepitaxial growth, the goal of which is the generation of significant advances in fundamental epitaxy theory.

The experimental investigations are also of two types. First, fundamental explorations are carried out to delineate mechanisms and general empirical principles of the heteroepitaxial growth process. Second, practical studies accompany the fundamental investigations so that useful developments can be immediately applied to the improvement of semiconductor films and thin-film devices on insulating substrates.

The work has emphasized the CVD method of growing semiconductor thin films because of its importance in the semiconductor industry. One of the unique aspects of the program is this emphasis on the study of fundamental mechanisms of CVD growth; most previous fundamental studies of epitaxy have concentrated upon physical vapor deposition (PVD) methods, partly because such studies are easier with PVD techniques.

The program emphasis is on films of Si and GaAs and substrates of sapphire ($A\ell_2O_3$) and spinel ($MgA\ell_2O_4$); nonstoichiometric spinel and beryllia (BeO) may also be included as substrate materials as the program progresses. The initial emphasis has been on the Si-on-$A\ell_2O_3$ system, with increasing attention being given to the Si-on-$MgA\ell_2O_4$ and GaAs-on-$A\ell_2O_3$ systems. Si and GaAs have been chosen because of the preeminence of the former in the semiconductor industry and the high-frequency and high-temperature attributes of the latter; in addition, they represent the elemental and compound semiconductors for which most comparative information exists. If further modifications in the semiconductor-insulator systems under study appear advisable as the work develops other materials will be introduced.

The program as described is carried on primarily at facilities of the Electronics Group of North American Rockwell Corporation (NR) by NR personnel. Parts of several of the subtasks are performed by personnel of the University of California at Los Angeles (UCLA), in the Department of Electrical Sciences and Engineering and in the Chemistry Department, by means of a subcontract from NR.

The accomplishments of the contract program to date are summarized by the present subtask structure as follows:

1. SUBTASK 1. THEORY OF EPITAXY AND HETEROEPITAXIAL INTERFACES

During the first year a formal theoretical method of replacing overgrowth atoms on a substrate with Gaussian mass distributions was further developed for those cases where the effective interatomic potential is known. The technique, applicable to irregular-shaped islands or films of finite extent, was applied to a simplified model to determine preferred orientation relationships from calculated film-substrate interaction energies. The method was not pursued further, however, because it was not sufficiently adaptable to real systems. Several other possible approaches to the theoretical modeling of heteroepitaxial systems were critically reviewed, including the Frank-Van der Merwe model, a Green's function/Wannier-function approach, a contrived potential-energy model, and the two-body interatomic potential method. It was concluded that most existing theories are inadequate for application to real systems.

The feasibility of a molecular orbital development of the heteroepitaxial interface was then investigated. However, during the past six months it was determined infeasible to apply this technique in a manner directly relevant to heteroepitaxy, so this effort has been terminated. The interatomic potential approach to heteroepitaxy has has been reinstigated, with the goal being the computer simulation of growth of Si on $A\ell_2O_3$. Mechanical stability conditions for an $A\ell_2O_3$ lattice modeled with two-body potentials were investigated and determined to the depth required for these applications. Computer programming of the $A\ell_2O_3$ lattice energy and elastic constants was begun for use in determining appropriate empirical potentials required for modeling this $A\ell_2O_3$ lattice. Successful modeling of the $A\ell_2O_3$ lattice is a major requirement for modeling Si growth on $A\ell_2O_3$.

In addition, during the past six months the application of the electron-on-network theory to the problem of determining surface configurations and interfacial binding energies in heteroepitaxial systems where the surface structure is allowed to relax has been investigated and appears promising for the real systems of interest. Normalized eigenvectors have been developed as a basis for a secular equation whose solution is fundamental to the solution of the total problem.

2. SUBTASK 2. DEPOSITION STUDIES AND FILM PREPARATION

In the first year it was determined that the electrical properties of undoped n-type heteroepitaxial Si films grown on various orientations of $A\ell_2O_3$ (and also $MgA\ell_2O_4$) by the CVD method of pyrolysis of SiH_4 are dominated by surface-state conduction for carrier concentrations of $\sim 10^{15}$ cm^{-3} or below. Essentially equivalent (100)- and (111)-oriented Si films were grown on $(01\bar{1}2)$ and $(10\bar{1}4)$ $A\ell_2O_3$ substrates at deposition temperatures below the autodoping range (~1050 C). $A\ell_2O_3$ orientations near the $(11\bar{2}0)$ plane, not previously used in heteroepitaxy studies, have been utilized as substrates for (111) Si heteroepitaxy; this has resulted in electron mobilities of 600-700 cm^2/V-sec for carrier concentrations of 10^{15} - 10^{17} cm^{-3}, which exceeds mobilities obtained on either $(01\bar{1}2)$ or $(10\bar{1}4)$ $A\ell_2O_3$ substrates.

Analysis of the data obtained during the past six months reveals the strong interrelationships that exist among the various parameters that have been selected as being most meaningful for optimizing Si growth on insulators. Evaluation of the electrical properties of Si films on $A\ell_2O_3$ orientations recognized years ago as providing reflective Si overgrowths is demonstrating that growth conditions (1) must be maximized for the substrate orientation chosen; (2) differ for those $A\ell_2O_3$ orientations which lead to the same Si orientation; (3) are dependent upon reactor geometry and gaseous atmosphere; and (4) should be optimized for the particular film thickness desired. It is still too early to determine if annealing during film growth or the use of water-cooled reactors is beneficial, but these factors are being evaluated. Preliminary studies of Si growth by SiH_4 pyrolysis at reduced pressures (1 to 10 torr) have been very encouraging, indicating single-crystal growth can be obtained over fairly wide temperature range, when conditions are optimized, on both $A\ell_2O_3$ and $MgA\ell_2O_4$ substrates. Brief investigation of the growth of Si films on $A\ell_2O_3$ and $MgA\ell_2O_4$ using He as the growth atmosphere and the carrier gas showed that epitaxial growth could be achieved, but the conditions for good quality growth remain to be established.

3. SUBTASK 3. ANALYSIS AND PURIFICATION OF CVD REACTANTS

During the first year, techniques of gas chromatography were developed for analysis of the reactants used for semiconductor heteroepitaxy by CVD. A general-purpose gas-handling system was constructed for the highly volatile and reactive gases studied, with silicone oil and polymer columns used for the chromatography. Several extraneous impurity peaks were observed in the chromatograms of SiH_4 samples; diborane (B_2H_6) was tentatively identified as a significant impurity (~10 ppm), although not confirmed by mass spectrometer techniques. Small quantities of purified SiH_4, free of diborane, were prepared by successive injections in the chromatograph; quantities were too small, however, for use in laboratory CVD experiments. During the past six months, samples of SiH_4 and of trimethylgallium (TMG) used for Si and GaAs CVD experiments have been analyzed for impurity content by sensitive mass spectrometric techniques. Disilane and trimethylsilane, together with several other impurities of less concern, were found in the SiH_4 samples. Analyses are still in progress on other TMG samples because of uncertainties in the analyses to date.

4. SUBTASK 4. PREPARATION AND CHARACTERIZATION OF SUBSTRATES

In the first year of the program it was demonstrated that $A\ell_2O_3$ surfaces prepared by mechanical polishing techniques and used routinely for semiconductor heteroepitaxy typically have severe surface and subsurface damage, with many scratches often several microns deep, often rendered invisible to close inspection by amorphous or fine-grained debris embedded in the scratches in the final polishing stages. Some improvement in mechanical polishing procedures was achieved in terms of the density and depth of such damage. Gas-phase etching/polishing procedures using SF_6 and various fluorinated halocarbons in the 1350-1500 C temperature range produced essentially scratch-free surfaces on $(01\bar{1}2)$ and near-$(11\bar{2}0)$ $A\ell_2O_3$ substrates. Extensive gas-phase etch-rate data were obtained as a function of crystallographic orientation in this temperature range.

During the past six months a much improved technique for polishing $(10\bar{1}4)$ $A\ell_2O_3$ has been developed, and excellent surfaces in this orientation are now being obtained. Gas-phase etching/polishing techniques have been further developed and exploited for (1) thinning $A\ell_2O_3$ substrates to thicknesses the order of 1 mil; (2) evaluating the effects of prolonged etching on $(01\bar{1}2)$, (0001), and ~$(11\bar{2}0)$ $A\ell_2O_3$; and (3) assessing the subsurface damage caused by various mechanical polishing procedures. Four sets of $A\ell_2O_3$ substrate wafers — in the (0001), $(01\bar{1}2)$, $(10\bar{1}4)$ and ~ $(11\bar{2}0)$ orientations — are being prepared for a series of experiments designed to establish correlations between Si film properties and $A\ell_2O_3$ substrate conditions. Routine characterization of substrate surfaces at various stages of preparation had continued with techniques of X-ray and electron diffraction analysis, optical and electron microscopy, and charged-particle back-scattering measurements.

5. SUBTASK 5. STUDIES OF IN SITU FILM GROWTH IN THE ELECTRON MICROSCOPE

In the first year of the program many of the modifications required in the electron microscope for in situ observation of the nucleation and early-stage growth of CVD semiconductor films on insulating substrates were completed. Provision for motion-picture recording of film growth was assembled and tested, and the heated specimen stage was installed and tested. The first in situ PVD experiments were carried out. In the past six months a series of electron microscope modifications and tests has been completed, culminating in a series of successful PVD experiments inside the electron microscope. Aluminum has been deposited onto a heated carbon substrate and a sequence of micrographs taken during the growth process, demonstrating the feasibility of performing in situ nucleation and growth studies in this equipment.

A transmission phosphor screen (for the motion picture camera) has been installed, permitting motion picture photography which does not interfere with the normal still photography. The auxiliary vacuum pumping system for the specimen chamber has been fabricated, installed and tested. The basic vacuum system of the microscope itself has been improved by addition of a cooled baffle, by polishing numerous O-ring grooves, and by thoroughly cleaning the microscope interior. A PVD source assembly has been fabricated, installed and used in conjunction with the specimen heater to perform the above PVD experiments. Calculations and design for the CVD microchamber have been completed; it and the differential pumping apertures are being fabricated. Work has begun on the production of the thin (200 Å) $A\ell_2O_3$ crystals required as substrates for the in situ CVD studies.

6. SUBTASK 6. EVALUATION OF FILM PROPERTIES

During the first year, the routine evaluation of film properties was carried out by established methods of X-ray and electron diffraction analysis, metallographic analysis, and electrical measurements of transport properties. In addition, a new technique for evaluating the characteristics of the interfacial region of heteroepitaxial films was developed, involving measurement of the photoelectron emission from monochromatically-illuminated films in the MIS configuration on insulating (viz., $A\ell_2O_3$) substrates. Relatively large photocurrents due to electron transport through thick (~10 mils) single-crystal $A\ell_2O_3$ substrates were measured as a function of photon energy. Photoelectric threshold energies, escape length (mean free path) of excited electrons, and band bending in the semiconductor film adjoining the interface were determined in the $Si/A\ell_2O_3$ and $GaAs/A\ell_2O_3$ systems. Observation of the energy spectrum of back-scattered proton or alpha-particle beams injected in channeling directions in heteroepitaxial semiconductor films was also investigated as a means of measuring the density and the location of structural defects in the films. Experiments indicated that Si/insulator films have less imperfect interfacial regions than do GaAs/insulator films. The best structures of those examined to date were found in (100) Si films on $(01\bar{1}2)$ $A\ell_2O_3$ substrates and in (111) Si films grown on near-$(11\bar{2}0)$ $A\ell_2O_3$ substrates.

During the past six months the thorough study of the effects of changes in deposition parameters on $Si/A\ell_2O_3$ film properties has continued. These studies have led to considerable insight into the factors which most profoundly influence film quality, and identification of conditions for optimized film growth on the various $A\ell_2O_3$

orientations is nearly complete. The importance of reactor geometry has been recognized and demonstrated. The extent of $A\ell$ autodoping from the substrate has been established, and appropriate annealing procedures for minimizing these effects have been determined. The use of new $A\ell_2O_3$ orientations for Si growth has led to substrates which appear to yield epitaxial films of as good or better quality than those previously obtained. The measurements of photoemission of electrons from heteroepitaxial semiconductor films and transport of electrons in $A\ell_2O_3$ have been carried further. Work functions of additional metals have been determined, and the mechanism of electron transport through the insulator is becoming better understood. Measurements of high-field transport properties of Si and GaAs heteroepitaxial films have been initiated.

7. SUBTASK 7. DESIGN AND FABRICATION OF DEVICES

During the first year apparatus for determining carrier lifetime by C-V measurement in MOS structures was designed, constructed and tested. A special MOS structure was designed for measurement of channel conductance, high- and low-field transport properties, and various interface characteristics of heteroepitaxial films. Initial attempts to fabricate Schottky-barrier diodes in $Si/A\ell_2O_3$ films as a means of evaluating their electrical properties were not successful. During the past six months preliminary design of a Schottky-barrier type of FET has been completed; experimental FET structures will be fabricated in GaAs/insulator films for operation at 1 GHz. Preliminary results on carrier lifetime in $Si/A\ell_2O_3$ films have been obtained, after initial development of the measurement technique on bulk single-crystal Si samples was completed and after impurity contamination problems encountered in the oxide growth process were solved. The device content of the program is gradually increasing, according to the original contract plan.

APPENDIX A

INTERIM REPORT ON ANALYSIS AND PURIFICATION OF CVD REACTANTS*

Early in this contract program it was clear that the probable impurity content of the various reactants used for the chemical vapor deposition of Si and GaAs heteroepitaxial films provided real limitations on the achievable impurity levels in the films themselves. A study was undertaken to attempt to identify the impurities present in these reactants and to establish the concentrations of the principal impurities that would influence the properties of the grown films if they become incorporated into the films.

During the first 12 months of the contract, studies were initiated at UCLA for this purpose. At that time these studies constituted Subtask 4, but at the start of the second year of the program the designation was changed to Subtask 3. (See Section 1.)

The plan was to analyze SiH_4 and trimethylgallium (TMG) first and then AsH_3, using techniques of gas chromatography and mass spectrometry. Among the various techniques available in analytical chemistry, this combination was selected as the most convenient method to analyze volatile inorganic compounds, as such components are expected to be present at the sub-ppm concentration level in the reactants of interest here.

Gas chromatography (GC) by itself is not an absolute method to identify the components of a sample. The general procedure used in qualitative GC is to compare experimental retention data with those obtained with reference samples. The results then have to be confirmed by an analytical method, preferably employing direct coupling from the detector of a gas chromatograph to the inlet of a mass spectrometer. Special adapters are needed to eliminate large excesses of carrier gas from the main flow. However, in these experiments the direct coupling was not available; the sample from the effluent of the gas chromatograph was collected in a special trap and then injected into a mass spectrometer.

Monosilane, SiH_4, was studied primarily. It was assumed that the contaminants originated in the $SiC\ell_4$ used to prepare SiH_4. Boron compounds, which may be present in $SiC\ell_4$, can be reduced to volatile hydrides such as diborane (B_2H_6). The relatively close boiling points of the pair SiH_4-B_2H_6 do not allow efficient elimination of the latter by typical industrial fractional condensation processes. But the difference of 30C in their boiling points is sufficient to separate these two compounds by analytical GC, if the right column packing is selected.

All of the reactant materials used in semiconductor heteroepitaxial studies by CVD are highly volatile and reactive gases. Special care was taken in this work to prevent hazardous contact of these gases with air and moisture.

*This work was done by Dr. Marie Dixmier and Prof. R. L. Pecsok of the Chemistry Department, UCLA, in the first year of the contract. The principal results were summarized in the Second Semiannual Report of this contract.

The references for this Appendix are grouped together at the end of the Appendix.

The general function of the gas handling system used in the present study (Figure A-1) was to introduce the sample under vacuum through a three-way valve, and to dispose of the sample by purging with He (at a high flow rate) to the burning port. A 500-mℓ stainless-steel trapping cylinder was used to temporarily condense the sample fraction before injection. Connections Swagelok fittings were made of 316 SS, as were the shut-off and metering valves. The injection valve was a three-way mini-volume Carle valve (No. 5521) with interchangeable loops of different volumes.

After extensive testing and some modification this system was shown to be explosion-proof, but for routine use leaks greater than ~1 torr must be avoided. The Carle valve was found to be less dependable than the other parts of the system. A bellows valve or a purge-model valve with a closed housing would be preferable for systems such as this.

In first experiments, classical gas-liquid chromatography was used. Nonpolar stationary phases such as silicone oil are known to separate silanes[1,2] or light boranes.[3,4,5] The first packing used was Dow-Corning silicone DC-200, 20 percent by weight on Chromosorb P, acid-washed and silanized. A Loenco gas chromatograph, Model 160, equipped with a 4.2 m x 6 mm o.d. stainless-steel column and a thermal conductivity detector, was used for the investigations. Isothermal elution at 40C was obtained with a He flow rate of 50 mℓ/min. The sample volume, measured in a 2.5 mℓ loop under 2.5 psi of SiH_4, was calculated to be about 4 mℓ at STP.

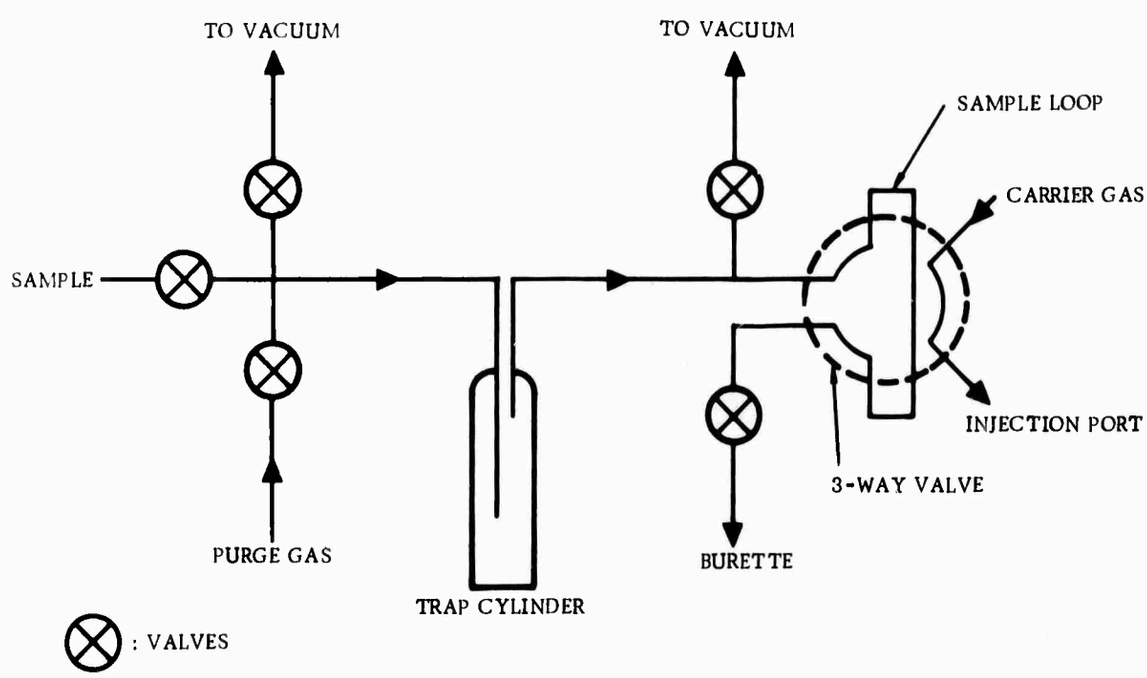

Figure A-1. Schematic Gas Sample Handling System for GC

Samples of semiconductor-grade SiH_4 from four different supply cylinders gave the same basic chromatogram (Figure A-2), with at least six impurities detected by the thermal conductivity detector. Retention indices versus n-paraffin homologs and concentrations in ppm calculated by the area method are given in Table A-1. Identification of one of these impurities as B_2H_6 was attempted by comparison with a known B_2H_6 reference sample.

It should be pointed out that in analytical GC, characterization of a given solute is given by a unique specific retention time. But in semipreparative GC, when large amounts of solute are injected, large variations of retention times can be expected because of overloading effects. Under these conditions, equilibrium distribution of the sample between the phases is not maintained, and the excess sample will travel at a higher speed through the column.[6] For large samples of both B_2H_6 and SiH_4 there is a decrease in retention times from the analytical data. Retention times were evaluated from experimental data with a 3 percent range of variation. With the DC-200 column, the B_2H_6 noncorrected retention time is 12 percent greater than for SiH_4. This small difference in retention times is not sufficient to separate these two compounds on a preparative scale, or even to detect B_2H_6 that is completely hidden in the main peak of SiH_4.

The experimental results confirm the general behavior of a silicone column toward nonpolar solutes: i.e., retention times are in order of their boiling points. As the chemical reactivities of SiH_4 and B_2H_6 are similar, it cannot be expected that

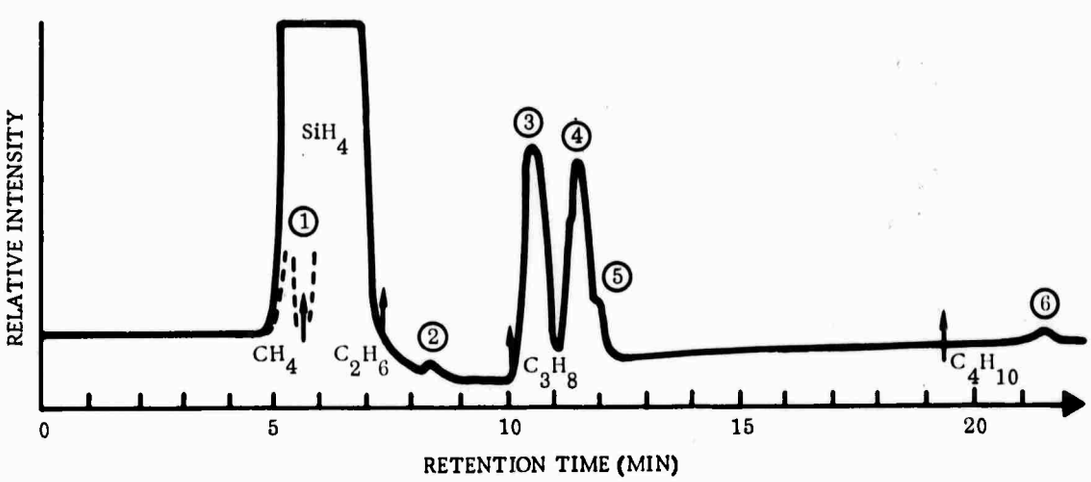

Figure A-2. SiH_4 Chromatogram on DC-200 Silicone Column Packing

Table A-1. Retention Index and Concentration of Impurities in SiH_4 Sample

Impurity	Concentration (ppm)	Retention Index
(1) H_2 + air	7000	-
(2)	< 10 ppm	250
(3)	260	305
(4)	415	323
(5)	10	-
(6)	<10	>400

a polar stationary phase will enhance their separation by specific selectivity. Thus, in order to increase the ratio of the retention times a solid packing having a large specific area was used. A second column was prepared with Chromosorb 102 (Johns Manville) as packing for gas-solid chromatography. This is a cross-linked copolymer of divinyl benzene-styrene which exhibits a surface area 100 times greater than the Chromosorb P used previously. This column was 5.4 m x 6 mm o.d., packed with 60 to 80 mesh Chromosorb 102. The column was first maintained at ambient temperature, with a He flow rate of 40 mℓ/min.

A typical chromatogram of a SiH_4 sample on the Chromosorb 102 colum is shown in Figure A-3. Four impurity peaks are evident before the main SiH_4 peak.

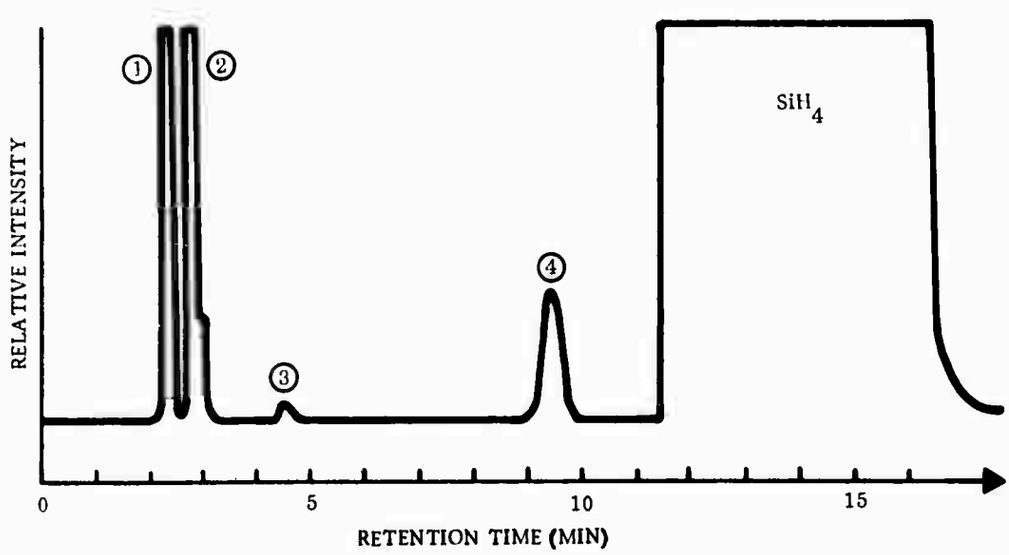

Figure A-3. SiH_4 and other Compounds on a Chromsorb 102 Column at Ambient Temperature

By comparison with reference samples these peaks appear to correspond to (1) H_2, (2) $N_2 + O_2$ (air), (3) CH_4, and (4) CO_2.

No impurities were detected after the SiH_4 peak. Unfortunately, with this chromatographic equipment, it was not possible to expect a large improvement in detection. However, the difference of retention times of SiH_4 and CH_4 was about three times larger with Chromosorb 102 than with the DC-200 column.

In order to reduce the retention times of solutes eluted after the SiH_4 peak, an isothermal chromatogram at 60C was obtained with a reference mixture of SiH_4 and B_2H_6 and is shown in Figure A-4. Retention data are expressed here in corrected retention distance

$$d'_R = d_R - d_M , \qquad \text{(A-1)}$$

where d_M is related to hydrogen and $d_R = t_R$ x (chart speed), with t_R the retention time in minutes and the recorder chart speed 1 in./min in this case.

It is interesting to compare the experimental retention data with the boiling points of the different compounds which might be present in the SiH_4 sample. This was done by the use of a thermodynamic relation derived from the Clausius-Clapeyron equation. This simplified relation is

$$\log d'_R \propto BP . \qquad \text{(A-2)}$$

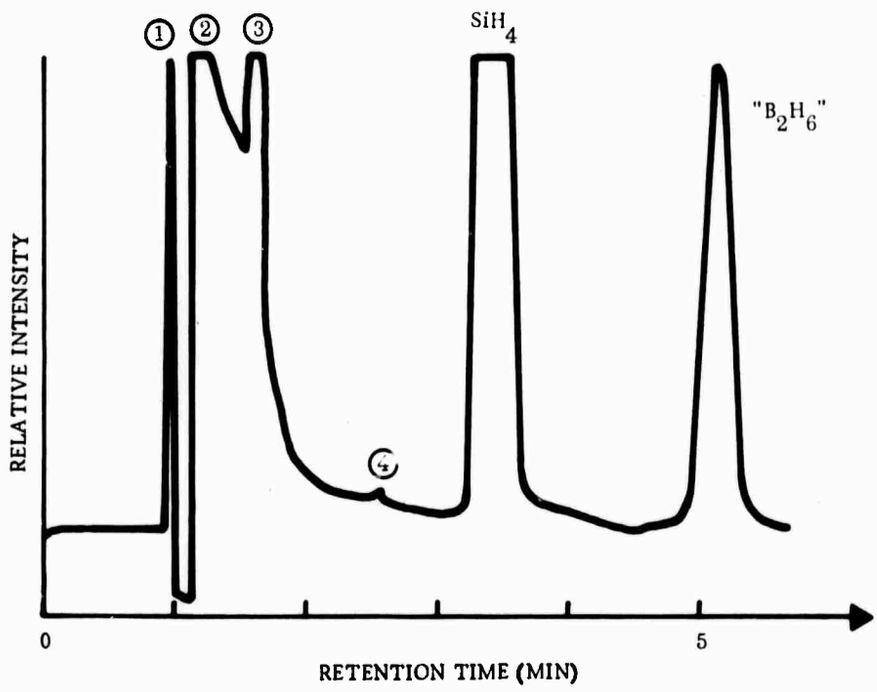

Figure A-4. Chromatogram at 60C of a Mixture of SiH_4 and B_2H_6 on a Chromsorb 102 Column

A classical calculation related d'_R to the vapor pressure of a given solute, and the vaporization enthalpy of the pure solute to its boiling point. Although this relation applies strictly to compounds of an homologous series, it is interesting to verify the behavior of C, Si, and boron hydrides on Chromosorb 102. Results are given in Table A-2.

The experimental values verify the relation of Equation (A-2) and confirm that, as in gas-liquid chromatography on a silicone oil, these solutes are eluted in the order of their boiling points. However, an important improvement is obtained with Chromosorb 102, specifically, the large increase of B_2H_6 retention versus that of SiH_4 – 80 percent compared with the 12 percent on the silicone DC-200 column. Even with large overloading of the Chromsorb 102 column with preparative injections of SiH_4, a good separation of the couple SiH_4 – B_2H_6 can be expected, sufficient to detect the latter at the sub-ppm level.

In order to confirm and identify the nature of the solutes, several collected effluents were injected into the CEC 21-620 mass spectrometer. In a 50 mℓ glass flask previously evacuated, the effluent stream of solute and carrier gas was trapped in totality. The time of collection was roughly one minute, selected near the maximum of the detector signal. As will be shown later, this technique gives good yields of recovery for preparative collection of purified samples, but for mass spectrometry the results were very poor. The main reason appeared to be that the sample was too dilute for the injection system of this mass spectrometer; the sample was diluted by a factor of 10^3 from the injection volume.

Attempts to identify peak 3 in the sample represented in Figure A-2 and even B_2H_6 in the sample of Figure A-3 failed. Only one impurity present in both the SiH_4 sample (Figure A-2) and the B_2H_6 reference mixture was identified and that was CH_4. Results from two collected samples compared with the theoretically expected relative intensities for the mass spectrometric analysis are given in Table A-3.

Table A-2. Comparison of Retention Data and Boiling Points of Solutes Eluted According to Figure A-3

	CH_4	SiH_4	B_2H_6
d'_R(mm)	28	115	207
log d'_R	1.45	2.06	2.32
BP(^oC)	-161.5	-112	-92.5

Table A-3. Mass Spectrometric Data for CH_4

Relative Intensity (70 V)			
m/e	1st Sample	2nd Sample	Theory
16	100	100	100
15	81.7	83.6	85.9
14	(33.4)	11.2	16.1

More informative results were obtained in collection experiments in some semi-preparative GC. Three series of successive GC collections of purified SiH_4 were obtained, with four, seven and 10 runs, respectively. In each run, the amount of SiH_4 collected was calculated to be 5 mg, corresponding to the injection volume of 4 ml. The recovered material was tested for purity by recycling the sample through the Chromosorb 102 column for the first two series and through both the DC-200 and Chromosorb 102 columns for the last series. Elimination of impurities 2 through 6 (see Figure A-2 and Table A-1) was demonstrated by elution of successive equal volumes of purified and crude SiH_4 on the DC-200 column.

In the Chromosorb 102 column, impurities 3 and 4 (see Figure A-3) were completely removed, but traces of air still remained. B_2H_6 was not detected in the SiH_4 sample with the Chromsorb 102 column because of the poor sensitivity of the thermal conductivity detector.

It is thus not possible to certify the dependability either of the gas chromatographic technique or the collection apparatus. However, the retention time of B_2H_6 on Chromosorb 102, almost two times larger than that of SiH_4, shows that GC can be a promising and efficient method to detect and even to separate B_2H_6 from SiH_4. Therefore, a compromise must be made between the reliability of preparative-scale GC and its limited production capability for industrial purposes.

REFERENCES

1. K. Borer and C. S. G. Phillips, Proc. Chem. Soc. 1959, 189.

2. G. S. G. Phillips and P. L. Timms, Anal. Chem. 35, 505 (1963).

3. G. R. Seely, J. P. Oliver and D. M. Ritter, Anal. Chem. 31, 1993 (1959).

4. K. Borer, A. B. Littlewood and C. S. G. Phillips, J. Inorg. Nucl. Chem. 15, 316 (1960).

5. H. W. Myers and R. F. Putnam, Anal. Chem. 34, 664 (1962).

6. A. B. Littlewood, Gas Chromatography (Academic Press, New York, 1970), p. 225.

APPENDIX B

BIBLIOGRAPHY: ELECTRON MICROSCOPE IN SITU NUCLEATION AND GROWTH STUDIES

Addendum to Appendix A, Second Semiannual Report

A. EXPERIMENTAL TECHNIQUES: CHEMICAL VAPOR DEPOSITION (CVD)

A16. G. Dalmai-Imelik and C. Leclercq, p 359 in reference G1.
"Etude de L'Evolution de Catalyseurs au cours de leur Preparation et de Reactione Catalytiques."

A17. J. Escaig and C. Sella, p 177 in reference G2.
"Celluie Porte-Objet Permettant L'Observation de Specimen Chauffes Sous Atmosphere Contrôlée."

B. RESULTS: CVD AND GAS REACTION ON HEATED SUBSTRATES

B17. N. Sasaki and R. Ueda, p 463 in reference G9.
"The Electronmicroscopic and Micro-diffraction Observation In Situ of Changes in Solids (Reduction of MoO_3)."

B18. R.K. Hart and J. K. Maurin, Surface Science 20, 285 (1970)
"The Nucleation and Growth of Oxide Islands on Aluminum."

B19. F. S. Feates, H. Morley, and P. S. Robinson, p 295 in reference G1.
"Controlled Atmosphere Electron Microscopy."

B20. F.S. Feates, P. S. Harris, R. T. K. Baker, p 357 in reference G1
"Catalytic Oxidation of Graphite by Continuous Electron Microscopic Observation."

B21. R. S. Gordon and W. D. Kingery, J. Amer. Ceram. Soc 49, 654 (1966) and 50, 8 (1967). "Thermal Decomposition of Brucite: I, Electron and Optical Microscope Studies; II, Kinetics of Decomposition in Vacuum."

B22. J. F. Goodman, Proc. Roy. Soc. A247, 346 (1958).
"The Decomposition of Magnesium Hydroxide in an Electron Microscope."

B23. P. L. Burnett, W. R. Mitchess, and C. L. Horick, p 446 in reference G12.
"Observations of the Thermal Decomposition of Brucite."

D. RESULTS: PHYSICAL VAPOR DEPOSITION

D16. T. E. Hutchinson, p 376 in reference G12.
"In situ Electron Microscope Investigations of the Growth and Structure of Thin Films."

Preceding page blank

D17. H. Poppa, p 378 in reference G12.
"Thin Film Nucleation and Growth Under Controlled Conditions."

E. (1-19) RELATED TOPICS: GAS INLET DEVICES

E10. R. C. Moretz, G. G. Hausner, and D. F. Parsons, p 44 in reference G14.
"New Design for a Differentially Pumped Hydration Chamber for a Siemens 1A."

E11. D. F. Parsons and R. C. Moretz, p 497 in reference G1.
"Microscopy and Diffraction of Water in the Electron Microscope."

E12. D. L. Allinson, p 169 in reference G1 vol I.
"Environmental Cell for Use in a High Voltage Electron Microscope."

E13. A. Fukami, K. Adachi, and M. Katoh, p 263 in reference G2.
"On a Study of New Micro Plastic Grid and its Applications."

E14. A. Fukami, T. Etoh, N. Ishihara, M. Katoh, and K. Fujiwara, p 171 in reference G1. "Pressurized Specimen Chamber for Electron Microscope."

E15. G. Dupouy, F. Perrier, and L. Durrieu, Rendus 251, 2836 (1960).
"L'Observation de la matière vivante au moyen d'un microscope électronique fonctionnant sans très haute tension" (The Observation of Living Material by Means of an Electron Microscope Operating at Very High Voltage)

E16. G. Dupouy, F. Perrier, and L. Durrieu, Comptes Rendus 254, 3786 (1962).
"L'Observation des objets en milieu gazeur. Application à l'étude de la contamination dans le microscope électronique." (The Observatio of Objects in the Midst of Gas. Application to the Study of Contamination in the Electron Microscope)

E17. P. R. Ward and R. F. Mitchell, p 44 in reference G15.
"An Electron Microscope Environmental Specimen Chamber."

E. (20-39) RELATED TOPICS: ION PUMPING AND RESIDUAL GAS ANALYSIS

E27. R. B. Marcus, C. J. Calbick, and T. T. Sheng, p 163 in reference G1.
"Improvements in an Electron Microscope for Clean, Quiet, Vibrationless Operation."

E28. R. E. Hartman and R. S. Hartman, Lab. Investigation 14, 409 (1965).
"Elimination of Potential Sources of Contaminating Material."

E29. R. E. Hartman and R. S. Hartman, p 74 in reference G14.
"Residual Gas Reactions in the Electron Microscope: IV. A Factor in Radiation Damage."

E30. R. E. Hartman, R. S. Hartman and P.L. Ramos, p 292 in reference G12.
"Residual Gas Reactions in the Electron Microscope: I. Qualitative Observations on the Water Gas Reaction."

E31. D. N. Braski, p 314 in reference G12. "A High Vacuum Electron Microscope."

E32. E. A. Buvinger, p 348 in reference G12. "Background Gas Reduction in the Electron Microscope."

E33. R. K. Hart, T. F. Kassner, and J. K. Maurin, Phil. Mag. 21, 453 (1970). "The Contamination of Surfaces during High Energy Electron Bombardment."

E (40-59) RELATED TOPICS: SPECIMEN HEATING STAGES

E45. K. Itoh, T. Itoh, and M. Watanabe, p 658 in reference G9. "The High Temperature Furance for the Electron Microscope."

E52. D. Jones, p 662 in reference G9. "A Specimen Furnace for the Reflection Electron Microscope."

E53. I. W. Sprys and P. C. J. Gallagher, p 312 in reference G12. "A New Hot Stage for the Philips EM200 and Its Calibration."

E (60-79) RELATED TOPICS: CINEMATOGRAPHY

E63. E. Sugata, Y. Nishitani, S. Kaneda, M. Tateishi, and H. Yoloya, p 452 in reference G9. "Fundamental Researches for Observing Specimens in Gas Layers."

E64. F. D. Lugton and C. E. Warble, Rev. Sci. Instr. 41, 1793 (1970). "High Resolution Cinematography at High Temperature in the Electron Microscope."

E65. M. J. Whelan, P. B. Hirsch, R. W. Horne, and W. Bollmann, Proc. Royal Soc. (London) A240 524 (1957). "Dislocations and Stacking Faults in Stainless Steel."

E66. K. Anderson, P. B. Kenway, p 244 in reference G12. "External Photography of the Microscope Image."

E67. J. W. S. Hearle, D. J. Clarke, B. Lomas, D. A. Reeves, and J. T. Sparrow, p 210 in reference G15. "A Simple Method of Recording Dynamic Events in the SEM Using a 16 mm Camera."

F. RELATED TOPICS: COOLING STAGES

F17. C. A. English and J. A. Venables, p 48 in reference G15. "The Design of Pressure Cells for Studying Condensed Gases."

G. GENERAL REFERENCES: ELECTRON MICROSCOPY CONFERENCES

G1. Electron Microscopy 1970 (Seventh International Congress on Electron Microscopy, Grenoble, 1970), Ed. P. Favard (Societe Francaise de Microscopie Electronique, Paris 1970), Vol. 1, Methods and General Techniques, Vol. 2, Physics.

G2. Electron Microscopy 1966 (Sixth International Congress for Electron Microscopy, Kyoto, 1966), Ed. R. Uyeda (Maruzen Co., Tokyo, 1966), Vol. 1, Physics.

G3. Electron Microscopy (Fifth International Congress for Electron Microscopy, Philadelphia, 1962), Ed. S. S. Breese, (Adademic Press, New York, 1962), Vol. 1, Physics and General Electron Microscopy.

G4. Fourth International Conference on Electron Microscopy (Berlin, 1958), Eds. W. Barqmann, G. Möllenstedt, H. Niehrs, R. Peters, E. Ruska, and C. Wolpers (Springer-Verlag, Berlin, 1960).

G5. Electron Microscopy (Proceedings of the Fourth European Regional Conference, Rome, 1968), Ed. D. A. Bocciarelli (Tipografia Poliglotta Vaticana, Rome, 1968).

G6. Electron Microscopy 1964 (Proceedings of the Third European Regional Conference, Prague, 1964), Ed. M. Titlbach (Publishing House of the Czechoslovak Academy of Sciences, Prague, and The Royal Microscopical Society, London, 1964), Vol. A, Physics.

G7. Proceedings of the (Second) European Regional Conference on Electron Microscopy (Delft 1960), Eds. A. L. Houwink and B. J. Spit (Nederlandse Vereniging voor Electronenmicroscopie, Delft, 1960), Vol. 1, Physics.

G8. Electron Microscopy (Proceedings of the Stockholm (First European Regional) Conference, 1956), Eds. F. S. Sjostrand and J. Rhodin (Almquist and Wiksell, Stockholm, 1956).

G9. Third International Conference on Electron Microscopy (London, 1954). Eds. V. E. Cosslett and R. Roso. (Royal Microscopical Society, London, 1954).

G10. Proceedings 28th Annual Meeting Electron Microscopy Society of America. (Houston, 1970) Ed. C. J. Arceneaux (Claitor's Publishing Division, Baton Rouge, 1970).

G11. Proceedings 27th Annual Meeting Electron Microscopy Society of America. (St. Paul, 1969) Ed. C. J. Arceneaux (Claitor's Publishing Division, Baton Rouge, 1969).

G12. Proceedings 26th Annual Meeting Electron Microscopy Society of America. (New Orleans, 1968) Ed. C. J. Arceneaux (Claitor's Publishing Division, Baton Rouge, 1968).

G13. Proceedings 25th Annual Meeting Electron Microscopy Society of America. (Chicago, 1967) Ed. C. J. Arceneaux (Claitor's Publishing Division, Baton Rouge, 1967).

G14. Proceedings 29th Annual Meeting Electron Microscopy Society of America. (Boston, 1971) Ed. C. J. Arceneaux (Claitor's Publishing Division, Baton Rouge, 1971).

G15. Electron Microscopy and Analysis (25th Meeting EMAG). Ed. W. C. Nixon (Institute of Physics, London, 1971).

REFERENCES

1. R. P. Ruth, "Fundamental Studies of Semiconductor Heteroepitaxy," First Semiannual Report, 28 January 1971, ARPA Order No. 1585, Contract No. DAAH01-70-C-1311. Prepared by North American Rockwell, Autonetics Division, Anaheim, CA, for USAMICOM, Redstone Arsenal, AL.

2. R. P. Ruth, "Fundamental Studies of Semiconductor Heteroepitaxy," Second Semiannual Report, July 1971, ARPA Order No. 1585, Contract No. DAAH01-70-C-1311. Prepared by North American Rockwell, Autonetics Division, Anaheim, CA, for USAMICOM, Redstone Arsenal, AL.

3. J. H. Van der Merwe, Single Crystal Films, ed. by M. H. Francombe and H. Sato (Pergamon Press, Oxford, 1964), p 137; J. Appl. Phys. 34, 117, 123 (1967); 41, 4725 (1970).

4. H. Reiss, J. Appl. Phys. 39, 5045 (1968).

5. M. Bettman, in Single Crystal Films, ed. by M. H. Francombe and H. Sato (Pergamon Press, Oxford, 1964), p 177.

6. N. H. Fletcher and P. L. Adamson, Phil. Mag. 14, 99 (1966).

7. E. B. Moore, Jr. and C. M. Carlson, Solid State Commun. 4, 47 (1966); A. J. Bennett, B. McCarroll and R. P. Messmer, Surface Sci. 24, 191 (1971); G. D. Watkins, R. P. Messmer, C. Weigal, D. Peak and J. W. Corbett, Phys. Rev. Lett. 27, 1573 (1971).

8. B. McCarroll and R. P. Messmer, Surface Sci. 27, 451 (1971).

9. Gordon Research Conference on Thin Films, Tilton, New Hampshire, August 9-13, 1971.

10. P. A. Tick and A. F. Witt, Surface Sci. 26, 165 (1971).

11. T. Johannesson and B. Persson, Physica Scripta. 2, 309 (1970); Phys. Stat. Sol. (a) 3, K251 (1970).

12. J. H. Gieske and G. R. Barsch, Phys. Stat. Sol. 29, 121 (1968).

13. O. L. Anderson, in Physical Acoustics, ed. by W. P. Mason, Vol. III, Part B (Academic Press, Inc., New York, 1965), p 43.

14. R. A. Swalin, J. Phys. Chem. Solids 18, 290 (1961).

15. a. H. Kuhn, Helv. Chim. Acta 31, 1441 (1948); 34, 1308 (1951); J. Chem. Phys. 17, 1198 (1949).

    b. K. Rudenberg and C. W. Scherr, J. Chem. Phys. 21, 1565 (1953).

Preceding page blank

16. E. W. Montroll, J. Math. Phys. 11, 635 (1970); with R. G. J. Mills, 2525 (1970).

17. R. F. C. Farrow and J. D. Filby, J. Electrochem. Soc. 118, 149 (1971).

18. G. L. Haller and R. W. Rice, J. Phys. Chem. 74, 4386 (1970).

19. D. W. Pashley, Phil. Mag. 10, 127 (1964).

20. L. J. van der Pauw, Phillips Tech. Rev. 20, 220 (1958-9).

21. H. M. Manasevit and A. C. Thorsen, "Heteroepitaxy of III-V Compound Semiconductors on Insulating Substrates," Final Report, January 1970, p 9, NASA Contract No. NAS 12-2010. Prepared by North American Rockwell, Autonetics Division, Anaheim, CA, for NASA/ERC, Boston, MA.

22. D. J. Dumin, Solid State Electron. 13, 415 (1970).

23. C. R. Viswanathan and R. Loo, Fifth International Vacuum Congress, Paper J-4, Boston, October 13, 1971.

24. M. Zerbst, Z. angew. Phys. 22, 30 (1966).

25. A. S. Grove, O. Leistiko, Jr., and C. T. Sah, J. Appl. Phys 35, 2695 (1964).